NUMERICAL STUDY ON CONVECTIVE BOUNDARY LAYER FLOW AND HEAT TRANSFER OF NANOFLUID OVER A WEDGE

RUHAILA MD KASMANI

FACULTY OF SCIENCE
UNIVERSITY OF MALAYA
KUALA LUMPUR

2016

NUMERICAL STUDY ON CONVECTIVE BOUNDARY LAYER FLOW AND HEAT TRANSFER OF NANOFLUID OVER A WEDGE

RUHAILA MD KASMANI

THESIS SUBMITTED IN FULFILMENT OF THE REQUIREMENTS FOR THE DEGREE OF DOCTOR OF PHILOSOPHY

FACULTY OF SCIENCE
UNIVERSITY OF MALAYA
KUALA LUMPUR

2016

ABSTRACT

The convective boundary layer flow, heat (and mass) transfer of nanofluid over a wedge are investigated. The fluid flow and heat transfer characteristics of nanofluid have received considerable attention due to wide range of engineering applications. In many boundary layer flow studies, it is found that nanofluid exhibits higher thermal conductivity and heat transfer coefficients compared to the conventional fluid. In this thesis, the mathematical nanofluid model proposed by Buongiorno is used to study the boundary layer flow of nanofluid past a wedge under the influence of various effects. The nanofluid model takes into account the transport mechanism of nanoparticles, namely the Brownian diffusion and thermophoresis. Based on this model, the mathematical formulation is developed to study the characteristics of flow, heat (and mass) transfer of six boundary layer flow problems. The problems are limited to steady, two-dimensional, laminar flow of incompressible viscous nanofluid along a wedge. The governing partial differential equations are reduced to a system of nonlinear ordinary differential equations using similarity transformation. The resulting system is solved numerically using the fourth-order Runge-Kutta-Gill method along with the shooting technique and Newton Raphson method. Then, the numerical values of the skin friction, heat (and mass) transfer coefficients are obtained for various values of the governing parameters such as wedge angle, heat generation/absorption, thermal radiation, Brownian motion, thermophoresis, suction, power law variation, Soret and Dufour effects. Comparisons with previously published work for verification and accuracy of the method used is performed and found to be in good agreement. The solutions are expressed graphically in terms of velocity, temperature, solutal concentration and nanoparticle volume fraction profiles. The effects of pertinent parameters entering into the problems on skin friction coefficient, local Nusselt number and local Sherwood number are discussed in detail.

ABSTRAK

Olakan aliran lapisan sempadan, pemindahan haba (dan jisim) bagi bendalir nano terhadap baji telah dikaji. Ciri aliran bendalir dan pemindahan haba bagi bendalir nano mendapat perhatian kerana mempunyai aplikasi kejuruteraan yang meluas. Dalam kebanyakan kajian aliran lapisan sempadan, didapati bendalir nano mempamerkan kebolehaliran terma dan pekali pemindahan haba yang lebih tinggi berbanding bendalir konvensional. Dalam tesis ini, model matematik bendalir nano yang dicadangkan oleh Buongiorno telah digunakan untuk mengkaji aliran lapisan sempadan bagi bendalir nano melalui baji yang dipengaruhi oleh pelbagai kesan. Model bendalir nano melibatkan mekanisma pengangkutan partikel nano iaitu pergerakan Brownian dan termoforesis. Berasaskan kepada model ini, formulasi matematik dibina untuk mengkaji ciri aliran, pemindahan haba (dan jisim) bagi enam masalah aliran lapisan sempadan. Masalah tersebut dihadkan kepada aliran laminar, mantap dua matra dalam nano bendalir likat tak mampat sepanjang baji. Persamaan pembezaan separa penakluk dijelmakan kepada sistem persamaan pembezaan biasa menggunakan penjelmaan keserupaan. Sistem persamaan yang terhasil diselesaikan secara berangka menggunakan kaedah Runge-Kutta-Gill dengan teknik tembakan dan kaedah Newton Raphson. Nilai berangka bagi pekali geseran kulit, pekali pemindahan haba (dan jisim) diperoleh untuk pelbagai nilai parameter seperti parameter sudut baji, penjanaan haba, sinaran terma, pergerakan Brownian, termoforesis, sedutan, kesan Soret dan Dufour. Perbandingan keputusan dengan kajian penerbitan terdahulu telah dilakukan bagi menentusah serta menguji ketepatan kaedah yang digunakan dan didapati hasil perbandingan sangat memuaskan. Penyelesaian berangka yang diperoleh dipersembahkan dalam bentuk graf dari segi profil-profil halaju, suhu, kepekatan solutal dan pecahan isipadu nanopartikel. Kesan pelbagai parameter berkenaan masalah ke atas pekali geseran kulit, nombor Nusselt setempat dan nombor Sherwood setempat dibincangkan secara terperinci.

ACKNOWLEDGEMENTS

I would like to express my deepest gratitude to Dr. S. Sivasankaran for his excellent guidance, great encouragement and invaluable advice throughout all stages in the completion of this study. I am also indebted to Dr. Zailan Siri for his insight and suggestions.

I would like to thank the Vice Chancellor of University of Malaya, who permitted me to take two years' leave from my teaching with full salary to undertake this study. My gratitude is extended to the entire staff of Institute of Mathematical Sciences and Centre for Foundation Studies in Science, University of Malaya for their constant support and encouragement.

My sincere thanks to all my friends for their cooperation, especially Cheong Huey Tyng for the help extended to me during my writing process.

Finally, a special gratitude to my husband, daughter and son for their sacrifices and tremendous patience throughout the study. I also deeply thank to my parents and family members for helping me stay motivated through the hard times.

TABLE OF CONTENTS

LIST OF FIGURES

LIST OF TABLES

LIST OF SYMBOLS AND ABBREVIATIONS

a, b, b_1, b_2, b_w	constants
c	specific heat capacity
C	solutal concentration
C_{fx}	local skin friction coefficient
d_p	nanoparticle diameter
D_B	Brownian diffusion coefficient
D_{CT}	Soret-type diffusivity
D_S	solutal diffusivity
D_T	thermophoretic diffusion coefficient
D_{TC}	Dufour-type diffusivity
f	dimensionless stream function
F_w	suction parameter
g	acceleration due to gravity
Gr_x	thermal Grashof number
Gr_x^*	solutal Grashof number
h_p	specific enthalpy of the nanoparticle material
$\mathbf{j}_{p,B}$	nanoparticle mass flux due to Brownian diffusion
$\mathbf{j}_{p,T}$	nanoparticle mass flux due to thermophoretic effect
k	thermal conductivity
k_B	Boltzmann's constant
k_1	Rosseland mean absorption coefficient
K_0	chemical reaction coefficient
K^*	chemical reaction parameter
Le	Lewis number
Ln	nanofluid Lewis number
m	wedge angle parameter
n_1, n_2	power index
N	buoyancy ratio

N_B	Brownian motion parameter
N_{CT}	Soret-type parameter
N_T	thermophoresis parameter
N_{TC}	Dufour-type parameter
Nu_x	local Nusselt number
P	pressure
Pr	Prandtl number
$\mathbf{q}$	energy flux
q_m	mass flux
q_r	radiation heat flux
q_w	wall heat flux
Q	heat generation/absorption coefficient
R	radiation parameter
Re_x	Reynolds number
Ri	Richardson number
S	nanoparticle volume fraction
Sh_x	local Sherwood number
t	time
T	temperature of the fluid
u, v	velocity component in x- and y-direction
U	free stream velocity
U_w	moving wedge velocity
$\mathbf{v}$	velocity vector
v_0	suction or injection
x, y	Cartesian coordinates

Greek symbols

α	thermal diffusivity
β	Hartree pressure gradient
β_C	volumetric concentration expansion coefficient
β_T	volumetric thermal expansion coefficient

β^*	thermophoretic coefficient
γ	dimensionless solutal concentration
δ	heat generation/absorption parameter
η	similarity variable
θ	dimensionless temperature
λ	moving wedge parameter
μ	dynamic viscosity
ν	kinematic viscosity
ξ	dimensionless distance
ρ	fluid density
σ	Stefan-Boltzmann constant
τ	ratio of heat capacity of nanoparticle and heat capacity of base fluid
τ^*	stress tensor
τ_w	shear stress
ϕ	dimensionless nanoparticle volume fraction
ψ	stream function
Ω	angle of the wedge

Subscripts

w	conditions at the surface of the wedge
∞	ambient conditions/free stream
f	base fluid
p	nanoparticle

Abbreviations

Ag	silver
Al_2O_3	alumina
Au	gold
Cu	copper
MHD	magnetohydrodynamics
TiO_2	titanium dioxide/titania

CHAPTER 1: INTRODUCTION

1.1 Fluid Dynamics

Fluid dynamics is categorized as the part of fluid mechanics that studies the causes and effects of the motion of fluid. Aerodynamics and hydrodynamics are the examples of several subdisciplines in fluid dynamics. Aerodynamics deals with the motion of air, particularly when it interacts with a solid object. Hydrodynamics concerned with studying the motion of liquids acting on solid body immersed in fluids.

1.1.1 Conservation laws

Fluid dynamics offers bountiful source of mathematical, experimental and computational challenges. Fluid dynamics aims to construct a mathematical theory of fluid motion, which govern by the conservation principles, specifically conservation of mass, conservation of momentum (also known as Newton's Second Law of Motion) and conservation of energy (also known as the First Law of Thermodynamics). These fundamental principles can be expressed in terms of mathematical equations. The applications of fluid dynamics are enormous including heating, ventilation, air conditioning systems, oil pipelines, aircraft designs and wind turbines.

1.2 Boundary Layer

The concept of boundary layer introduced by Ludwig Prandtl in a paper presented on August 12, 1904 at the Third International Congress of Mathematicians in Heidelberg, Germany is one of the cornerstones of modern fluid dynamics (Curle, 1962). The classical theories of inviscid flow assumed that the viscous forces in a fluid are small in comparison with the inertia forces. This would seem a reasonable assumption since the viscosity of many fluids is extremely low. However, Prandtl observed that the viscous forces can still be locally important in certain regions of flow. He remarked that as the fluid passed a surface of an object, the fluid which is immediately adjacent to the surface sticks to the surface due to the effect of friction. This creates a thin layer near the surface in which the velocity changes enormously from zero to the stream value away from the surface. This layer is referred to as the boundary layer in which the frictional effects are experienced. Prandtl simplified the equations of fluid flow by splitting the flow field into two regions. In the thin boundary layer, viscosity and the skin friction drag are dominant. Outside the boundary layer, the flow is inviscid. With the advent of the boundary layer concept, Prandtl showed that the Navier-Stokes equations can be significantly reduced to a simpler form. The application of boundary layer theory is mainly to the aerodynamics industries; designing special aircraft wing sections to avoid boundary layer separation.

1.3 Heat Transfer

Heat transfer refers to the exchange of thermal energy due to a temperature difference. It occurs from the part of high temperature to another part of lower temperature. Heat transfer changes the internal energy of both objects involved according to the first law of thermodynamics. Three primary modes of heat transfer are conduction, convection and radiation.

1.3.1 Conduction

Conduction can be described as the transfer of energy within an object or between objects that are in physical contact. It occurs in solid or fluid. Heat conduction also referred as a microscopic phenomenon in which the temperature gradient present in a stationary medium. Energy is transmitted through collisions between neighboring molecules, atoms and electrons. Here are some examples of the process of conduction:

- A metal spoon immersed in a cup of boiling liquid will eventually be warmed.
- The heat from a hot liquid makes the cup itself hot.
- The metal skillet or pot is heated by a stove burner. Heat will transfer from the stove burner to the skillet or pot.
- A light bulb that is turned on because electricity travels through the wires due to conduction of electricity.

1.3.2 Convection

Convection refers to the process of heat transfer through the collective movement of particles within fluids (liquids or gases). Unlike conduction, convection is a macroscopic phenomenon. The fluid particles themselves transit and carry energy from a high temperature area to a low temperature area. The direction of heat convection depends on the relative magnitude of the temperature of the fluid and the surface. Here are some examples of the process of convection:

- The metal pot that holds water is heated by a stove burner. As the pot becomes hot, the water at the bottom of the pot becomes warmer. Hot particles of water begin to rise to the top of the pot and cooler particles of water move down to replace it, causing a circular motion.
- The warm air rising from the radiator then falling back to the floor as cool air.
- A heater inside a hot air balloon heats the air and so the air moves upward. This causes the balloon to rise because the hot air gets trapped inside. When the pilot want to descend, he releases some of the hot air and cool air takes it place, causing the balloon to lower.

1.3.3 Radiation

Radiation can be described as the process of heat transfer by means of electromagnetic waves. It is generated by a direct result of the random movements of atoms and molecules in matter. All matter with a temperature greater than absolute zero emits thermal radiation. Here are some examples of thermal radiation:

- The sun radiates heat in all directions. The heat is transferred to the surface of the Earth through space between the Earth and the sun.
- A camp fire heats a person who sit in front of it.
- The visible light and infrared light emitted by an incandescent light bulb.
- A microwave oven emits thermal radiation to heat up food.

1.4 Types of Convection

Convection may occurs by density differences caused by temperature differences within fluid motion. This fluid motion is associated with the aggregates of a great number of molecules. Convection takes place by mainly two mechanisms, advection and diffusion. Advection is the energy transferred by the bulk or macroscopic motion of the fluid. Diffusion is the energy transfer due to random molecular motion. Convection can be classified in terms of being natural, forced or as a combination of both of them.

1.4.1 Natural Convection

Natural convection happens when the flow is induced by density differences caused by the temperature variations in the fluid. The fluid motion is not generated by any external induced flow. Buoyancy works as the driving force for natural convection. Examples of natural convection include:

- The air circulation of the oceans during days and nights.
- The rising plume of smoke from fire.
- Free air cooling of hot components of a circuit boards.
- The formation of micro structures during the cooling of molten metals.

1.4.2 Forced Convection

In contrast to natural convection, forced convection is a mechanism in which the fluid motion is generated by an external agent such as a fan, a pump, a blower or a suction device. Examples of forced convection flow can be found in:

- Centralized heating.
- Air conditioning.
- Steam turbines.
- Heat exchangers.

1.4.3 Mixed Convection

Mixed convection is a combination of forced and free convection to transfer heat. It occurs when both pressure forces and buoyant forces interact simultaneously. Examples of mixed convection flow can be found in:

- Nuclear reactor.
- Solar energy storage.
- Refrigeration devices.

1.4.4 Double Diffusive Convection

Double diffusive convection occurs when the fluid is subjected by two different density gradients, which have different rates of diffusion. The density variations may be triggered by gradients in the concentration of the fluid, or by differences in temperature. Temperature and concentration gradients can often diffuse with time, reducing their ability to drive the convection, and requiring that gradients in other regions of the flow exist in order for convection to continue. Examples of double diffusive convection can be found in:

- adding one tea spoon of sugar into a cup of hot coffee.
- oceanography: heat and salt concentrations exist with different gradients and diffuse at differing rates.
- geology: the layered convection exists in magma reservoirs from which pyroclastic flows are erupted.

1.5 Mass Transfer

Mass transfer takes place when there is a difference in the concentration of some chemical species in a mixture. A species concentration gradient in a mixture provides the driving potential for transport of that species. Mass transfer commonly involves diffusion. Mass diffusion occurs in liquids, solids and gases. However, since mass transfer is strongly influenced by molecular spacing, diffusion occurs more easily in gases than in liquids.

It also happens without difficulty in liquids than in solids. Examples of mass transfer process include:

- The evaporation of water from a pond to the atmosphere.
- the purification of blood in the kidneys and liver.
- The transfer of water vapor into dry air in home humidifier.
- The distillation of alcohol.

1.6 Nanofluid

The major use of conventional fluids, such as water, ethylene glycol and oil, is as a medium for convective heat transfer. However, they have lower ability to conduct heat compared to metals. Metals have thermal conductivities up to several times higher than these fluids. In order to produce an efficient medium for convective heat transfer that would maintained as fluid, but has the thermal conductivity of a metal, thus it is necessary to combine both fluids and metals. So there is a strong need to develop advanced heat transfer fluids with substantially higher conductivities to enhance thermal characteristics (Khan et al., 2013). Nanofluid consists of uniformly dispersed and suspended nanometer-scale solid particles into base fluid. Choi (1995) introduced the term nanofluid as reference to a liquid containing nanoparticles with average sizes below 100 nm. The nanoparticles are made of oxides, metals and carbides, nitride and even immiscible nanoscale liquid droplets. The shape of nanoparticles can be spherical, rod-like or tubular shapes and they can be dispersed individually. The common nanoparticles that have been used are aluminum, copper, iron and titanium or their oxides. For the base fluids, the commonly used fluids are water, ethylene glycol and oils.

Nanofluid is said to differ from the conventional fluid because of the following reasons:

- It possesses high specific surface area and therefore more heat transfer surface between particles and fluids.
- It reduced particle clogging as compared to conventional slurries, thus promoting system miniaturization.

- It has adjustable properties, including thermal conductivity and surface wettability, by varying particle concentrations to suit different applications.

Nanofluids may be used in a wide variety of industries, ranging from transportation to energy production, in electronics systems, as well as in the field of biotechnology. The following examples show that how nanotechnology can be integrated into each of these industrial areas:

- engine cooling.
- electronic cooling.
- nuclear systems cooling.
- biomedical applications.
- refrigeration (domestic refrigerators and chillers).
- drag reductions.

1.7 Research Objectives

This study embarks on the following objectives:

1. To formulate mathematical models for convective flow, heat (and mass) transfer of nanofluid under the influence of various effects.
2. To develop numerical algorithm for solving the model problems.
3. To investigate the influences of thermal radiation, heat generation/absorption, chemical reaction and suction on convective heat transfer of nanofluid along a wedge.
4. To investigate the Soret and Dufour effects on double diffusive convective flow of nanofluid over a moving wedge in the presence of suction, .
5. To investigate the effects of thermal radiation, Soret and Dufour on mixed convective flow of nanofluid over a wedge with power law variation in surface temperature and species concentration.

1.8 Thesis Organization

This thesis is organized into 9 chapters. Starting with a general introduction to fluid dynamics, Chapter 1 evolves through boundary layer, heat transfer and mass transfer. The chapter then stated the objectives of the study.

Reviews of past research works on wedge flow of nanofluid with various effects are given in Chapter 2. From the review, it is revealed that a significant scope exists to investigate the convective heat and mass transfer of nanofluid along a wedge.

From the descriptions of the mathematical modeling on the convective boundary layer flow of nanofluid over a wedge, the governing equations of the problem are given in Chapter 3. A detailed explanations on similarity transformations is also included. As part of this research, a numerical routine is presented in order to solve the equations.

Chapters 4 through 8, respectively, deal with 6 different research problems. Chapter 4 consists of two research problems. In the first problem, the convective flow and heat transfer of heat generating nanofluid over a wedge with suction/injection are analyzed. The second problem of Chapter 4 presents the convective flow and heat transfer of heat generating nanofluid over a wedge with suction and thermal radiation. The convective flow and heat transfer of heat generating nanofluid over a wedge with suction and chemical reaction are analyzed in Chapter 5. Chapter 6 presents the double diffusive convective flow of nanofluid over a moving wedge with suction, Soret and Dufour effects. Chapter 7 focuses on the double diffusive convective flow of nanofluid over a wedge with suction, thermal radiation, Soret and Dufour effects. Chapter 8 discusses the double diffusive convective flow of nanofluid over a wedge with power law variation in surface temperature in the presence of suction, thermal radiation, Soret and Dufour effects.

The conclusion and recommendations for future work are given in Chapter 9.

CHAPTER 2: LITERATURE SURVEY

Numerous studies have been conducted on various convective boundary layer flow phenomena past different types of geometries. One of the most frequently studied is the wedge flows. Fig. 2.1 shows the configurations of the horizontal and vertical wedge. The horizontal flow circumstance is the one in which the plane of the wedge is aligned with the free stream velocity, U as shown in Fig. 2.1(a). The vertical wedge in Figs. 2.1(b) and 2.1(c) show that the flow moves parallel to the axis of the wedge in the downward and upward directions, respectively, with free stream velocity. In addition, the buoyancy forces aid or oppose the development of the boundary layer flow, depending on the orientation of the wedge. The wedge angle is denoted by $\Omega = \beta\pi$, where β is the Hartree pressure gradient. Jaluria (1980) stated that the wedge geometry comprises a few practical circumstances such as stagnation point flow and the flow over horizontal surfaces. The case of $\beta = 0$ corresponds to the horizontal plate as shown in the Fig. 2.2(a). Meanwhile, Fig. 2.2(b) shows the vertical plate case for $\beta = 1$. The latter case is also known as stagnation point flow.

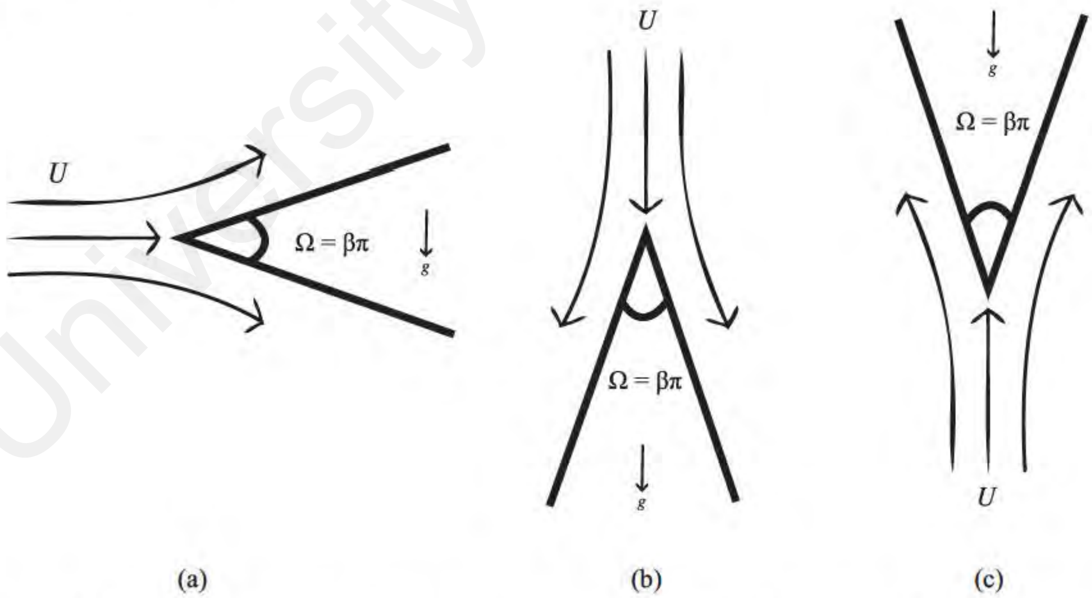

Figure 2.1: The (a) horizontal wedge; (b) vertical wedge downward flow; (c) vertical wedge upward flow configurations

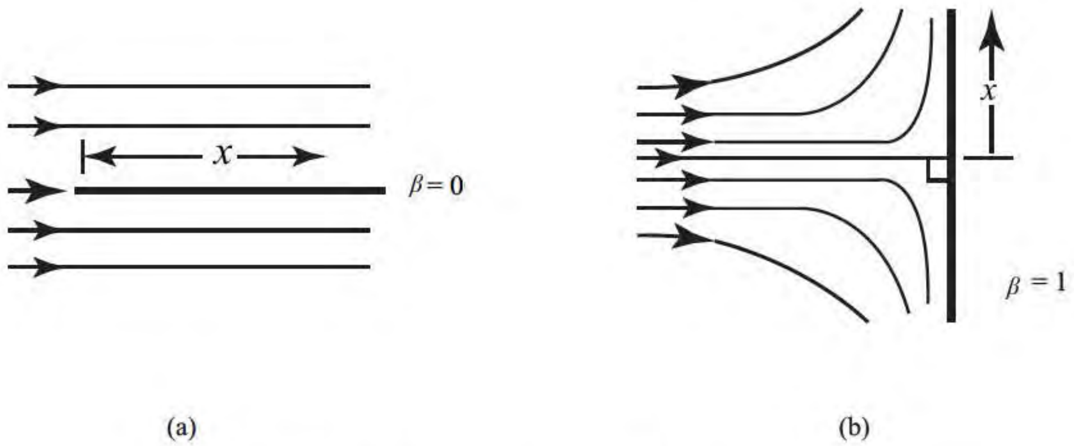

Figure 2.2: The (a) horizontal plate; (b) stagnation point flow

2.1 Boundary Layer Flow over a Wedge

The wedge flows are also called the Falkner and Skan flows after the authors who first published their boundary layer solutions. Falkner & Skan (1931) introduced the velocity gradient which occurs in two-dimensional potential flow between two straight walls meeting at an angle. The authors considered that the velocity of the free stream (inviscid flow) in the x direction is $U = U_\infty x^m$ where U_∞ and m are constants. The index m is a wedge angle parameter and m is a function of β such that $m = \beta/(2-\beta)$. Based on these considerations, they gave the general form of the boundary layer equations and obtained the approximate solutions by applying two-step numerical procedures. Its similar solution was later studied by Hartree (1937) using the differential analyzer. Schuh (1947) employed the exact velocity distributions of Hartree (1937) for the constant property values when $\mathrm{Pr} = 0.7$. The heat produced by friction and compression were neglected in Schuh (1947) and Falkner & Skan (1931), but, partially accounted in the work of Levy (1952), who investigated the heat transfer and laminar boundary layer flow over the wedge with power-law variation in surface temperature. A comprehensive study on the Falkner-Skan solutions has been carried out by Stewartson (1954). He figured out that there exists a further solution within the region of pressure gradient, $-0.199 < \beta < 0$ and the velocity profile demonstrates the back flows. A detailed discussion on the solutions with back flow for $\beta \to 0$ can be found in the work by Brown & Stewartson (1966) and Libby & Li (1967). Stewart & Prober (1962) investigated the heat and mass transfer along a wedge. They obtained the boundary layer solutions for the flow of binary constant-property mixtures over plane and wedge by using direct or inverse interpolation of the tabulated solutions. The exact numerical solutions are also given in this paper for the Prandtl and Schmidt numbers from 0.1 to 10. Later, Prober & Stewart (1963) studied the heat and mass transfer along a wedge by using the perturbation method. Gunness & Gebhart (1965) considered the simultaneous phenomena of forced and natural convective flow over an isothermal wedge. The numerical results are obtained for surface shear and heat-transfer rates with different values of wedge angle when $\mathrm{Pr} = 0.7$. The effect of changing surface heat flux on convective boundary layer flow over a wedge was studied by Chen & Chao (1970). They restricted their investigation to the determination of the entire time-history of the heat transfer process in Falkner-Skan flow subsequent to a step change in the wedge's surface temperature or heat flux. Chao & Cheema (1971) examined the steady forced convection past a wedge with a step discontinuity in temperature. They obtained a solution which describes the arbitrary variations of surface temperature. Drake & Riley (1975), Chen & Radulovic (1973) and Jeng et al. (1978) used the solution method introduced by Chao & Cheema (1971) for solving the convective heat transfer with non-isothermal surfaces. Drake & Riley (1975) provided an extension to the results of Chao & Cheema (1971) for small Prandtl number. Chen & Radulovic (1973) focused on the analytical solution of laminar boundary layer flow of power law fluids past a wedge. Jeng et al. (1978) generalized the work by Chao & Cheema (1971) by handling the axis-symmetric boundary layer flows. Later, Unsworth & Chiam (1980) adopted the same mathematical formulation as Drake & Riley (1975) for various values of Prandtl numbers ranging from 0.001 to 20000.

An approximate solution of the impulsive motion of a wedge in viscous fluid was obtained by Smith (1967) by using the momentum integral method. However, Nanbu (1971) claimed that Smith (1967) gave a very strange result that the time required for the unsteady boundary layer to settle into its steady state tends to infinity as the wedge angle tends to π. Thus, Nanbu (1971) solved the same problem with some improved aspects by the finite difference method where the effect of pressure gradient of the boundary layer was clarified. Watkins (1976) extended the previous works of Smith (1967) and Nanbu (1971) by considering the unsteady heat transfer in impulsive Falkner-Skan flows past a semi-infinite wedge. King & Varwig (1971) presented an analytical study of the hypersonic boundary layer over a wedge with uniform blowing and viscous interaction. They found that the effect of viscous interaction dominates the flow when the interaction is strong and the effects of blowing become more important as the strength of the viscous interaction decreases. Olsson (1973) used an integral method to solve the problem of heat transfer from a finite wedge-shaped fin with limited heat conductivity. The solution of Falkner-Skan equation for a wide range of Prandtl numbers was studied by Lin & Lin (1987). In addition, the asymptotic approach for heat transfer of boundary layer flow past a wedge for small Prandtl numbers was studied by a number of authors (Chen (1985), Chen (1986) and Herwig (1987)).

2.2 Boundary Layer Flow of Nanofluid over a Wedge

Fluid flow and heat transfer characteristics of nanofluid have received considerable attention due to wide range of engineering applications such as in engine cooling, solar water heating, cooling of electronics, cooling of transformer oil, improving diesel generator efficiency, cooling of heat exchanging devices, improving heat transfer efficiency of chillers, domestic refrigerator-freezers, cooling in machining, in nuclear reactor and defense (Das et al., 2007). Nanofluid is a dispersion of metallic or non-metallic nanometer-sized particles in a liquid resulting in the modification of the carrier fluid properties such as thermal conductivity, viscosity, density, and heat transfer capability. Undoubtedly, nanofluids exhibit some unique features that are quite different from conventional colloidal suspensions. The work of Choi (1995) was one of the first attempts to study the enhancement of thermal conductivity of fluids with nanoparticles. They performed experiments and found that nanofluids are expected to exhibit high thermal conductivities compared to conventional fluids. Numerous studies have been conducted afterward concerning on mathematical and numerical modeling of convective heat transfer in nanofluid, for example, Tiwari & Das (2007) and Buongiorno (2006). The former approach analyzes the behaviour of nanofluids taking into account the solid volume fraction of the nanofluid. On the other hand, Buongiorno (2006) stated that nanoparticles absolute velocity can be viewed as the sum of the base fluid velocity and a slip velocity, with total of seven slip mechanisms involved: inertia, Brownian diffusion, thermophoresis, diffusiophoresis, Magnus effect, fluid drainage and gravity. He indicated from those seven that only Brownian diffusion and thermophoresis are important slip mechanisms in nanofluids. Based on this finding, he developed a mathematical nanofluid model by taking into account the Brownian motion and thermophoresis effects on flow and heat transfer fields.

Many researchers have employed numerical techniques to explore the convective heat transfer of nanofluids over a wedge by using the model proposed by Tiwari & Das (2007). Yacob et al. (2011a) used an implicit finite difference scheme known as the Keller-box method to solve the Falkner-Skan equation for a static or moving wedge in nanofluids with prescribed surface heat flux. Later, Yacob et al. (2011b) investigated the same problem but excluded the surface heat flux effect. Both Yacob et al. (2011a) and Yacob et al. (2011b) considered three different types of nanofluids, namely copper (Cu), alumina (Al_2O_3) and titanium dioxide (TiO_2) with water as the base fluid. Their results revealed that the skin friction coefficient and the heat transfer rates are highest for copper-water nanofluids compared to alumina-water and titanium-water nanofluids. Salem et al. (2014) investigated the numerical solutions for hydromagnetic flow over a moving wedge in Cu-water nanofluid with viscous dissipation. They found that the temperature of the fluid increases on increasing the magnetic field and viscous dissipation parameters. Rahman et al. (2012) investigated the hydromagnetic slip flow of water based nanofluids past a wedge with convective surface in the presence of heat generation or absorption. Their results indicated that the velocity increases with the increase of the Biot number, wedge angle, thermal buoyancy, slip, magnetic field and heat generation parameters. In addition, Rahman et al. (2012) concluded that the rate of heat transfer in the Cu-water nanofluid is found to be higher than the rate of heat transfer in the TiO_2-water and Al_2O_3-water nanofluids. Detailed numerical studies on the Hiemenz flow of Cu-water nanofluid over a wedge embedded in a porous medium with thermal radiation and suction or injection had been carried out by Raman et al. (2014), Kandasamy et al. (2012), Kandasamy et al. (2013) and Mohamad et al. (2013). Kandasamy et al. (2012) also considered the influence of thermal stratification at the boundary condition in their study. Meanwhile, both Kandasamy et al. (2013) and Mohamad et al. (2013) performed numerical studies on the unsteady flow. Unsteady MHD non-Darcy Cu-water nanofluid flow along a wedge embedded in a porous medium was reported by Kandasamy et al. (2014). They found out that the temperature of the nanofluid increases with the increase of unsteadiness parameter. Su & Zheng (2013) investigated the Hall effect on MHD flow and heat transfer of nanofluids over a stretching wedge in the presence of velocity slip and Joule heating. They analyzed four different types of water-base nanofluids containing copper (Cu), silver (Ag), alumina (Al_2O_3), and titania (TiO_2) nanoparticles. They found that an increase in nanoparticle volume fraction leads to an increase in the fluid temperature. Kameswaran et al. (2014) conducted a study of combined heat and mass transfer over an isothermal wedge immersed in nanofluid. They compared two types of nanofluids, Ag-water and Au-water nanofluids. They observed that the skin friction and heat transfer rates are more enhanced in the case of gold nanoparticles compared with silver nanoparticles.

Many research works have been performed on convective flow and heat transfer over a wedge by employing the nanofluid model proposed by Buongiorno (2006). The numerical solutions of the mixed convective boundary layer flow of nanofluid over a vertical wedge embedded in a porous medium, can be found in the work by Gorla et al. (2011), Chamkha et al. (2012), Chamkha et al. (2014) and James et al. (2015). The results obtained in Gorla et al. (2011) showed that the Nusselt number decreases on increasing the value of thermophoresis and Brownian motion parameters. Chamkha et al. (2012) and Chamkha et al. (2014) provide extension work of Gorla et al. (2011) for thermal radiation effect and non-Newtonian base fluid, respectively. Chamkha et al. (2012) found that the local Nusselt number increases when either buoyancy ratio, or the Brownian motion, or the thermophoresis, or the radiation–conduction or Lewis number increases. Chamkha et al. (2014) used power law fluid or also known as the Ostwald-de Waele fluid to describe the behaviour of non-Newtonian fluid. James et al. (2015) investigated the influence of thermal radiation, chemical reaction, variable viscosity and suction of nanofluid flow over a permeable wedge embedded in saturated porous medium. They concluded that the nanoparticle volume fraction thickness decreases with the increase of chemical reaction parameter and Lewis number. Khan & Pop (2013) investigated the boundary layer flow of nanofluid past a moving wedge. They found that the temperature of nanofluid increases when increasing both Brownian motion and thermophoresis parameters. Chamkha &

Rashad (2014) studied the MHD forced convection flow of a nanofluid adjacent to a non-isothermal wedge. The results indicated that owing to the presence of the Brownian motion and the thermophoresis effects, the local Nusselt number decreases while the local Sherwood number increases. Khan et al. (2014) numerically analyzed the MHD boundary layer flow of nanofluid past a wedge in the presence of thermal radiation, heat generation and chemical reaction. Their results indicated that the nanoparticle volume fraction increases on increasing the heat generation and chemical reaction parameters.

2.3 Boundary Layer Flow over a Moving Wedge

A milestone contribution in wedge flow was made by Falkner & Skan (1931) who first published their boundary layer solutions. Since then, the boundary layer flow and heat transfer along a wedge has been theoretically developed. However, the abundant literature on the boundary layer flow over a wedge is limited to static wedge and little attention was given to moving ones. Boundary layer separation can be prevented by moving the wedge wall in the flow direction. A moving wall could remove the existence of the velocity difference between the wall and the outer flow.

Riley & Wiedman (1989) studied the effect of moving boundary of the Falkner-Skan flow in a viscous fluid. They obtained multiple solutions for various values of wedge angle parameter. Ishak et al. (2007) extended the paper by Riley & Wiedman (1989) to the case when the walls of the moving wedge are permeable with suction and injection effects. The results reported were consistent with those found by Riley & Wiedman (1989). There have been several studies on boundary layer flow of non-Newtonian fluid over a moving wedge, for example: Ishak et al. (2006), Ishak et al. (2011), Akçay & Yükselen (2011) and Postelnicu & Pop (2011). All of these investigations have demonstrated that the non-Newtonian fluids display a drag reduction compared to Newtonian fluids. Butt & Ali (2013) considered the convective flow and heat transfer past a static and moving wedge. They figured out that when the wedge and fluid are moving in opposite directions, the momentum boundary layer is thicker than the case when the fluid and the wedge are moving in same direction. Ahmad & Khan (2013) analyzed the heat transfer of a viscous fluid with the effect of heat generation/absorption and viscous dissipation over a moving wedge with convective boundary condition in the presence of suction and injection. It is shown that the dimensionless velocity and temperature depend upon the stretching/shrinking, suction/injection, and pressure gradient parameters. The study of MHD laminar boundary layer flow past a moving wedge was considered by Jafar et al. (2013) and Ahmad & Khan (2014). Jafar et al. (2013) focused on the parallel free stream of an electrically conducting fluid with the induced magnetic field. Meanwhile, Ahmad & Khan (2014) examined the combined effects of heat and mass transfer of MHD flow over a moving wedge with viscous dissipation, heat source/sink and convection boundary condition.

2.4 Boundary Layer Flow over a Wedge with Suction/Injection

Suction and injection (blowing) are known as the useful techniques to prevent boundary layer separation. Schlichting & Gersten (2000) mentioned that the separation of the boundary layer is generally undesirable since it leads to great losses of energy. The wall of the wedge is assumed to be permeable, so that fluid can be sucked or blown through the narrow slits on the wall. Separation can be almost completely prevented by this continuous suction or injection because the boundary layer can be given enough kinetic energy.

Investigation on boundary layer fluid flows along a wedge with suction or injection has increased and has been widely emphasized. The effect of injection/suction on the velocity and temperature distributions within the boundary layer has important applications in engineering processes such as the design of the thrust bearings, the entrance region of the pipe flow and the reduction of the drag force. Watanabe (1990) investigated the behaviour of incompressible laminar boundary layer in forced flow over a wedge with uniform suction or injection. It is found that the velocity distributions become thick and temperature distributions become thin, as the suction/injection parameter is increased. Later, Watanabe et al. (1994) investigated the mixed convection boundary layer flow over a wedge in the presence of suction and injection. Their results indicated that the skin friction and heat transfer rate increase on decreasing the buoyancy parameter. Kafoussias & Nanousis (1997) considered the MHD laminar boundary layer flow over a wedge with suction or injection. They obtained that the velocity profile increases on increasing the suction parameter. Nanousis (1999) extended the previous work of Kafoussias & Nanousis (1997) by considering the mixed convection flow. He indicated that the fluid velocity increases as the value of the buoyancy parameter increases. Yih (1998) studied the forced convection with uniform heat flux in the presence of suction or injection. The results indicated that the local skin friction coefficient and the local Nusselt number increase owing to suction of fluid. This trend reversed for blowing of the fluid. Kumari (1998) examined the effect of large blowing rates on the unsteady conducting fluid flow over an infinite wedge with magnetic field. The author concluded that the boundary layer thickness increases on increasing the blowing rate and magnetic parameter. Meanwhile, Hossain et al. (2000) investigated the effects of temperature dependent viscosity and thermal conductivity on forced convective flow with surface heat flux and suction. They concluded that both the local skin-friction coefficient and local Nusselt number increase as suction parameter increases. Kumari et al. (2001) investigated the MHD mixed convection flow over a vertical wedge embedded in a porous medium with suction or injection. They found that both the skin friction coefficient and heat transfer rate increase with suction. The mixed convection flow over a vertical wedge was considered by Singh et al. (2009). A detailed analytical solution of heat transfer and boundary layer flow over a wedge with suction or injection by using Gyarmati's variational technique can be found in Chandrasekar (2003). Later, Chandrasekar & Baskaran (2008) and Chandrasekar & Shanmugapriya (2008) provide the extension work of Chandrasekar (2003) for MHD flow and mixed convection flow, respectively. Meanwhile, Yao (2009) obtained the analytical solutions of Falkner-Skan problem with suction by using the Homotopy analysis method. In addition, further solutions of the boundary layer flow of a second grade fluid over a wedge with suction or injection, can be found in the works by Massoudi & Ramezan (1989), Hsu et al. (1997) and Hsiao (2011).

2.5 Boundary Layer Flow over a Wedge with Chemical Reaction

Chemical reactions are classified into two categories; viz., homogeneous reaction, which involves only single phase reaction and heterogeneous reaction, which involves two or more phases and occur at the interface between fluid and solid or between two fluids separated by an interface. The important applications of homogeneous reactions are the combination of common household gas and oxygen to produce a flame and the reactions between aqueous solutions of acids and bases. Thamelis (1995) stated that the majority of chemical reactions encountered in applications are first-order and heterogeneous reactions such as hydrolysis of methyl acetate in the presence of mineral acids and inversion of cane sugar in the presence of mineral acids. A chemical reaction is said to be first-order when a reaction rate depends on a single substance and the value of the exponent is one. Midya (2012) observed from their study that the first-order chemical reaction is very important in chemical engineering where the chemical reactions take place between a foreign mass and the working fluid.

There are comparatively a few studies on the wedge flow in the presence of chemical reaction. Kandasamy et al. (2005) studied the effect of chemical reaction on heat and mass transfer along a wedge with heat source, suction and injection. They concluded that the increase of chemical reaction decelerates the fluid motion, temperature distribution and concentration of the fluid along the wall of the wedge, due to the uniform suction and heat source. Kandasamy & Palanimani (2007) obtained numerical solutions of heat and mass transfer on MHD flow over a wedge embedded in a porous medium with chemical reaction. Kandasamy et al. (2008) considered the thermophoresis and chemical reaction effects on non-Darcy mixed convective heat and mass transfer past a porous wedge with variable viscosity in the presence of suction or injection. They found that the skin friction, heat and mass rates decrease with the increase of Forchheimer number, thermophoresis and chemical reaction parameters. Later, Muhaimin et al. (2009) extended the work of Kandasamy et al. (2008) by considering the influence of magnetic field. They indicated that the velocity of the fluid increases on increasing the strength of magnetic field. Ganapathirao et al. (2013) investigated the non-uniform slot suction/injection on unsteady mixed convection flow over a wedge with chemical reaction and heat generation/absorption. Deka & Sharma (2013) used Falkner-Skan transformations to solve MHD mixed convection flow past a wedge under variable temperature and chemical reaction. The unsteady mixed convection flow past a wedge in the presence of chemical reaction, heat generation/absorption and suction/injection was carried out by Ganapathirao et al. (2015). They found that the local skin friction coefficient increases with the increase of buoyancy ratio parameter for an accelerating flow. Loganathan et al. (2010) used the local non-similarity transformation for solving the MHD mixed convection, heat and mass transfer over a wedge embedded in a porous medium. They incorporated the effects of chemical reaction and suction or injection. Their results indicated that the velocity and concentration of the fluid decrease with the increase of chemical reaction parameter and Schmidt number.

2.6 Boundary Layer Flow over a Wedge with Radiation

It is well known that thermal radiation changes the temperature distribution by playing a role like controlling heat transfer process such as in polymer processing and nuclear reactor cooling system. Ahmed et al. (2014) stated that the role of thermal radiation is of major importance in the designing of many advanced energy convection systems operating at high temperature. Bhuvaneswari et al. (2012) mentioned that the study of convective heat transfer in the presence of thermal radiation has attracted many investigators over the past few decades due to its wide range of applications in the petroleum industry, geothermal problems and boundary layer control in aerodynamics. Thus, a significant amount of research has been carried out to study the effect of thermal radiation on convective flow.

Yih (2001) investigated the effect of thermal radiation on mixed-convection flow over an isothermal wedge embedded in a saturated porous medium. The results indicated that the local Nusselt number increases on increasing the wedge angle and radiation parameters. The effect of radiation on convective flow and heat transfer over a wedge with variable viscosity was studied by Elbashbeshy & Dimian (2002). It is shown that increasing both the viscosity and radiation parameters tend to enhance the local Nusselt number and local skin friction coefficient. Chamkha et al. (2003) studied the influence of thermal radiation on MHD forced convection flow over a non-isothermal wedge in the presence of heat generation or absorption. They found that the local Nusselt number decreases on increasing the thermal radiation parameter. Mukhopadhyay (2009) examined the effects of temperature-dependent viscosity and thermal radiation along a symmetric wedge. The results indicated that the temperature decreases with increasing the value of radiation parameter and Prandtl number. Pal & Mondal (2009) extended the previous work of Mukhopadhyay (2009) by considering the MHD forced convection over a non-isothermal wedge. The effects of viscous dissipation, Joule heating, stress work, heat generation/absorption and suction/injection were also included. Their results indicated that the temperature increases on increasing the thermal radiation and magnetic parameters. Su et al. (2012) presented the analytical solutions of the influence of thermal radiation and ohmic heating on MHD heat and mass transfer over a permeable stretching wedge. Rashidi et al. (2014) studied the effect of thermal radiation on MHD mixed convective heat transfer of a viscoelastic fluid flow over a porous wedge. They found that increasing the thermal radiation parameter reduces the heat transfer coefficient between the wedge and the fluid.

2.7 Boundary Layer Flow over a Wedge with Heat Generation or Absorption

Heat generation or absorption in boundary layer flow is very important because it may change the temperature distribution. The investigation on boundary layer flow with heat generation or absorption has considerable practical applications related to nuclear reactor cores, fibre and combustion modeling, electronic chips and semi-conductor wafers. Thus, there are many remarkable works have been done to reveal the effect of heat generation or absorption in boundary layer flow along a wedge.

Chamkha et al. (2000) investigated the MHD natural convection of heat and mass transfer over a vertical wedge embedded in a porous medium with heat generation or absorption. They considered two cases of thermal boundary conditions, namely the uniform wall temperature and the uniform wall heat flux. They concluded that the Nusselt number increases on increasing the absorption parameter for both cases. Rashad & Bakier (2009) studied the MHD convective forced flow and heat transfer of heat generating fluid past a wedge embedded in a non-Darcy porous medium with uniform surface heat flux. They found that the Nusselt number and the skin friction coefficient are significantly affected by the porosity and heat generation/absorption parameters. Salem (2010) considered the effect of temperature-dependent viscosity on free convective boundary layer flow and heat transfer over a vertical wedge in a non-Darcy porous medium with heat generation or absorption. The results showed that the velocity and temperature of the fluid decrease on increasing the heat absorption parameter. Ashwini & Eswara (2012) examined the MHD Falkner-Skan boundary layer flow with internal heat generation or absorption and figured out that the effect of heat generation or absorption is found to be very significant on heat transfer, but its effect on the skin friction is negligible. The influence of heat generation or absorption on the non-linear slip flow and heat transfer over a wedge with temperature dependent was studied by Rahman & Al-Hadhrami (2013). Prasad et al. (2013) obtained the numerical solutions on MHD mixed convection flow over a permeable non-isothermal wedge by using the implicit finite difference scheme. They also include the effects of viscous dissipation, internal heat generation/absorption, thermal radiation, Joule heating and stress work. They observed that the temperature distribution decreases on increasing the heat sink parameter while a reversed trend is obtained for the heat source.

2.8 Boundary Layer Flow over a Wedge with Soret and Dufour Effects

The Dufour or diffusion-thermal effect is the contribution to the thermal energy flux due to concentration gradients. On the other hand, Soret or thermo-diffusion effect is referred as the diffusion of mass due to temperature gradient. Soret and Dufour effects are very important where more than one chemical species is present under a large temperature gradient. These effects have many applications such as semiconductor wafer, electrostatic precipitators, manufacturing of optical fiber and drug discovery. Cheng (2012) investigated the Soret and Dufour effects on mixed convection, heat and mass transfer over a downward-pointing vertical wedge embedded in a porous medium with constant wall temperature and concentration. The results showed that the local Nusselt number decreases while the local Sherwood number slightly increases on increasing the values of the Dufour parameter. Meanwhile, an increase in the Soret number tends to decrease the local Sherwood number. Pal & Mondal (2013) investigated the influences of thermophoresis, Soret and Dufour on MHD heat and mass transfer over a non-isothermal wedge with thermal radiation and Ohmic dissipation. They observed that the concentration profile increases on increasing the Soret parameter while a reverse trend is observed for temperature. The temperature increases and the concentration decreases on increasing the Dufour parameter.

CHAPTER 3: MATHEMATICAL FORMULATION

3.1 Introduction

In this chapter, an overview of the governing equations of the nanofluid flow within the boundary layer is given. The similarity and local similarity solutions to the momentum, thermal, concentration and nanoparticle volume fraction equations are thoroughly explained. The local skin friction, Nusselt number and Sherwood number are then discussed. The numerical solutions using the fourth-order Runge-Kutta-Gill method along with the shooting technique and Newton Raphson method are explained in detail.

3.2 The Boundary Layer Flow Model

Mathematical modeling of fluid flow is based on the partial differential equations which govern the physical behaviour of the flows. These governing equations represent mathematical statements of the related conservation law of physics. The physical laws which govern the boundary layer flow under the influence of specified forces are as follows:

1. Based on the conservation of mass, the mass of a fluid is conserved across the entire domain.
2. Based on the Newton's second law of motion, the rate of change of momentum equals the sum of the forces on a fluid particle.
3. Based on the the first law of thermodynamics, the rate of change of energy is equal to the sum of the rate of heat addition to and the rate of work done on a fluid particle.

In addition to the statements above, in the present study, it is necessary to include the assumptions of nanofluid that describe the constitutive behaviour of the fluid. The nanofluid is a dilute solid-liquid mixture with a uniform volume fraction of nanoparticles dispersed within the base liquid. Following the nanofluid model proposed by Buongiorno (2006), the assumptions are as follows:

1. The fluid is incompressible.

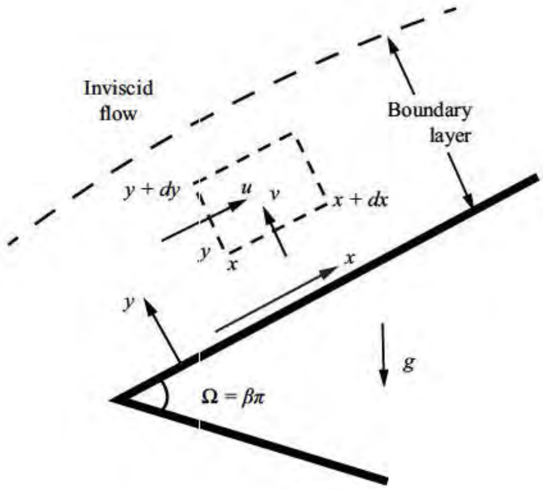

Figure 3.1: A small volume element in the boundary layer region

2. There are no chemical reactions. The nanoparticles are chosen for their chemical inertness with the base fluid.

3. There are no external forces. The nanoparticles are carried by the turbulent eddies and other diffusion mechanisms are negligible.

4. The base liquid and nanoparticles are in thermal equilibrium. This situation showed that as the nanoparticles move in the surrounding fluid, they achieved thermal equilibrium with it very rapidly.

5. There is no slip at the wall.

6. There is no energy dissipation in the boundary layer.

Thus, with all these assumptions, the governing equations of the present problem can be derived.

3.2.1 The Continuity Equation

The continuity equation is the mathematical representation which states about the conservation of mass. It expresses the fact that, the rate of increase of mass in fluid element equals the net rate of flow of mass into fluid element. Consider a small volume element of fluid located at the point (x, y) in the boundary layer as shown in Fig. 3.1. If ρ is the fluid density, the amount of fluid flowing in the x-direction through the face of element located at x is $\rho u \, dy$, and the amount flowing through the opposite face located at $(x + dx)$ is

$$\left[\rho u + \frac{\partial}{\partial x}(\rho u)dx\right] dy. \tag{3.1}$$

Therefore, the amount of fluid leaving the element in the x-direction per unit volume is $(\partial/\partial x)(\rho u)$. Similarly, for the y-direction is

$$\left[\rho v + \frac{\partial}{\partial y}(\rho v)dy\right] dx, \tag{3.2}$$

where the amount of fluid leaving the element in the y-direction per unit volume is $(\partial/\partial y)(\rho v)$. In the steady state, the amount of fluid leaving the volume element per unit volume is zero. Thus,

$$\frac{\partial}{\partial x}(\rho u) + \frac{\partial}{\partial y}(\rho v) = 0. \tag{3.3}$$

When the density ρ is uniform, it can be taken outside and we obtain

$$\frac{\partial u}{\partial x} + \frac{\partial v}{\partial y} = 0. \tag{3.4}$$

3.2.2 The Momentum Equation

The momentum equation is based on the basic law of mechanics (Newton's second law). The law states that the rate of change of the momentum of the fluid element is equal to the external force exerted on the element and is in the direction of that force. Following Buongiorno (2006), the momentum equation for the nanofluid with negligible external forces is

$$\rho\left[\frac{\partial \mathbf{v}}{\partial t} + \mathbf{v}\cdot\nabla\mathbf{v}\right] = -\nabla P - \nabla\cdot\tau^*, \tag{3.5}$$

where $\mathbf{v}$ is the nanofluid velocity, t is time and P is the pressure. The stress tensor, τ^* can be expanded by assuming Newtonian behaviour and incompressible flow:

$$\tau^* = -\mu\left[\nabla\mathbf{v} + (\nabla\mathbf{v})^T\right], \tag{3.6}$$

where μ is the coefficient of the viscosity of the fluid and the superscript T indicates the transpose of $\nabla\mathbf{v}$. For a steady flow, we have $\partial u/\partial t = 0$ and by definition, $\partial x/\partial t = u$ and

$\partial y/\partial t = v$, Eq. 3.5 becomes

$$\rho u\frac{\partial u}{\partial x} + \rho v\frac{\partial u}{\partial y} = -\frac{dp}{dx} + \mu\frac{\partial^2 u}{\partial y^2}. \tag{3.7}$$

At the beginning of the mainstream, the total pressure force acting on the fluid element per unit volume is therefore can be written as

$$-\frac{dp}{dx} = \rho U\frac{dU}{dx}, \tag{3.8}$$

where U is the free stream velocity. Applying Eq. 3.8 in Eq. 3.7, the momentum equation which will be used later

$$u\frac{\partial u}{\partial x} + v\frac{\partial u}{\partial y} = U\frac{dU}{dx} + \nu\frac{\partial^2 u}{\partial y^2}, \tag{3.9}$$

where $\nu = \mu/\rho$ is the kinematic viscosity of the fluid.

3.2.3 The Nanoparticle Volume Fraction Equation

It is important to add the continuity equation for the nanoparticles in the present problem because the fluid around the nanoparticles can be regarded as a continuum. The nanoparticle absolute velocity can be viewed as the sum of the base fluid velocity and a relative (slip) velocity. Buongiorno (2006) stated that the Brownian diffusion and thermophoresis are considered as the slip mechanisms. Thus, the nanoparticle volume fraction can be written as

$$\frac{\partial S}{\partial t} + \mathbf{v}\cdot\nabla S = -\frac{1}{\rho_p}\nabla\cdot\mathbf{j}_p, \tag{3.10}$$

where S is the nanoparticle volume fraction and $\mathbf{j}_p$ is the nanoparticle mass flux which can be expressed as

$$\mathbf{j}_p = \mathbf{j}_{p,B} + \mathbf{j}_{p,T} = -\rho_p D_B \nabla S - \rho_p D_T \frac{\nabla T}{T}, \tag{3.11}$$

where ρ_p is nanoparticle density, T is temperature, $\mathbf{j}_{p,B}$ and $\mathbf{j}_{p,T}$ are the nanoparticle mass flux due to Brownian diffusion and thermophoretic effect, respectively. $D_B = k_B T/3\pi\mu d_p$ is the Brownian diffusion coefficient, which is given by the Einstein-Stokes's equation, where k_B is the Boltzmann's constant and d_p is the nanoparticle diameter. $D_T = \beta^*\mu C/\rho$

is the thermophoretic diffusion coefficient where $\beta^* = 0.26k_f/(2k_f + k_p)$ is the thermophoretic coefficient with k_f and k_p are the thermal conductivity of the base fluid and nanoparticle, respectively. A detailed explanation and derivation of $\mathbf{j}_{p,B}$ and $\mathbf{j}_{p,T}$ can be found in Buongiorno (2006). Substituting Eq. 3.11 in Eq. 3.10 yield

$$\frac{\partial S}{\partial t} + \mathbf{v} \cdot \nabla S = \nabla \cdot \left[D_B \nabla S + D_T \frac{\nabla T}{T} \right]. \tag{3.12}$$

Eq. 3.12 states that the nanoparticles can move homogeneously with the fluid, but they also possess a slip velocity relatively to the fluid which is due to Brownian diffusion and thermophoresis. For a steady state condition, Eq. 3.12 becomes

$$u\frac{\partial S}{\partial x} + v\frac{\partial S}{\partial y} = D_B \frac{\partial^2 S}{\partial y^2} + \left(\frac{D_T}{T_\infty}\right) \frac{\partial^2 T}{\partial y^2}, \tag{3.13}$$

where D_B and D_T are the Brownian diffusion coefficient and thermophoretic diffusion coefficient, respectively.

3.2.4 The Thermal Energy Equation

The thermal energy equation is a statement about the first law of thermodynamics. It expresses the fact that the rate of change of the thermal energy of the volume element per unit volume. Following Buongiorno (2006), the thermal energy equation for the nanofluid is

$$(\rho c)_f \left[\frac{\partial T}{\partial t} + \mathbf{v} \cdot \nabla T \right] = -\nabla \cdot \mathbf{q} + h_p \nabla \cdot \mathbf{j}_p + (\rho c)_f \, D_{TC} \nabla^2 C, \tag{3.14}$$

where $(\rho c)_f$ is the heat capacity of the base fluid, c is the specific heat, C is the solutal concentration, h_p is the specific enthalpy of the nanoparticle material, D_{TC} is the Dufour diffusivity and $\mathbf{q}$ is the energy flux relative to the nanofluid velocity $\mathbf{v}$ which can be defined as

$$\mathbf{q} = -k \nabla T + h_p \mathbf{j}_p, \tag{3.15}$$

where k is the thermal conductivity. Substituting Eq. 3.15 in Eq. 3.14 yield

$$
\begin{aligned}
(\rho c)_f\left[\frac{\partial T}{\partial t}+\mathbf{v}\cdot\nabla T\right] &= \nabla\cdot k\nabla T-\nabla\cdot(h_p\mathbf{j}_p)+h_p\nabla\cdot\mathbf{j}_p+(\rho c)_f\,D_{TC}\nabla^2 C \\
&= \nabla\cdot k\nabla T-h_p\nabla\cdot\mathbf{j}_p-\mathbf{j}_p\cdot\nabla h_p+h_p\nabla\cdot\mathbf{j}_p+(\rho c)_f\,D_{TC}\nabla^2 C \\
&= \nabla\cdot k\nabla T-c_p\mathbf{j}_p\cdot\nabla T+(\rho c)_f\,D_{TC}\nabla^2 C, \qquad (3.16)
\end{aligned}
$$

where $\nabla h_p = c_p\nabla T$ and c_p is the nanoparticle specific heat. It is worth to note that if $\mathbf{j}_p = 0$, Eq 3.16 becomes the common energy equation for a pure fluid. Substituting Eq. 3.11 into Eq. 3.16 gives

$$
(\rho c)_f\left[\frac{\partial T}{\partial t}+\mathbf{v}\cdot\nabla T\right]=\nabla\cdot k\nabla T+(\rho c)_p\left[D_B\nabla S\cdot\nabla T+D_T\frac{\nabla T\cdot\nabla T}{T}\right]+(\rho c)_f\,D_{TC}\nabla^2 C. \qquad (3.17)
$$

Note that $(\rho c)_p$ is the heat capacity of the nanoparticles. If we assume that the thermal properties of the nanofluid are uniform and the flow is steady, then the thermal energy equation becomes

$$
u\frac{\partial T}{\partial x}+v\frac{\partial T}{\partial y}=\alpha\frac{\partial^2 T}{\partial y^2}+\tau\left[D_B\frac{\partial S}{\partial y}\frac{\partial T}{\partial y}+\left(\frac{D_T}{T_\infty}\right)\left(\frac{\partial T}{\partial y}\right)^2\right]+D_{TC}\frac{\partial^2 C}{\partial y^2}, \qquad (3.18)
$$

where $\alpha = k/(\rho c)_f$ is the thermal diffusivity and $\tau = (\rho c)_p/(\rho c)_f$ is the ratio of the heat capacity of nanoparticle and heat capacity of the base fluid.

3.2.5 The Concentration Equation

In general, there may be a number of chemical components in the fluid. This normally happens when there be a transfer of mass to or from the fluid at the surface. At the body surface, some particular component of the fluid has concentration, which is determined by the conditions of thermal equilibrium. Following Kuznetsov & Nield (2011), the concentration or mass diffusion equation of the boundary layer is

$$
\frac{\partial C}{\partial t}+\mathbf{v}\cdot\nabla C = D_S\nabla^2 C+D_{CT}\nabla^2 T, \qquad (3.19)
$$

where C is the solutal concentration, D_S is the solutal diffusivity and D_{CT} is the Soret diffusivity. For a steady flow condition and using boundary layer assumptions, Eq. 3.19 becomes

$$u\frac{\partial C}{\partial x}+v\frac{\partial C}{\partial y}=D_S\frac{\partial^2 C}{\partial y^2}+D_{CT}\frac{\partial^2 T}{\partial y^2}. \tag{3.20}$$

In summary, Eq. 3.4 represents the continuity equation of the nanofluid, Eq. 3.9 denotes the nanofluid momentum equation, Eq. 3.13 indicates the nanoparticle volume fraction equation, Eq. 3.18 represents the thermal energy equation and Eq. 3.20 indicates the solutal concentration equation. All these equations comprise a complete set of equations which explains the transport model of nanofluid. The model can be solved once the boundary and initial conditions are known. This nanofluid model developed by Buongiorno (2006) describes as a two-phase flow analysis and nonhomogeneous.

3.2.6 The Boundary Conditions

In all boundary layer problems, the boundary conditions play an important role which dictate the particular solutions to be obtained from the governing equations. The governing equations, Eqs. 3.4, 3.9, 3.13, 3.18 and 3.20 can be solved step-by-step by marching downstream from where the flow encounters a body, subject to specified inflow conditions at the encounter and specified boundary conditions at the outer edge of boundary layer. The velocity boundary conditions are

1. for suction/injection; $\quad u=0, \quad v=v_0 \quad \text{at} \quad y=0,$

2. for moving wedge with suction/injection; $\quad u=U_w, \quad v=v_0 \quad \text{at} \quad y=0,$

3. as $\quad y\to\infty; \quad u\to U,$

where v_0 is the suction ($v_0<0$) or injection ($v_0>0$) across the wedge surface. The velocity of the moving wedge is denoted as U_w.

The boundary conditions for temperature are

1. for constant temperature; $\quad T=T_w \quad \text{at} \quad y=0,$

2. for power law variation; $\quad T=T_w=T_\infty+b_1x^{n_1} \quad \text{at} \quad y=0,$

3. as $\quad y\to\infty; \quad T\to T_\infty,$

where T_w is temperature at the wedge wall, T_∞ is the ambient values of temperature, b_1 and n_1 are constants.

The boundary conditions of nanoparticles volume fraction are:

1. for constant nanoparticle volume fraction; $S = S_w$ at $y = 0$,

2. as $y \to \infty$; $S \to S_\infty$,

where S_w is the nanoparticle volume fraction at the wedge wall and S_∞ is the ambient value of nanoparticle volume fraction.

The solutal concentration boundary conditions are:

1. for constant concentration; $C = C_w$ at $y = 0$,

2. for power law variation; $C = C_w = C_\infty + b_2 x^{n_2}$ at $y = 0$,

3. as $y \to \infty$; $C \to C_\infty$,

where C_w is the solutal concentration at the wedge wall, C_∞ is the ambient value of solutal concentration, b_2 and n_2 are constants.

3.2.7 The Stream Function

By introducing the stream function, the velocity components u and v can be replaced by a single function ψ. The boundary layer problem can be solved and simplified by choosing a stream function ψ which satisfies the continuity equation 3.4 automatically. The stream function $\psi(x,y)$ is defined by the equations

$$u = \frac{\partial \psi}{\partial y} \quad \text{and} \quad v = -\frac{\partial \psi}{\partial x}. \tag{3.21}$$

3.3 Similarity Solutions of the Boundary Layer Equations

The use of the word similar was explained in Evans (1968). For most flows, the shape of velocity profile varies gradually as x changes. This means that the manner of increase or decrease of velocity in the x-direction is the same for all values of y. Since the velocity profiles for these flows have a similar shape, such boundary layer may be described as similar and the corresponding solutions to the governing equations as similarity solution. The mathematical statement that expresses the velocity profiles at all x-positions are geometrically similar, differing only by a multiplying factor, is given as follows:

$$u = f[y \cdot p(x)]. \tag{3.22}$$

Kays & Crawford (1980) derived and explained in detail of Eq. 3.22 in order to prove the assumption that the solution can be expressed in this form truly leads to such solution. The similarity solution procedure is described below for the general case of convective boundary layer flow of nanofluid along a wedge. Fig. 3.2 shows that the x-axis is extending along the wedge surface, while the y-axis normal to the surface of the wedge. The flow is assumed to be in the x direction. The total angle of the wedge is denoted as $\Omega = \beta\pi$, where $\beta = 2m/(m+1) \geq 0$. The governing equations derived in Section 3.2 describing the continuity, momentum, nanoparticles volume fraction, thermal energy and solutal concentration can be written as

$$\frac{\partial u}{\partial x} + \frac{\partial v}{\partial y} = 0, \tag{3.23}$$

$$u\frac{\partial u}{\partial x} + v\frac{\partial u}{\partial y} = U\frac{dU}{dx} + \nu\frac{\partial^2 u}{\partial y^2}, \tag{3.24}$$

$$u\frac{\partial S}{\partial x} + v\frac{\partial S}{\partial y} = D_B\frac{\partial^2 S}{\partial y^2} + \left(\frac{D_T}{T_\infty}\right)\frac{\partial^2 T}{\partial y^2}, \tag{3.25}$$

$$u\frac{\partial T}{\partial x} + v\frac{\partial T}{\partial y} = \alpha\frac{\partial^2 T}{\partial y^2} + \tau\left[D_B\frac{\partial S}{\partial y}\frac{\partial T}{\partial y} + \left(\frac{D_T}{T_\infty}\right)\left(\frac{\partial T}{\partial y}\right)^2\right] + D_{TC}\frac{\partial^2 C}{\partial y^2}, \tag{3.26}$$

$$u\frac{\partial C}{\partial x} + v\frac{\partial C}{\partial y} = D_S\frac{\partial^2 C}{\partial y^2} + D_{CT}\frac{\partial^2 T}{\partial y^2}. \tag{3.27}$$

Following Falkner & Skan (1931), the free stream or potential flow velocity is

$$U = ax^m. \tag{3.28}$$

Clearly, the constant a is the value of U at the point where x is of unit length. The exponent m is the wedge angle parameter which depends on the pressure gradient, β in the stream

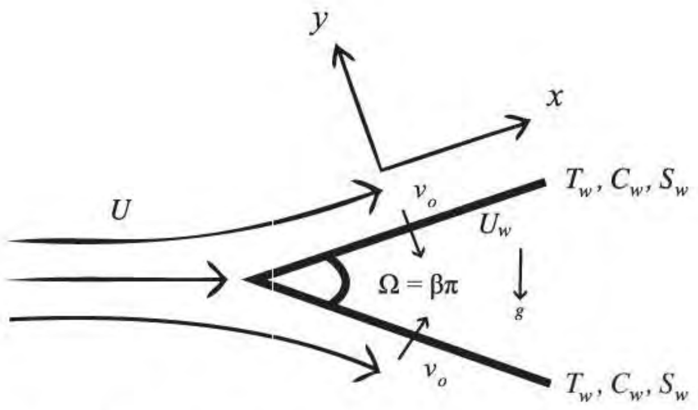

Figure 3.2: The physical configuration of the wedge

direction. By differentiation of Eq. 3.28, it is shown that both m and β are related by the reciprocal relationships

$$\beta = \frac{2m}{m+1}, \qquad m = \frac{\beta}{2-\beta}. \tag{3.29}$$

By evaluating ψ and its derivatives, from the first term of Eq. 3.21, we obtain

$$\psi = \sqrt{\frac{2U\nu x}{m+1}} f(\eta) = h(x) f(\eta), \tag{3.30}$$

and the dimensionless distance from the wall is defined as

$$\eta = \sqrt{\frac{(m+1)U}{2\nu x}} y = p(x) y. \tag{3.31}$$

We can derive

$$h(x)p(x) = \sqrt{\frac{2U\nu x}{m+1}} \sqrt{\frac{(m+1)U}{2\nu x}} = U, \qquad \frac{dU}{dx} = \frac{mU}{x},$$

$$\frac{dh}{dx} = h\left(\frac{m+1}{2x}\right), \qquad \frac{dp}{dx} = p\left(\frac{m-1}{2x}\right), \quad \frac{\partial \eta}{\partial x} = \frac{p'\eta}{p}.$$

The velocity components u and v, as given in Eq. 3.21, in terms of new variables η and f are

$$u = U\frac{\partial f}{\partial \eta}, \qquad v = -\left[h' f + h\left(\frac{\partial f}{\partial x} + \frac{\partial f}{\partial \eta}\frac{p'\eta}{p}\right)\right]. \tag{3.32}$$

The momentum equation 3.24 can be transformed to (η, f) using Eqs. 3.32.

$$U\frac{\partial f}{\partial \eta}\frac{\partial}{\partial x}\left(U\frac{\partial f}{\partial \eta}\right) - \left[h'f + h\left(\frac{\partial f}{\partial x} + \frac{\partial f}{\partial \eta}\frac{p'\eta}{p}\right)\right]\frac{\partial}{\partial y}\left(U\frac{\partial f}{\partial \eta}\right)$$
$$= \nu\frac{\partial^2}{\partial y^2}\left(U\frac{\partial f}{\partial \eta}\right) + U\frac{mU}{x}.$$

After some calculations, the result is

$$\frac{\partial^3 f}{\partial \eta^3} + f\frac{\partial^2 f}{\partial \eta^2} + \frac{2m}{m+1}\left(1 - \left(\frac{\partial f}{\partial \eta}\right)^2\right) = \frac{2x}{m+1}\left(\frac{\partial^2 f}{\partial x \partial y}\frac{\partial f}{\partial \eta} - \frac{\partial^2 f}{\partial \eta^2}\frac{\partial f}{\partial x}\right). \tag{3.33}$$

Eq. 3.33 is the ordinary differential equation which governs the distribution of fluid velocity.

The nanoparticle volume fraction, thermal energy and solutal concentration equations also contain the velocity components u and v. To establish the conditions which the nanoparticle volume fraction, S, the fluid temperature, T and solutal concentration, C must satisfy for similar solutions to Eqs. 3.25−3.27, we shall go through the transformation to the (η, f)-coordinates in some detail. The variation of S, T and C must be restricted to satisfy the conditions for the similarity of the nanoparticle volume fraction, temperature and concentration profiles. Thus, the dimensionless nanoparticle volume fraction, ϕ, dimensionless temperature, θ and dimensionless concentration, γ are defined as

$$\phi(\eta) = \frac{S - S_\infty}{S_w - S_\infty}, \qquad \theta(\eta) = \frac{T - T_\infty}{T_w - T_\infty}, \qquad \gamma(\eta) = \frac{C - C_\infty}{C_w - C_\infty}. \tag{3.34}$$

Substituting Eq. 3.32 and 3.34 into Eqs. 3.25−3.27, we obtain

$$\frac{\partial^2 \phi}{\partial \eta^2} + \Pr\,\mathrm{Ln} f\frac{\partial \phi}{\partial \eta} + \frac{N_T}{N_B}\frac{\partial^2 \theta}{\partial \eta^2} = \Pr\,\mathrm{Ln}\frac{2x}{m+1}\left(\frac{\partial f}{\partial \eta}\frac{\partial \phi}{\partial x} - \frac{\partial f}{\partial x}\frac{\partial \phi}{\partial \eta}\right), \tag{3.35}$$

$$\frac{\partial^2 \theta}{\partial \eta^2} + \Pr f\frac{\partial \theta}{\partial \eta} + N_B\frac{\partial \phi}{\partial \eta}\frac{\partial \theta}{\partial \eta} + N_T\left(\frac{\partial \theta}{\partial \eta}\right)^2 + N_{TC}\frac{\partial^2 \gamma}{\partial \eta^2} = \Pr\frac{2x}{m+1}\left(\frac{\partial f}{\partial \eta}\frac{\partial \theta}{\partial x} - \frac{\partial f}{\partial x}\frac{\partial \theta}{\partial \eta}\right), \tag{3.36}$$

$$\frac{\partial^2 \gamma}{\partial \eta^2} + \Pr\,\mathrm{Le} f\frac{\partial \gamma}{\partial \eta} + N_{CT}\,\mathrm{Le}\frac{\partial^2 \theta}{\partial \eta^2} = \Pr\,\mathrm{Le}\frac{2x}{m+1}\left(\frac{\partial f}{\partial \eta}\frac{\partial \gamma}{\partial x} - \frac{\partial f}{\partial x}\frac{\partial \gamma}{\partial \eta}\right). \tag{3.37}$$

In Eqs. 3.35−3.37, the following dimensionless variables have been used

$$\Pr = \frac{\nu}{\alpha}, \quad \text{Prandtl number,} \tag{3.38}$$

$$\text{Le} = \frac{\alpha}{D_S}, \quad \text{Lewis number,} \tag{3.39}$$

$$\text{Ln} = \frac{\alpha}{D_B}, \quad \text{nanofluid Lewis number,} \tag{3.40}$$

$$N_B = \frac{\tau D_B(S_w - S_\infty)}{\alpha}, \quad \text{Brownian motion parameter,} \tag{3.41}$$

$$N_T = \frac{\tau D_T(T_w - T_\infty)}{\alpha T_\infty}, \quad \text{thermophoresis parameter,} \tag{3.42}$$

$$N_{CT} = \frac{D_{CT}(T_w - T_\infty)}{\alpha(C_w - C_\infty)}, \quad \text{Soret-type parameter,} \tag{3.43}$$

$$N_{TC} = \frac{D_{TC}(C_w - C_\infty)}{\alpha(T_w - T_\infty)}, \quad \text{Dufour-type parameter.} \tag{3.44}$$

3.3.1 The Dimensionless Boundary Conditions

The velocity boundary conditions which the variable f must satisfy are

1. for suction/injection; $\dfrac{\partial f}{\partial \eta} = 0, \quad \dfrac{f}{2}\left(\dfrac{x}{U}\dfrac{dU}{dx}\right) + x\dfrac{\partial f}{\partial x} = F_w \quad \text{at} \quad \eta = 0,$
2. for moving wedge with suction/injection;
   $\dfrac{\partial f}{\partial \eta} = \lambda, \quad \dfrac{f}{2}\left(\dfrac{x}{U}\dfrac{dU}{dx}\right) + x\dfrac{\partial f}{\partial x} = F_w \quad \text{at} \quad \eta = 0,$
3. as $\eta \to \infty; \quad \dfrac{\partial f}{\partial \eta} \to 1,$

where the moving wedge parameter is denoted as $\lambda = U_w/U$. The suction $(F_w > 0)$ or injection $(F_w < 0)$ parameter is denoted as $F_w = -v_0 \text{Re}_x^{1/2}/U$ where $\text{Re}_x = Ux/\nu$ is the Reynolds number.

The temperature boundary conditions which the variable θ must satisfy are

1. for constant temperature; $\theta = 1 \quad \text{at} \quad \eta = 0,$
2. for power law variation; $\theta = 1 \quad \text{at} \quad \eta = 0,$
3. as $\eta \to \infty; \quad \theta \to 0.$

The boundary conditions of nanoparticles volume fraction which the variable ϕ must satisfy are:

1. for constant nanoparticle volume fraction; $\phi = 1$ at $\eta = 0$,
2. as $\eta \to \infty$; $\phi \to 0$.

The solutal concentration boundary conditions which the variable γ must satisfy are

1. for constant concentration; $\gamma = 1$ at $\eta = 0$,
2. for power law variation; $\gamma = 1$ at $\eta = 0$,
3. as $\eta \to \infty$; $\gamma \to 0$.

3.3.2 Local Similarity Solution

Consider the general transformation of independent variables in the Eqs. 3.33, 3.35, 3.36 and 3.37 from (x, y) to (ξ, η). Following Kafoussias & Nanousis (1997), ξ is denoted as the dimensionless distance along the wedge and

$$\xi = bx^{(1-m)/2}. \tag{3.45}$$

Using Eq. 3.45 and its derivative with respect to x, Eqs. 3.33, 3.35, 3.36 and 3.37 become

$$\frac{\partial^3 f}{\partial \eta^3} + f\frac{\partial^2 f}{\partial \eta^2} + \frac{2m}{m+1}\left(1 - \left(\frac{\partial f}{\partial \eta}\right)^2\right) = \frac{1-m}{m+1}\xi\left(\frac{\partial^2 f}{\partial \xi \partial \eta}\frac{\partial f}{\partial \eta} - \frac{\partial^2 f}{\partial \eta^2}\frac{\partial f}{\partial \xi}\right), \tag{3.46}$$

$$\frac{\partial^2 \phi}{\partial \eta^2} + \mathrm{Pr}\ \mathrm{Ln} f\frac{\partial \phi}{\partial \eta} + \frac{N_T}{N_B}\frac{\partial^2 \theta}{\partial \eta^2} = \mathrm{Pr}\ \mathrm{Ln}\frac{1-m}{m+1}\left(\frac{\partial f}{\partial \eta}\frac{\partial \phi}{\partial \xi} - \frac{\partial f}{\partial \xi}\frac{\partial \phi}{\partial \eta}\right), \tag{3.47}$$

$$\begin{aligned}\frac{\partial^2 \theta}{\partial \eta^2} + \mathrm{Pr} f\frac{\partial \theta}{\partial \eta} + N_B\frac{\partial \phi}{\partial \eta}\frac{\partial \theta}{\partial \eta} + N_T\left(\frac{\partial \theta}{\partial \eta}\right)^2 + N_{TC}\frac{\partial^2 \gamma}{\partial \eta^2}\\ = \mathrm{Pr}\frac{1-m}{m+1}\xi\left(\frac{\partial f}{\partial \eta}\frac{\partial \theta}{\partial \xi} - \frac{\partial f}{\partial \xi}\frac{\partial \theta}{\partial \eta}\right),\end{aligned} \tag{3.48}$$

$$\frac{\partial^2 \gamma}{\partial \eta^2} + \mathrm{Pr}\ \mathrm{Le} f\frac{\partial \gamma}{\partial \eta} + NCT\ \mathrm{Le}\frac{\partial^2 \theta}{\partial \eta^2} = \mathrm{Pr}\ \mathrm{Le}\frac{1-m}{m+1}\left(\frac{\partial f}{\partial \eta}\frac{\partial \gamma}{\partial \xi} - \frac{\partial f}{\partial \xi}\frac{\partial \gamma}{\partial \eta}\right). \tag{3.49}$$

The boundary condition which involves the suction/injection effect becomes

$$\frac{f}{2}\left(\frac{x}{U}\frac{dU}{dx}\right)+x\frac{\partial f}{\partial x}=\frac{f}{2}(m+1)+\frac{1-m}{2}\xi\frac{\partial f}{\partial \xi}=F_w$$

It may be observed that if either ξ or derivative with respect to ξ remains in the transformed Eqs. 3.46−3.49, similarity solutions will not exist. However, when dropping the terms containing partial derivatives with respect to ξ and retaining ξ as a parameter, this approach is called local similarity assumption. Kays & Crawford (1980) mentioned that the resulting solutions is generally valid if ξ and the discarded derivatives are small. Thus, the local similarity solution of Eqs. 3.46−3.49 are obtained by deleting the terms containing partial derivatives with respect to ξ, and consider ξ as a parameter. By employing this assumptions, Eqs. 3.46−3.49 reduce to

$$f'''+ff''+\frac{2m}{m+1}\left(1-(f')^2\right)=0, \tag{3.50}$$

$$\phi''+\Pr\,\mathrm{Ln}f\phi'+\frac{N_T}{N_B}\theta''=0, \tag{3.51}$$

$$\theta''+\Pr f\theta'+N_B\phi'\theta'+N_T\left(\theta'\right)^2+N_{TC}\gamma''=0, \tag{3.52}$$

$$\gamma''+\Pr\,\mathrm{Le}f\gamma'+N_{CT}\,\mathrm{Le}\theta''=0, \tag{3.53}$$

where primes denote as the differentiation with respect to η. The boundary condition which involves the suction/injection effect becomes $f=\frac{2}{m+1}F_w$.

3.3.3 The Skin Friction, Nusselt Number and Sherwood Number

The skin friction, heat and mass transfer rates are the important parameters in thermal engineering applications. The skin friction, Nusselt number and Sherwood number are defined as follows

$$C_{fx}=\frac{\tau_w}{\rho_f U^2},\quad Nu_x=\frac{xq_w}{k(T_w-T_\infty)},\quad Sh_x=\frac{xq_m}{D_B(C_w-C_\infty)}, \tag{3.54}$$

where

$$\tau_w = \mu \left(\frac{\partial u}{\partial y}\right)_{y=0}, \quad q_w = -k\left(\frac{\partial T}{\partial y}\right)_{y=0}, \quad q_m = -D_B\left(\frac{\partial C}{\partial y}\right)_{y=0}, \tag{3.55}$$

are shear stress, heat flux and mass flux, respectively. Employing Eqs. 3.21 and 3.34, the local skin friction coefficient, local Nusselt number and local Sherwood number can be written, respectively as

$$C_{fx}(\mathrm{Re}_x)^{1/2} = f''(0)\sqrt{\frac{m+1}{2}}, \tag{3.56}$$

$$Nu_x(\mathrm{Re}_x)^{-1/2} = -\theta'(0)\sqrt{\frac{m+1}{2}}, \tag{3.57}$$

$$Sh_x(\mathrm{Re}_x)^{-1/2} = -\gamma'(0)\sqrt{\frac{m+1}{2}}. \tag{3.58}$$

3.4 Numerical Method

The nonlinear ordinary differential Eqs. 3.50−3.53 are of the third order in f and second order in θ, ϕ and γ. These equations are numerically solved by employing the fourth-order Runge-Kutta-Gill method (Gill, 1951) integrated with shooting technique and Newton Raphson method (Cebeci & Keller, 1971). We define:

$$\begin{gathered} f = Y_1, \quad f' = Y_2, \quad f'' = Y_3, \quad \theta = Y_4, \quad \theta' = Y_5, \\ \gamma = Y_6, \quad \gamma' = Y_7, \quad \phi = Y_8, \quad \phi' = Y_9. \end{gathered} \tag{3.59}$$

We also define the following:

$$\begin{gathered} f' = F_1, \quad f'' = F_2, \quad f''' = F_3, \quad \theta' = F_4, \quad \theta'' = F_5, \\ \gamma' = F_6, \quad \gamma'' = F_7, \quad \phi' = F_8, \quad \phi'' = F_9. \end{gathered} \tag{3.60}$$

Substitute Eqs. 3.59 and 3.60 into Eqs. 3.50−3.53, these equations are reduced to a system of nine simultaneous equations of first order as follows:

$$F_1 = Y_2, \tag{3.61}$$

$$F_2 = Y_3, \tag{3.62}$$

$$F_3 = -Y_1Y_3 - \frac{2m}{m+1}(1 - Y_2Y_2), \tag{3.63}$$

$$F_4 = Y_5, \tag{3.64}$$

$$F_5 = -\mathrm{Pr}Y_1Y_5 - N_BY_7Y_5 - N_T(Y_5)^2 + N_{TC}F_7, \tag{3.65}$$

$$F_6 = Y_7, \tag{3.66}$$

$$F_7 = -\mathrm{Pr}\ \mathrm{Le}Y_1Y_7 + N_{CT}\mathrm{Le}F_5, \tag{3.67}$$

$$F_8 = Y_9, \tag{3.68}$$

$$F_9 = -\mathrm{Pr}\ \mathrm{Ln}Y_1Y_9 - \frac{N_T}{N_B}F_5. \tag{3.69}$$

Assuming the boundary conditions have the specific case as follows:

$$Y_1 = \frac{2}{m+1}F_w, \quad Y_2 = 0, \quad Y_4 = 1, \quad Y_6 = 1, \quad Y_8 = 1, \quad \text{at} \quad \eta = 0, \tag{3.70}$$

$$Y_2 \to 1, \quad Y_4 \to 0, \quad Y_6 \to 0, \quad Y_8 \to 0, \quad \text{as} \quad \eta \to \infty. \tag{3.71}$$

It is worth mentioning that the values of Y_3, Y_5, Y_7, and Y_9 at $\eta = 0$ are needed for solving the Eqs. 3.61−3.69. Since the four values are unknown, the initial guesses for $Y_3(0) = s$, $Y_5(0) = t$, $Y_7(0) = sc$, and $Y_9(0) = np$ are chosen and denoted as s, t, sc and np. The problem is to find s, t, sc and np such that the solutions of Eqs. 3.61−3.70 satisfy the outer boundary conditions 3.71. We indicate the solutions of this initial value problem by

$$\mathbf{F}[Y_1(\eta,s),Y_2(\eta,s),\ldots,Y_9(\eta,s)], \quad \mathbf{F}[Y_1(\eta,t),Y_2(\eta,t),\ldots,Y_9(\eta,t)],$$
$$\mathbf{F}[Y_1(\eta,sc),y_2(\eta,sc),\ldots,Y_9(\eta,sc)], \quad \mathbf{F}[Y_1(\eta,np),Y_2(\eta,np),\ldots,Y_9(\eta,np)].$$

To find the value of s, we define such that

$$\varphi(s) \equiv [Y_2(\eta_\infty,s) - 1, Y_4(\eta_\infty,s), Y_6(\eta_\infty,s), Y_8(\eta_\infty,s)] = 0. \tag{3.72}$$

To solve Eq. 3.72, we employ Newton Raphson method (Griffiths & Higham, 2010). For some initial estimate s^0 of the root, this yields the iterates s^k, defined by

$$s^{k+1} = s^k - \frac{\varphi(s^k)}{d\varphi(s^k)/ds}, \tag{3.73}$$

where $k = 0, 1, 2, 3, \ldots$ and

$$\varphi(s^k) = [Y_2(\eta_\infty, s^k) - 1, Y_4(\eta_\infty, s^k), Y_6(\eta_\infty, s^k), Y_8(\eta_\infty, s^k)], \tag{3.74}$$

$$d\varphi(s^k)/ds = \frac{\partial [Y_2(\eta_\infty, s^k) - 1, Y_4(\eta_\infty, s^k), Y_6(\eta_\infty, s^k), Y_8(\eta_\infty, s^k)]}{\partial s}. \tag{3.75}$$

In order to obtain the derivative of Y_2, Y_4, Y_6 and Y_8 with respect to s, we take the derivatives of Eqs. 3.61−3.69 with respect to s (Cebeci & Keller, 1971). This leads to the following linear differential equations, known as the variational equations for Eqs. 3.61−3.69. Thus, we have:

$$\begin{gathered} f_s = Y_{10}, \quad f_s' = Y_{11}, \quad f_s'' = Y_{12}, \quad \theta_s = Y_{13}, \quad \theta_s' = Y_{14}, \\ \gamma_s = Y_{15}, \quad \gamma_s' = Y_{16}, \quad \phi_s = Y_{17}, \quad \phi_s' = Y_{18}. \end{gathered} \tag{3.76}$$

We also define the following:

$$\begin{gathered} f_s' = F_{10}, \quad f_s'' = F_{11}, \quad f_s''' = F_{12}, \quad \theta_s' = F_{13}, \quad \theta_s'' = F_{14}, \\ \gamma_s' = F_{15}, \quad \gamma_s'' = F_{16}, \quad \phi_s' = F_{17}, \quad \phi_s'' = F_{18}. \end{gathered} \tag{3.77}$$

The following equations are the derivative of Eqs. 3.61−3.69 with respect to s:

$$F_{10} = Y_{11}, \tag{3.78}$$

$$F_{11} = Y_{12}, \tag{3.79}$$

$$F_{12} = -(Y_{10}Y_3 + Y_1Y_{12} + \frac{2m}{m+1}(2Y_2Y_{11}), \tag{3.80}$$

$$F_{13} = Y_{14}, \tag{3.81}$$

$$F_{14} = -\Pr(Y_{10}Y_5 + Y_1Y_{14}) - N_B(y_{18}Y_5 + Y_9Y_{14}) - 2N_TY_5Y_{14} + N_{TC}F_{16}, \tag{3.82}$$

$$F_{15} = Y_{16}, \tag{3.83}$$

$$F_{16} = -\text{Pr Le}(Y_{10}Y_7 + Y_1Y_{16}) + N_{CT}\text{Le}F_{14}, \tag{3.84}$$

$$F_{17} = Y_{18}, \tag{3.85}$$

$$F_{18} = -\text{Pr Ln}(Y_{10}Y_9 + Y_1y_{18}) - \frac{N_T}{N_B}F_{14}. \tag{3.86}$$

We repeat the same process in order to find one of the solutions for this initial value problem, $[y_1(\eta,t), Y_2(\eta,t), \ldots, Y_9(\eta,t)]$. To find the value of t, we define such that

$$\varphi(t) \equiv [Y_2(\eta_\infty,t) - 1, Y_4(\eta_\infty,t), Y_6(\eta_\infty,t), Y_8(\eta_\infty,t)] = 0. \tag{3.87}$$

Eq. 3.87 can be solved by using Newton Raphson method. For some initial estimate t^0 of the root, this yields the iterates t^k, defined by

$$t^{k+1} = t^k - \frac{\varphi(t^k)}{d\varphi(t^k)/dt}, \tag{3.88}$$

where $k = 0, 1, 2, 3, \ldots$ and

$$\varphi(t^k) = [Y_2(\eta_\infty,t^k) - 1, Y_4(\eta_\infty,t^k), Y_6(\eta_\infty,t^k), Y_8(\eta_\infty,t^k)], \tag{3.89}$$

$$d\varphi(t^k)/dt = \frac{\partial[Y_2(\eta_\infty,t^k) - 1, Y_4(\eta_\infty,t^k), Y_6(\eta_\infty,t^k), Y_8(\eta_\infty,t^k)]}{\partial t}. \tag{3.90}$$

For derivatives with respect to t, we have:

$$f_t = Y_{19}, \quad f_t' = Y_{20}, \quad f_t'' = Y_{21}, \quad \theta_t = Y_{22}, \quad \theta_t' = Y_{23},$$
$$\gamma_t = Y_{24}, \quad \gamma_t' = Y_{25}, \quad \phi_t = Y_{26}, \quad \phi_t' = Y_{27}. \tag{3.91}$$

We also define the following:

$$F_{19} = f_t', \quad F_{20} = f_t'', \quad F_{21} = f_t''', \quad F_{22} = \theta_t', \quad F_{23} = \theta_t'',$$
$$F_{24} = \gamma_t', \quad F_{25} = \gamma_t'', \quad F_{26} = \phi_t', \quad F_{27} = \phi_t''. \tag{3.92}$$

The following equations are the derivative of Eqs. 3.61−3.69 with respect to t:

$$F_{19} = Y_{20}, \tag{3.93}$$

$$F_{20} = Y_{21}, \tag{3.94}$$

$$F_{21} = -(Y_{19}Y_3 + Y_1Y_{21} + \frac{2m}{m+1}(2Y_2Y_{20}), \tag{3.95}$$

$$F_{22} = Y_{23}, \tag{3.96}$$

$$F_{23} = -\Pr(Y_{19}Y_5 + Y_1Y_{23}) - N_B(Y_{27}Y_5 + Y_9Y_{23}) - 2N_TY_5Y_{23} + N_{TC}F_{25}, \tag{3.97}$$

$$F_{24} = Y_{25}, \tag{3.98}$$

$$F_{25} = -\Pr\,\mathrm{Le}(Y_{19}Y_7 + Y_1Y_{25}) + N_{CT}\mathrm{Le}F_{23}, \tag{3.99}$$

$$F_{26} = Y_{27}, \tag{3.100}$$

$$F_{27} = -\Pr\,\mathrm{Ln}(Y_{19}Y_9 + Y_1Y_{27}) - \frac{N_T}{N_B}F_{23}. \tag{3.101}$$

We indicate $[Y_1(\eta,sc),Y_2(\eta,sc),\ldots,Y_9(\eta,sc)]$ as one of the solutions for this initial value problem. To find the value of sc, we define such that

$$\varphi(sc) \equiv [Y_2(\eta_\infty,sc) - 1, Y_4(\eta_\infty,sc), Y_6(\eta_\infty,sc), Y_8(\eta_\infty,sc)] = 0. \tag{3.102}$$

The Newton Raphson method can be used for solving Eq. 3.102. For some initial estimate $(sc)^0$ of the root, this yields the iterates $(sc)^k$, defined by

$$(sc)^{k+1} = (sc)^k - \frac{\varphi((sc)^k)}{d\varphi((sc)^k)/d(sc)}, \tag{3.103}$$

where $k = 0,1,2,3,\ldots$ and

$$\varphi((sc)^k) = [Y_2(\eta_\infty,(sc)^k) - 1, Y_4(\eta_\infty,(sc)^k), Y_6(\eta_\infty,(sc)^k), Y_8(\eta_\infty,(sc)^k)], \tag{3.104}$$

$$d\varphi((sc)^k)/d(sc) = \frac{\partial[Y_2(\eta_\infty,(sc)^k) - 1, Y_4(\eta_\infty,(sc)^k), Y_6(\eta_\infty,(sc)^k), Y_8(\eta_\infty,(sc)^k)]}{\partial(sc)}. \tag{3.105}$$

The derivative of Eqs. 3.61−3.69 with respect to sc:

$$
\begin{aligned}
f_{sc} = Y_{28}, \quad f'_{sc} = Y_{29}, \quad f''_{sc} = Y_{30}, \quad \theta_{sc} = Y_{31}, \quad \theta'_{sc} = Y_{32}, \\
\gamma_{sc} = Y_{33}, \quad \gamma'_{sc} = Y_{34}, \quad \phi_{sc} = Y_{35}, \quad \phi'_{sc} = Y_{36}.
\end{aligned} \tag{3.106}
$$

We also define the following:

$$
\begin{aligned}
F_{28} = f'_{sc}, \quad F_{29} = f''_{sc}, \quad F_{30} = f'''_{sc}, \quad F_{31} = \theta'_{sc}, \quad F_{32} = \theta''_{sc}, \\
F_{33} = \gamma'_{sc}, \quad F_{34} = \gamma''_{sc}, \quad F_{35} = \phi'_{sc}, \quad F_{36} = \phi''_{sc}.
\end{aligned} \tag{3.107}
$$

The following equations are the derivative of Eqs. 3.61−3.69 with respect to sc:

$$F_{28} = Y_{29}, \tag{3.108}$$

$$F_{29} = Y_{30}, \tag{3.109}$$

$$F_{30} = -(Y_{28}Y_3 + Y_1Y_{30} + \frac{2m}{m+1}(2Y_2Y_{29}), \tag{3.110}$$

$$F_{31} = Y_{32}, \tag{3.111}$$

$$F_{32} = -\Pr(Y_{28}Y_5 + Y_1Y_{23}) - N_B(Y_{36}Y_5 + Y_9Y_{32}) - 2N_TY_5Y_{32} + N_{TC}F_{34}, \tag{3.112}$$

$$F_{33} = Y_{34}, \tag{3.113}$$

$$F_{34} = -\Pr\,\mathrm{Le}(Y_{28}Y_7 + Y_1Y_{34}) + N_{CT}\mathrm{Le}F_{32}, \tag{3.114}$$

$$F_{35} = Y_{36}, \tag{3.115}$$

$$F_{36} = -\Pr\,\mathrm{Ln}(Y_{28}Y_9 + Y_1Y_{36}) - \frac{N_T}{N_B}F_{32}. \tag{3.116}$$

Again, the same procedure is applied in order to find the unknown value of np. We indicate $[Y_1(\eta, np), Y_2(\eta, np), \ldots, Y_9(\eta, np)]$ as one of the solution for the initial value problem. We now define

$$\varphi(np) \equiv [Y_2(\eta_\infty, np) - 1, Y_4(\eta_\infty, np), Y_6(\eta_\infty, np), Y_8(\eta_\infty, np)] = 0. \tag{3.117}$$

The Newton Raphson method can be used for solving Eq. 3.117. For some initial estimate $(np)^0$ of the root, this yields the iterates $(np)^k$, defined by

$$(np)^{k+1} = (np)^k - \frac{\varphi((np)^k)}{d\varphi((np)^k)/d(np)}, \tag{3.118}$$

where $k = 0, 1, 2, 3, \ldots$ and

$$\varphi((np)^k) = [Y_2(\eta_\infty, (np)^k) - 1, Y_4(\eta_\infty, (np)^k), Y_6(\eta_\infty, (np)^k), Y_8(\eta_\infty, (np)^k)], \tag{3.119}$$

$$d\varphi((np)^k)/d(np) = \frac{\partial[Y_2(\eta_\infty, (np)^k) - 1, Y_4(\eta_\infty, (np)^k), Y_6(\eta_\infty, (np)^k), Y_8(\eta_\infty, (np)^k)]}{\partial(np)}. \tag{3.120}$$

For derivatives with respect to np, we have:

$$\begin{gathered} f_{np} = Y_{37}, \quad f'_{np} = Y_{38}, \quad f''_{np} = Y_{39}, \quad \theta_{np} = Y_{40}, \quad \theta'_{np} = Y_{41}, \\ \gamma_{np} = Y_{42}, \quad \gamma'_{np} = Y_{43}, \quad \phi_{np} = Y_{44}, \quad \phi'_{np} = Y_{45}. \end{gathered} \tag{3.121}$$

We also define the following:

$$\begin{gathered} F_{37} = f'_{np}, \quad F_{38} = f''_{np}, \quad F_{39} = f'''_{np}, \quad F_{40} = \theta'_{np}, \quad F_{41} = \theta''_{np}, \\ F_{42} = \gamma'_{np}, \quad F_{43} = \gamma''_{np}, \quad F_{44} = \phi'_{np}, \quad F_{45} = \phi''_{np}. \end{gathered} \tag{3.122}$$

The following equations are the derivative of Eqs. 3.61−3.69 with respect to np:

$$F_{37} = Y_{38}, \tag{3.123}$$

$$F_{38} = Y_{39}, \tag{3.124}$$

$$F_{39} = -(Y_{37}Y_3 + Y_1Y_{39} + \frac{2m}{m+1}(2Y_2Y_{38}), \tag{3.125}$$

$$F_{40} = Y_{41}, \tag{3.126}$$

$$F_{41} = -\Pr(Y_{37}Y_5 + Y_1Y_{41}) - N_B(Y_{45}Y_5 + Y_9Y_{41}) - 2N_TY_5Y_{41} + N_{TC}F_{43}, \tag{3.127}$$

$$F_{42} = Y_{43}, \tag{3.128}$$

$$F_{43} = -\Pr \mathrm{Le}(Y_{37}Y_7 + Y_1Y_{43}) + N_{CT}\mathrm{Le}F_{41}, \tag{3.129}$$

$$F_{44} = Y_{45}, \tag{3.130}$$

$$F_{45} = -\Pr \mathrm{Ln}(Y_{37}Y_9 + Y_1Y_{45}) - \frac{N_T}{N_B}F_{41}. \tag{3.131}$$

It is worth mentioning that, $F_1 - F_{45}$ are a system of first order ordinary differential equations which govern the distribution of nanofluid velocity, temperature, solutal concentration and nanoparticle volume fraction. We use the Newton Raphson method to solve the unknown variables, s, t, sc and np. Newton Raphson method is an iterative root-finding technique using the partial derivative of the function as the new system of equations. In this case, we start with the estimate values $\left(s^{(0)}, t^{(0)}, sc^{(0)}, np^{(0)}\right)$ by the shooting method. The Newton Raphson algorithm is expanded to include partial derivatives with respect to each variable's dimension (Bazaraa et al., 2006). This would yield the derivative of $\mathbf{F}(F_1, F_2, \ldots, F_9)$ with respect to s, t, sc and np.

$$\begin{aligned} &\mathbf{F_s}(F_{10}, F_{11}, \ldots, F_{18}), \quad \mathbf{F_t}(F_{19}, F_{20}, \ldots, F_{27}), \\ &\mathbf{F_{sc}}(F_{28}, F_{29}, \ldots, F_{36}), \quad \mathbf{F_{np}}(F_{37}, F_{38}, \ldots, F_{45}). \end{aligned} \tag{3.132}$$

Thus, we need to find $\mathbf{F_s} = 0$, $\mathbf{F_t} = 0$, $\mathbf{F_{sc}} = 0$ and $\mathbf{F_{np}} = 0$ simultaneously. Following Saaty & Bram (1964) and Cebeci & Keller (1971), this yield a system of algebraic equations which satisfy the boundary conditions when $\eta \to \infty$.

$$\begin{aligned} f'_s s + f'_t t + f'_{sc}(sc) + f'_{np}(np) + f' - 1 = 0, \\ \theta_s s + \theta_t t + \theta_{sc}(sc) + \theta_{np}(np) + \theta = 0, \\ \gamma_s s + \gamma_t t + \gamma_{sc}(sc) + \gamma_{np}(np) + \gamma = 0, \\ \phi_s s + \phi_t t + \phi_{sc}(sc) + \phi_{np}(np) + \phi = 0. \end{aligned} \tag{3.133}$$

Rearrange the system 3.133, this yield a matrix equation:

$$\begin{bmatrix} f'_s & f'_t & f'_{sc} & f'_{np} \\ \theta_s & \theta_t & \theta_{sc} & \theta_{np} \\ \gamma_s & \gamma_t & \gamma_{sc} & \gamma_{np} \\ \phi_s & \phi_t & \phi_{sc} & \phi_{np} \end{bmatrix} \begin{bmatrix} s \\ t \\ sc \\ np \end{bmatrix} = \begin{bmatrix} 1-f' \\ -\theta \\ -\gamma \\ -\phi \end{bmatrix}. \tag{3.134}$$

This matrix equation 3.134 can be solved by the Cramer's rule for the system . Thus, the determinant of five matrices are:

$$D = \begin{vmatrix} f'_s & f'_t & f'_{sc} & f'_{np} \\ \theta_s & \theta_t & \theta_{sc} & \theta_{np} \\ \gamma_s & \gamma_t & \gamma_{sc} & \gamma_{np} \\ \phi_s & \phi_t & \phi_{sc} & \phi_{np} \end{vmatrix}, \quad D_s = \begin{vmatrix} 1-f' & f'_t & f'_{sc} & f'_{np} \\ -\theta & \theta_t & \theta_{sc} & \theta_{np} \\ -\gamma & \gamma_t & \gamma_{sc} & \gamma_{np} \\ -\phi & \phi_t & \phi_{sc} & \phi_{np} \end{vmatrix}, \quad D_t = \begin{vmatrix} f'_s & 1-f' & f'_{sc} & f'_{np} \\ \theta_s & -\theta & \theta_{sc} & \theta_{np} \\ \gamma_s & -\gamma & \gamma_{sc} & \gamma_{np} \\ \phi_s & -\phi & \phi_{sc} & \phi_{np} \end{vmatrix},$$

$$D_{sc} = \begin{vmatrix} f'_s & f'_t & 1-f' & f'_{np} \\ \theta_s & \theta_t & -\theta & \theta_{np} \\ \gamma_s & \gamma_t & -\gamma & \gamma_{np} \\ \phi_s & \phi_t & -\phi & \phi_{np} \end{vmatrix}, \quad D_{np} = \begin{vmatrix} f'_s & f'_t & f'_{sc} & 1-f' \\ \theta_s & \theta_t & \theta_{sc} & -\theta \\ \gamma_s & \gamma_t & \gamma_{sc} & -\gamma \\ \phi_s & \phi_t & \phi_{sc} & -\phi \end{vmatrix}.$$

The corrections are then added to the solution vector:

$$s^* = s + \frac{D_s}{D}, \quad t^* = t + \frac{D_t}{D}, \quad sc^* = sc + \frac{D_{sc}}{D}, \quad np^* = np + \frac{D_{np}}{D}, \tag{3.135}$$

where s^*, t^*, sc^* and np^* are the new guess values. Eq. 3.135 can be iterated until it converges within a tolerance.

Once the initial-value problem given by $F_1 - F_{45}$ are solved, s, t, sc and np are known, we use the fourth order Runge-Kutta-Gill method (Gill, 1951) to solve the system. The system of simultaneous equations of first order is solved numerically using fourth-order Runge-Kutta-Gill method from $\eta = 0$ to an appropriate finite value of $\eta \to \infty$, say η_∞. The value of η_∞ is selected to vary from 5 to 7, depending on the set of the physical parameters. The step size of $\triangle\eta = 0.01$ is found to be satisfactory in obtaining the numerical solutions. For convergence, the maximum absolute relative difference between two iterations is employed within a pre-assigned tolerance, $\varepsilon \leq 10^{-5}$. If the difference meets the convergence criteria, the solution is assumed to have converged and the iterative process is terminated. Following Gill (1951), the Runge-Kutta formula is:

$$
\begin{aligned}
Y_{i+1} &= Y_i + \frac{1}{6}hk_1 + \frac{1}{3}\left(\frac{2-\sqrt{2}}{2}\right)hk_2 + \frac{1}{3}\left(\frac{2+\sqrt{2}}{2}\right)hk_3 + \frac{1}{6}hk_4, \\
k_1 &= F(Y_i), \\
k_2 &= F\left(Y_i + \frac{h}{2}k_1\right), \\
k_3 &= F\left[Y_i + \left(\frac{\sqrt{2}-1}{2}\right)hk_1 + \left(\frac{2-\sqrt{2}}{2}\right)hk_2\right], \\
k_4 &= F\left[Y_i - \frac{\sqrt{2}}{2}hk_2 + \left(\frac{2+\sqrt{2}}{2}\right)hk_3\right],
\end{aligned}
\tag{3.136}
$$

where h is the step size and $i = 1, 2, 3, \ldots, 45$.

3.5 Code Validation

Validation of the computer code is very important in the numerical simulation. Thus, an examination of the present data against the existing results has been done in order to verify the accuracy of the present computer code. Comparative studies of the present results for $f''(0)$ and $-\theta(0)$ with Watanabe et al. (1994), Kumari et al. (2001) and Ganapathirao et al. (2013) for various values of m when $\Pr = 0.73$ are presented in Table 3.1. Watanabe et al. (1994) used Runge-Kutta-Gill method, Kumari et al. (2001) used the Keller box method and Ganapathirao et al. (2013) used finite difference method to solve the system of ordinary differential equations in their work. It can be seen from Table 3.1 that the present results coincide very well up to 3 significant digits with previous results, which confirms that the numerical method used in this study is accurate.

Table 3.1: Comparison of $f''(0)$ and $-\theta(0)$ with those of Watanabe et al. (1994), Kumari et al. (2001) and Ganapathirao et al. (2013) when $\mathrm{Pr} = 0.73$ and $\lambda = F_w = N_B = N_T = N_{CT} = N_{TC} = \mathrm{Le} = \mathrm{Ln} = 0$.

m	Watanabe et al. (1994)		Kumari et al. (2001)		Ganapathirao et al. (2013)		Present	
	$f''(0)$	$-\theta(0)$	$f''(0)$	$-\theta(0)$	$f''(0)$	$-\theta(0)$	$f''(0)$	$-\theta(0)$
0	0.46960	0.42015	0.46975	0.42079	0.46972	0.42055	0.46960	0.42016
0.0141	-	-	0.50472	0.42635	0.50481	0.42614	0.50461	0.42578
0.0435	0.56898	0.43548	0.56904	0.43597	0.56890	0.43544	0.56898	0.43548
0.0909	0.65498	0.44740	0.65501	0.44770	0.65493	0.44740	0.65498	0.44730
0.1429	0.73200	0.45693	0.73202	0.45728	0.73196	0.45707	0.73200	0.45694
0.2000	0.80213	0.46503	0.80214	0.46534	0.80215	0.46517	0.80213	0.46503
0.3333	0.92765	0.47814	0.92766	0.47840	0.92767	0.47841	0.92765	0.47814
0.5	1.03890	0.48848	-	-	1.03893	0.48851	1.03890	0.48849

CHAPTER 4: CONVECTIVE FLOW AND HEAT TRANSFER OF NANOFLUID OVER A WEDGE WITH SUCTION

Investigation on boundary layer flows with suction or injection has been widely emphasized. The velocity and temperature distributions within the boundary layers in the presence of suction/injection have many important applications in engineering processes such as the design of the thrust bearings, the entrance region of the pipe flow and the reduction of the drag force. Moreover, the effect of suction can significantly change the flow field as well as the skin friction, heat and mass transfer coefficients. It is often necessary to postpone or prevent separation of boundary layer to reduce drag force. This chapter consists of two problems. The first problem considered the effect of heat generation/absorption on convective flow and heat transfer of nanofluid over a wedge with suction/injection. In the second problem, we extend the first problem by the inclusion of thermal radiation.

4.1 Convective Flow and Heat Transfer of Nanofluid over a Wedge with Heat Generation/Absorption in the Presence of Suction/Injection

4.1.1 Mathematical Formulation

Consider a steady two-dimensional incompressible laminar boundary layer flow of a nanofluid as shown in the Fig. 3.2. The free stream velocity is denoted as $U = ax^m$ where a is a constant while the exponent m is a wedge angle parameter and m is a function of β such that $m = \beta/(2-\beta) \geq 0$. The base fluid and nanoparticles are in thermal equilibrium. The x and y axes are measured parallel to the wedge wall direction and normal to it respectively, with the associated velocity components u and v. T is the temperature and S is the nanoparticle volume fraction. The constant temperature and nanoparticle volume fraction at the wedge wall are denoted as T_w and S_w, respectively. Ambient values of temperature and nanoparticle volume fraction are taken as T_∞ and S_∞, respectively. The effects of Brownian motion and thermophoresis are included for the nanofluid based on the Buongiorno's model (Buongiorno, 2006). The suction and injection on the wall are included in the problem. Further, the boundary layer flow is considered in presence of heat source or heat sink. It is assumed that there is no chemical reaction between the nanoparticle and base fluid. Taking the above assumptions into consideration, the governing equations describing momentum, energy and nanoparticle volume fraction along with the boundary conditions can be written as

$$\frac{\partial u}{\partial x} + \frac{\partial v}{\partial y} = 0, \tag{4.1}$$

$$u\frac{\partial u}{\partial x} + v\frac{\partial u}{\partial y} = \nu\frac{\partial^2 u}{\partial y^2} + U\frac{dU}{dx}, \tag{4.2}$$

$$u\frac{\partial T}{\partial x} + v\frac{\partial T}{\partial y} = \alpha\frac{\partial^2 T}{\partial y^2} + \tau\left[D_B\frac{\partial S}{\partial y}\frac{\partial T}{\partial y}\left(\frac{D_T}{T_\infty}\right)\left(\frac{\partial T}{\partial y}\right)^2\right] + Q(T - T_\infty), \tag{4.3}$$

$$u\frac{\partial S}{\partial x} + v\frac{\partial S}{\partial y} = D_B\frac{\partial^2 S}{\partial y^2} + \frac{D_T}{T_\infty}\frac{\partial^2 T}{\partial y^2}, \tag{4.4}$$

$$\begin{aligned} &u = 0, \quad v = v_0, \quad T = T_w, \quad S = S_w, \quad \text{at} \quad y = 0, \\ &u \to U, \quad T \to T_\infty, \quad S \to S_\infty, \quad \text{as} \quad y \to \infty, \end{aligned} \tag{4.5}$$

where ν is the kinematic viscosity, $\alpha = k/(\rho c)$ is nanofluid thermal diffusivity, k is thermal conductivity, ρ is the fluid density, c is the specific heat, τ is the ratio of the heat capacity of nanoparticle and heat capacity of the base fluid, D_B is the Brownian diffusion coefficient, D_T is the thermophoretic diffusion, Q is the heat generation/absorption coefficient and v_0 is the suction/injection parameter.

To obtain similarity solution, we introduce the following dimensionless variables:

$$\eta = y\sqrt{\frac{(m+1)U}{2\nu x}}, \quad \psi = f(\eta)\sqrt{\frac{2U\nu x}{m+1}}, \quad \theta(\eta) = \frac{T - T_\infty}{T_w - T_\infty}, \quad \phi(\eta) = \frac{S - S_\infty}{S_w - S_\infty}, \tag{4.6}$$

where η is the similarity variable, ψ is the stream function defined as $u = \frac{\partial \psi}{\partial y}$ and $v = -\frac{\partial \psi}{\partial x}$. Substituting Eq. 4.6 into Eqs.4.2−4.4, we obtain the following system of nonlinear ordinary differential equations:

$$f''' + ff'' + \frac{2m}{m+1}\left(1 - (f')^2\right) = 0, \tag{4.7}$$

$$\theta'' + \Pr f\theta' + N_B\phi'\theta' + N_T\left(\theta'\right)^2 + \frac{2m}{m+1}\Pr\xi^2\delta\theta = 0, \tag{4.8}$$

$$\phi'' + \Pr\,\mathrm{Ln} f\phi' + \frac{N_T}{N_B}\theta'' = 0, \tag{4.9}$$

where prime denotes the partial differentiation with respect to η, $\Pr = \nu/\alpha$ is the Prandtl number, $N_B = \tau D_B(S_w - S_\infty)/\alpha$ is the Brownian parameter, $N_T = \tau D_T(T_w - T_\infty)/\alpha T_\infty$ is the thermophoresis parameter, $\delta = Q/ab^2$ is the heat generation/absorption parameter and $\mathrm{Ln} = \alpha/D_B$ is the nanofluid Lewis number. The boundary conditions 4.5 then become

$$\begin{aligned} f &= \frac{2}{m+1}F_w, \quad f' = 0, \quad \theta = 1, \quad \phi = 1, \quad \text{at} \quad \eta = 0, \\ f' &\to 1, \quad \theta \to 0, \quad \phi \to 0, \quad \text{as} \quad \eta \to \infty, \end{aligned} \tag{4.10}$$

where $F_w = -v_0\mathrm{Re}_x^{1/2}/U$ is the suction parameter and $\mathrm{Re}_x = Ux/\nu$ is the Reynolds number. The main physical quantities of interest are the skin friction coefficient and the local Nusselt number, which are proportional to the quantities of $f''(0)$ and $-\theta(0)$, respectively. These physical parameters can be defined as $C_{fx} = \tau_w/\rho_f U^2$ and $Nu_x = xq_w/k(T_w - T_\infty)$, where $\tau_w = \mu\left(\frac{\partial u}{\partial y}\right)_{y=0}$ and $q_w = -k\left(\frac{\partial T}{\partial y}\right)_{y=0}$, are shear stress and heat flux, respectively. Using Eq. 4.6, the local skin friction coefficient and local Nusselt number can be written, respectively as

$$C_{fx}(\mathrm{Re}_x)^{1/2} = f''(0)\sqrt{\frac{m+1}{2}}, \quad Nu_x(\mathrm{Re}_x)^{-1/2} = -\theta'(0)\sqrt{\frac{m+1}{2}}. \tag{4.11}$$

4.1.2 Results and Discussion

Table 4.1 presents the values of $f''(0)$ and $-\theta'(0)$ for various combination of parameters. In all works in this thesis, the Prandtl number for the base fluid was fixed as $\Pr = 6.2$. From Table 4.1, the value of $f''(0)$ increases on increasing the wedge angle and suction parameters. However, the value of $f''(0)$ remains unchanged when the values of δ, N_B, N_T and Ln increase. The value of $-\theta'(0)$ shows a decreasing pattern when m, δ, N_B, N_T and Ln parameters increase. However, the value of $-\theta'(0)$ increases on increasing the suction/injection parameter.

Fig. 4.1 displays the velocity, temperature and nanoparticle volume fraction profiles

Table 4.1: The values of $f''(0)$ and $-\theta'(0)$ for various values of m, F_w, δ, N_B, N_T and Ln

m	F_w	δ	N_B	N_T	Ln	$f''(0)$	$-\theta'(0)$
0.0909						1.34053	3.32223
0.2000	0.5	0.2	0.1	0.1	5	1.39034	3.01618
0.3333						1.43445	2.71710
	-0.1					0.96241	0.03918
	-0.05					1.00017	0.16660
0.0909	0	0.1	0.1	0.1	5	1.03890	0.31831
	0.7					1.66859	3.66353
	1					1.97741	5.26688
		-0.5					4.55591
		-0.2					4.07799
0.0909	0.5	0	0.1	0.1	5	1.34053	3.72112
		0.5					2.60585
		1					0.63972
			0.3				1.50831
0.0909	0.5	0.2	0.5	0.1	5	1.34053	0.56172
			0.7				0.14375
				0.3			1.51107
0.0909	0.5	0.2	0.2	0.5	5	1.34053	0.98019
				0.7			0.61277
					3.5		3.58531
0.0909	0.5	0.2	0.1	0.1	7	1.34053	3.09228
					10		2.88194

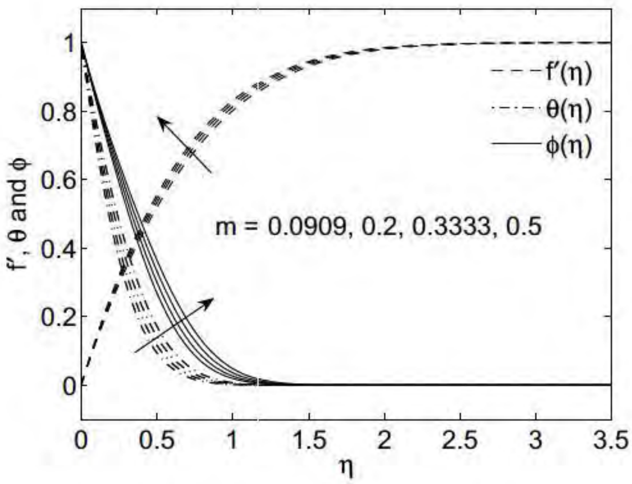

Figure 4.1: The distributions of f', θ and ϕ for different values of m when $N_T = N_B = 0.1$, $\delta = 0.2$, $F_w = 0.5$, $\xi = 1$ and $\mathrm{Ln} = 5$

against η for different values of the wedge angle, m. As for $m = 0$ (0°), it corresponds to the boundary layer flow past a flat horizontal surface, whereas $m = 1$ (180°) represents to the boundary layer flow near the stagnation point of a vertical plate. It can be seen that the velocity, temperature and nanoparticle volume fraction profiles increase on increasing the wedge angle parameter, m. Therefore the thickness of the hydrodynamic boundary layer decreases with the increase of m.

The impact of thermophoresis on the dimensionless temperature and nanoparticle volume fraction is depicted in the Fig. 4.2(a). It is found that the nanofluid velocity remains unchanged on increasing the thermophoresis parameter. The temperature and nanoparticle volume fraction profiles increase on increasing the value of N_T. The effect of Brownian motion is presented in the Fig. 4.2(b). It is observed that the temperature increases with the increase of N_B, while the volume fraction of nanofluid decreases on increasing the value of N_B. The Brownian motion parameter doesn't cause any significant effect on the velocity of the fluid.

The dimensionless temperature and nanoparticle volume fraction as a function of η are presented in the Figs. 4.3(a) and 4.3(b), respectively for various values of heat generation $(\delta > 0)$ and heat absorption $(\delta < 0)$. It is observed that the temperature increases as the value of δ increases for $\delta > 0$. Therefore, due to the presence of heat generation, it is apparent that there is an increase in the thermal state of the fluid. For heat absorption, the same situation is revealed for the temperature of the fluid. The nanoparticle volume frac-

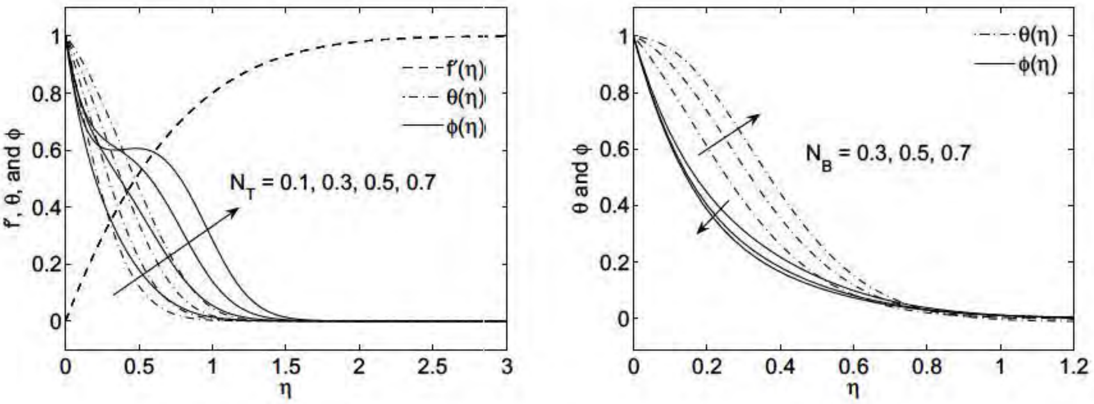

(a) **(b)**

Figure 4.2: The distributions of f', θ and ϕ for different values of: (a) N_T when $N_B = 0.2$; (b) N_B when $N_T = 0.1$; with $m = 0.0909$, $\delta = 0.2$, $F_w = 0.5$, $\xi = 1$ and $\text{Ln} = 5$

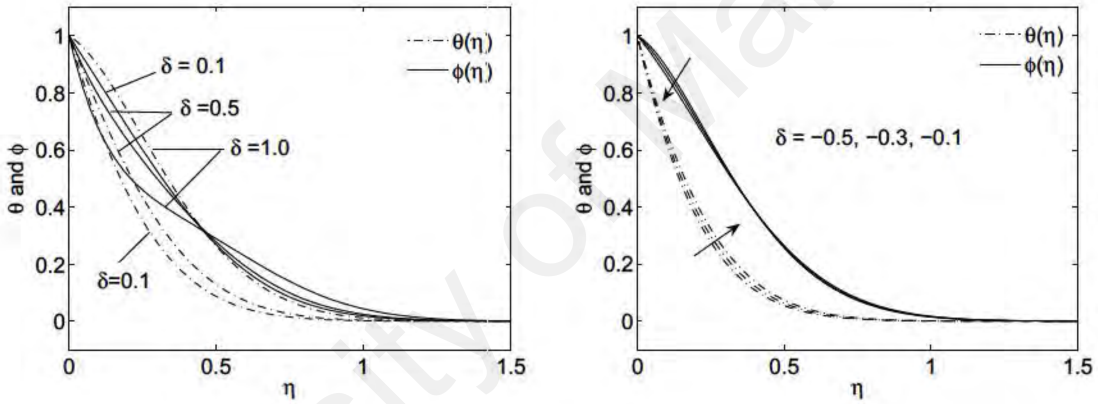

(a) **(b)**

Figure 4.3: The temperature,θ and nanoparticle volume fraction,ϕ for various values of (a) heat generation ($\delta > 0$) and; (b) heat absorption ($\delta < 0$); when $m = 0.0909$, $N_T = N_B = 0.1$, $F_w = 0.5$, $\xi = 1$ and $\text{Ln} = 5$

tion profile decreases with the increase of heat generation parameter when $\eta < 0.5$. On the other hand, when η is approximately greater than 0.5 ($\eta > 0.5$), the nanoparticle volume fraction profile increases on increasing the heat generation parameter. Fig. 4.3(b) shows that the nanoparticle volume fraction distribution decreases with the increase of heat absorption parameter. As we move away from the wedge surface, the nanoparticle volume fraction distribution is getting more closer to each other for the values of $\delta = -0.5, -0.3$ and -0.1. The internal heat absorption could not help to improve the distribution of the temperature and nanoparticle volume fraction.

The influence of suction on the velocity, temperature and nanoparticle volume fraction

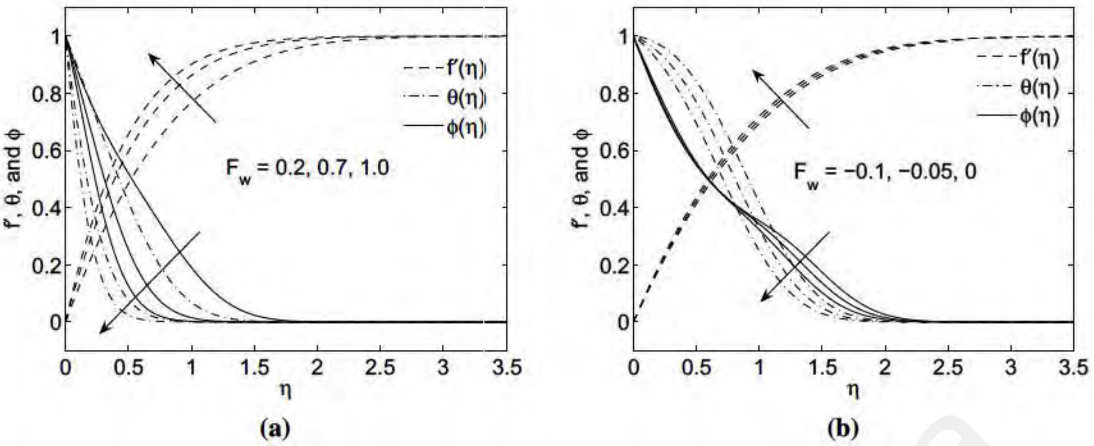

Figure 4.4: The distributions of f', θ and ϕ for different values of: (a) suction ($F_w > 0$) and; (b) injection ($F_w < 0$); when $m = 0.5$, $N_T = N_B = 0.1$, $\delta = 0.1$, $\xi = 1$ and $\mathrm{Ln} = 5$

profiles is displayed in the Fig. 4.4(a). It can be seen that the velocity profile increases on increasing the suction parameter. However, the opposite results are observed for temperature and nanoparticle volume fraction distributions as the suction parameter increases. Fig. 4.4(b) depicts the effect of injection on the velocity, temperature and nanoparticle volume fraction profiles. It is observed that the velocity profile increases on increasing the injection parameter. On the other hand, the temperature profile decreases with the increase of injection parameter. The nanoparticle volume fraction profile affects in very different manner when increasing the injection parameter. That is, there is no change in boundary layer when $\eta < 1$ and then the nanoparticle volume fraction boundary layer decreases on increasing F_w values.

4.2 The Effects of Thermal Radiation and Suction on Convective Heat Transfer of Nanofluid along a Wedge in the Presence of Heat Generation/Absorption

4.2.1 Mathematical Formulation

We consider the two-dimensional, steady, laminar boundary layer flow over a wedge immersed in nanofluid. The nanofluid is a dilute solid-liquid mixture with a uniform volume fraction of nanoparticle dispersed within the base fluid. The base fluid and nanoparticles are in thermal equilibrium. The effects of Brownian motion and thermophoresis are included for the nanofluid. The free stream velocity of the potential flow outside the boundary layer is denoted as U. Taking the above assumptions into consideration, the governing equations can be expressed as

$$\frac{\partial u}{\partial x}+\frac{\partial v}{\partial y}=0, \tag{4.12}$$

$$u\frac{\partial u}{\partial x}+v\frac{\partial u}{\partial y}=\nu\frac{\partial^2 u}{\partial y^2}+U\frac{dU}{dx}, \tag{4.13}$$

$$u\frac{\partial T}{\partial x}+v\frac{\partial T}{\partial y}=\alpha\frac{\partial^2 T}{\partial y^2}+\tau\left[D_B\frac{\partial S}{\partial y}\frac{\partial T}{\partial y}\left(\frac{D_T}{T_\infty}\right)\left(\frac{\partial T}{\partial y}\right)^2\right]+Q(T-T_\infty)-\frac{1}{\rho c}\frac{\partial q_r}{\partial y}, \tag{4.14}$$

$$u\frac{\partial S}{\partial x}+v\frac{\partial S}{\partial y}=D_B\frac{\partial^2 S}{\partial y^2}+\frac{D_T}{T_\infty}\frac{\partial^2 T}{\partial y^2}. \tag{4.15}$$

The radiative heat flux, $q_r=(-4\sigma/3k_1)(\partial T^4/\partial y)$ is employed accordance with the Rosseland approximation where σ and k_1 are the Stefan-Boltzmann constant and the Rosseland mean absorption coefficient, respectively. The fluid-phase temperature differences within the flow are assumed to be sufficiently small so that T^4 may be expressed as a linear function of temperature. This is done by expanding T^4 in a Taylor series about the free stream temperature T_∞ and neglecting the higher-order terms to yield $T^4 \cong 4T_\infty^3 T-3T_\infty^4$. Using this expression, the radiative heat flux in Eq. 4.14 becomes, $q_r=(-16\sigma T_\infty^3/3k_1)(\partial T/\partial y)$. The boundary conditions for the present problem are

$$\begin{gathered} u=0, \quad v=v_0, \quad T=T_w, \quad S=S_w, \quad \text{at} \quad y=0, \\ u\to U, \quad T\to T_\infty, \quad S\to S_\infty, \quad \text{as} \quad y\to\infty, \end{gathered} \tag{4.16}$$

where T_w and S_w are the constant temperature and nanoparticle volume fraction at the wedge wall, T_∞ is the ambient temperature, S_∞ is the nanoparticle volume fraction far away from the wedge and v_0 is the suction velocity at the wall. The continuity equation 4.12, can be satisfied automatically by defining the stream function such that $u=\partial\psi/\partial y$ and $v=-\partial\psi/\partial x$. Substituting Eq. 4.6 into Eqs. 4.13–4.15, we get the dimensionless ordinary differential equations.

$$f'''+ff''+\frac{2m}{m+1}\left(1-(f')^2\right)=0, \tag{4.17}$$

$$\left(1+\frac{4}{3R}\right)\theta''+\mathrm{Pr}f\theta'+N_B\phi'\theta'+N_T\left(\theta'\right)^2+\frac{2m}{m+1}\mathrm{Pr}\xi^2\delta\theta=0, \tag{4.18}$$

$$\phi'' + \Pr \mathrm{Ln} f \phi' + \frac{N_T}{N_B}\theta'' = 0, \tag{4.19}$$

with the following boundary conditions

$$\begin{aligned} f &= \frac{2}{m+1}F_w, \quad f' = 0, \quad \theta = 1, \quad \phi = 1, \quad \text{at} \quad \eta = 0, \\ f' &\to 1, \quad \theta \to 0, \quad \phi \to 0, \quad \text{as} \quad \eta \to \infty, \end{aligned} \tag{4.20}$$

where prime denotes the partial differentiation with respect to η, $R = k_1 k / 4\sigma T_\infty^3$ is the radiation parameter, $\Pr = \nu/\alpha$ is the Prandtl number, $N_B = \tau D_B(S_w - S_\infty)/\alpha$ is the Brownian parameter, $N_T = \tau D_T(T_w - T_\infty)/\alpha T_\infty$ is the thermophoresis parameter, $\delta = Q/ab^2$ is the heat generation/absorption parameter, $\mathrm{Ln} = \alpha/D_B$ is the nanofluid Lewis number, $F_w = -v_0 \mathrm{Re}_x^{1/2}/U$ is the suction parameter and $\mathrm{Re}_x = Ux/\nu$ is the Reynolds number. The main physical quantities of interest are the skin friction coefficient and the local Nusselt number, which are proportional to the values of $f''(0)$ and $-\theta(0)$, respectively. These physical parameters can be defined as $C_{fx} = \tau_w/\rho_f U^2$ and $Nu_x = xq_w/k(T_w - T_\infty)$, where

$$\tau_w = \mu \left(\frac{\partial u}{\partial y}\right)_{y=0}, \quad q_w = -k\left(\frac{\partial T}{\partial y}\right)_{y=0} - \frac{4\sigma}{3k_1}\left(\frac{\partial T^4}{\partial y}\right)_{y=0}, \tag{4.21}$$

are shear stress and heat flux, respectively. Using Eq. 4.6, the local skin friction coefficient and local Nusselt number can be written, respectively as

$$C_{fx}(\mathrm{Re}_x)^{1/2} = f''(0)\sqrt{\frac{m+1}{2}}, \quad Nu_x(\mathrm{Re}_x)^{-1/2} = -\theta'(0)\left(1 + \frac{4}{3R}\right)\sqrt{\frac{m+1}{2}}. \tag{4.22}$$

4.2.2 Results and Discussion

Fig. 4.5(a) shows the velocity, temperature and nanoparticle volume fraction profiles for various values of wedge angle parameter. The dimensionless velocity profile represents the fluid flow phenomenon toward the flow field. It can be observed that the fluid velocity increases as the wedge angle parameter increases and thus the hydrodynamic boundary layer becomes thin as m increases. It can be seen that both temperature and nanoparticle volume fraction profiles increase on increasing the values of m. The velocity, temperature and nanoparticle volume fraction profiles for various values of suction are demonstrated

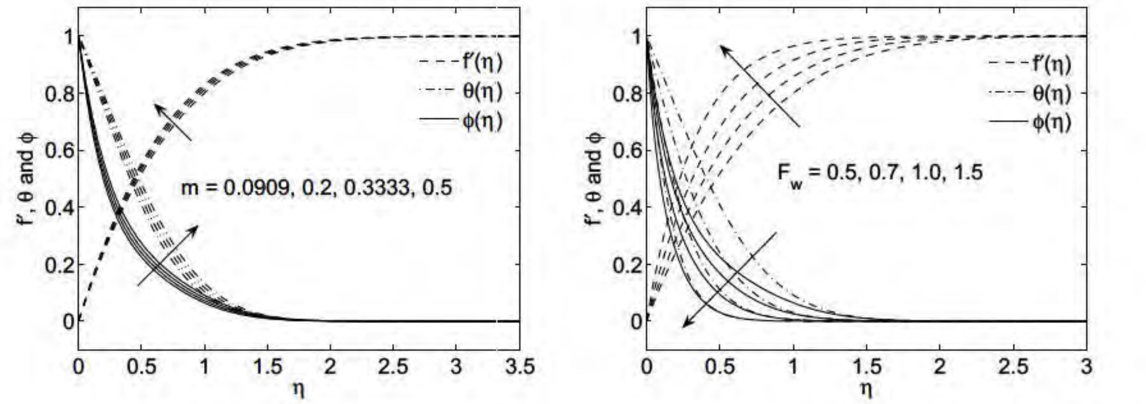

(a) (b)

Figure 4.5: The distributions of f', θ and ϕ for different values of: (a) m when $F_w = 0.5$; (b) F_w when $m = 0.0909$; with $N_T = N_B = 0.1$, $\delta = 0.5$, $R = 1$, $\xi = 1$ and $\mathrm{Ln} = 5$

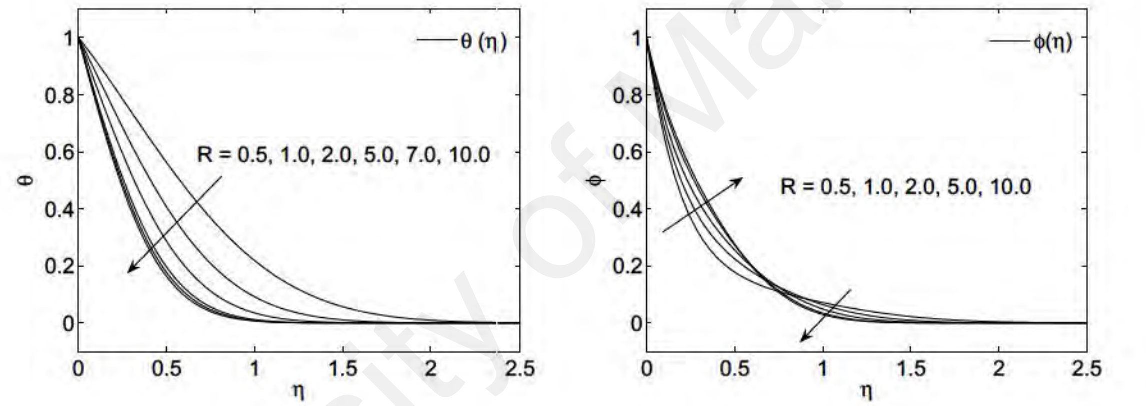

(a) (b)

Figure 4.6: The distributions of: (a) θ and; (b) ϕ; for different values of R when $m = 0.0909$, $F_w = 0.5$, $N_T = N_B = 0.1$, $\delta = 0.5$, $\xi = 1$ and $\mathrm{Ln} = 5$

in Fig. 4.5(b). The velocity profile increases and both temperature and nanoparticle volume fraction distributions decrease on increasing the value of F_w. These situations lead to reduce the hydrodynamic boundary layer thickness and the thermal boundary layer thickness.

Figs. 4.6(a) and 4.6(b) display the effect of thermal radiation on temperature and nanoparticle volume fraction distributions, respectively. The temperature profile decreases on increasing the thermal radiation parameter. Meanwhile, from the Fig. 4.6(b), we observed that the nanoparticle volume fraction profile exhibits different behaviour before and after certain points of η. For $\eta < 0.7$ the nanoparticle volume fraction distribution increases and after that point it decreases. It is worth mentioning here that the thermal

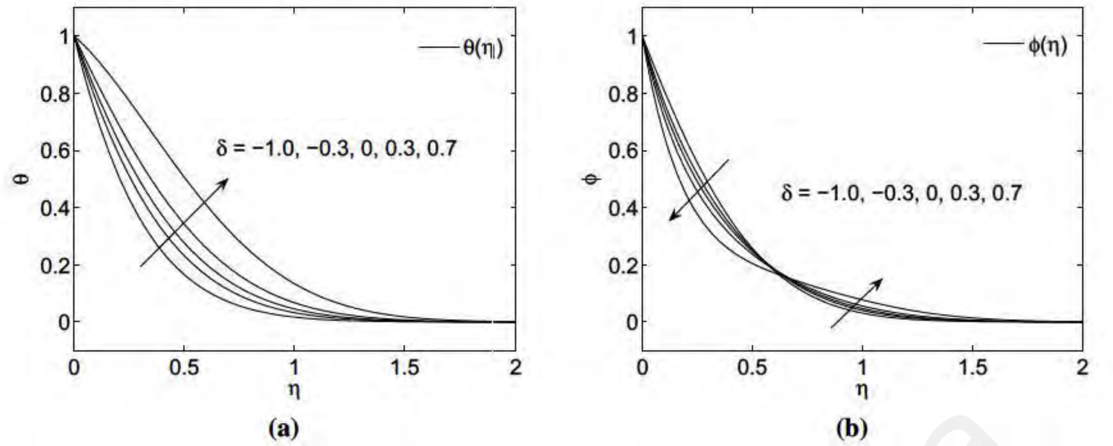

Figure 4.7: The distributions of: (a) θ and; (b) ϕ; for different values of δ when $m = 0.0909$, $F_w = 0.5$, $N_T = N_B = 0.1$, $R = 1$, $\xi = 1$ and $\mathrm{Ln} = 5$

radiation parameter doesn't cause any significant effect on the velocity of the fluid.

Figs. 4.7(a) and 4.7(b) present the effect of heat generation/absorption on the temperature and nanoparticle volume fraction profiles, respectively. The temperature profile increases on increasing the heat generation/absorption parameter. Increasing the value of δ causes the boundary layer thickness to decrease significantly as seen in Fig. 4.7(a). We observed two different types of behaviour for the nanoparticle volume profile on increasing δ along the domain. That is, ϕ decreases on increasing δ up to $\eta = 0.6$ and then we observed the opposite trend in ϕ.

Brownian motion is a random motion of particles suspended in the fluid which results from their collision with the atoms or molecules of the fluid. The effect of Brownian motion parameter on temperature and concentration profiles is shown in Fig. 4.8(a). As the Brownian motion parameter intensifies (N_B increases), the temperature profile and the thermal boundary layer thickness increase. This is due to the increase in the frequency of collisions of the fluid particles with nanoparticles. Meanwhile, the opposite behaviour is observed for the nanoparticle volume fraction profile. The nanoparticle volume fraction profile decreases as the Brownian motion parameter increases. This situation shows the weakening of nanoparticle volume fraction boundary layer thickness. Fig. 4.8(b) shows that, as the thermophoresis parameter increases, both the temperature and nanoparticle volume fraction profiles increase. The influence of thermophoresis on temperature distribution has similar effect with wedge angle parameter, heat generation/absorption and

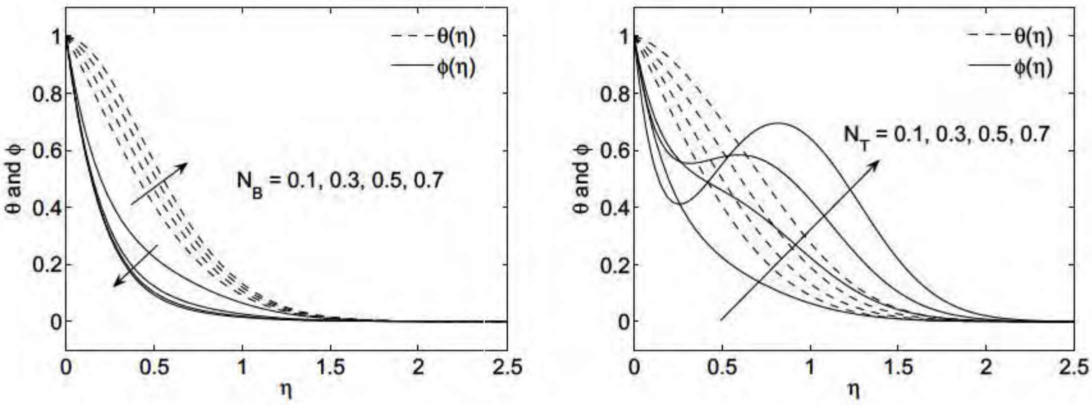

(a) (b)

Figure 4.8: The distributions of θ and ϕ for different values of: (a) N_B when $N_T = 0.1$; (b) N_T when $N_B = 0.1$; with $m = 0.0909$, $F_w = 0.5$, $\delta = 0.5$, $R = 1$, $\xi = 1$ and $\mathrm{Ln} = 5$

Brownian motion parameters. That is, the increases in the value of N_T cause the thermal boundary layer thickness to increase significantly. As the thermophoresis strengthen i.e for $N_T = 0.7$, the nanoparticle volume fraction curve drops quickly for $\eta < 0.3$ and started rising for certain range of η i.e for $0.3 < \eta < 0.9$. However, it slipped back after $\eta > 0.9$ and continued declining and finally converges to 0 as $\eta \to \infty$. It can be concluded that, the nanoparticle volume fraction profile decreases with thermophoresis effect. The nanoparticle volume fraction profile behaves in different manner near the plate and near the free stream which can be seen from the Figs. 4.6(b), 4.7(b) and 4.8(b).

CHAPTER 5: CONVECTIVE FLOW AND HEAT TRANSFER OF HEAT GENERATING NANOFLUID OVER A WEDGE WITH SUCTION AND CHEMICAL REACTION

This chapter has undertaken to discuss the effects of first-order chemical reaction, heat generation or absorption and suction on boundary layer flow of nanofluid past a wedge. The influence of wedge angle parameter, thermophoresis, Dufour and Soret type diffusivity are also included.

5.1 Mathematical Formulation

We consider the two-dimensional, steady, laminar boundary layer flow of nanofluid over a wedge with heat and mass transfer in the presence of heat generation/absorption. The velocity components u and v are associated along the x-axis and y-axis, respectively as depicted in the Fig. 3.2. The first-order chemical reaction is taking place in the flow which moves with the free stream velocity, U. The total angle of the wedge is denoted as $\Omega = \beta\pi$, where β is the Hartree pressure gradient. T_w and C_w are the constant temperature and solutal concentration at the wedge wall, T_∞ is the ambient temperature and C_∞ is the solutal concentration of the fluid far away from the wedge. The nanofluid is a dilute solid-liquid mixture with a uniform volume fraction of nanoparticle dispersed within the base fluid. The base fluid and nanoparticles are in thermal equilibrium. The suction velocity on the wall is considered. Taking the above assumptions into consideration, the governing equations describing momentum, energy and solutal concentration can be written as

$$\frac{\partial u}{\partial x} + \frac{\partial v}{\partial y} = 0, \tag{5.1}$$

$$u\frac{\partial u}{\partial x} + v\frac{\partial u}{\partial y} = \nu\frac{\partial^2 u}{\partial y^2} + U\frac{dU}{dx}, \tag{5.2}$$

$$u\frac{\partial T}{\partial x} + v\frac{\partial T}{\partial y} = \alpha\frac{\partial^2 T}{\partial y^2} + \tau\left(\frac{D_T}{T_\infty}\right)\left(\frac{\partial T}{\partial y}\right)^2 + D_{TC}\frac{\partial^2 C}{\partial y^2} + Q(T - T_\infty), \tag{5.3}$$

$$u\frac{\partial C}{\partial x} + v\frac{\partial C}{\partial y} = D_S\frac{\partial^2 C}{\partial y^2} + D_{CT}\frac{\partial^2 T}{\partial y^2} - K_0(C - C_\infty), \tag{5.4}$$

where K_0 is the chemical reaction coefficient. The boundary conditions for Eqs. 5.1–5.4 are expressed as:

$$
\begin{aligned}
u = 0, \quad v = v_0, \quad T = T_w, \quad C = C_w, \quad \text{at} \quad y = 0, \\
u \to U, \quad T \to T_\infty, \quad C \to C_\infty, \quad \text{as} \quad y \to \infty,
\end{aligned} \tag{5.5}
$$

The mathematical analysis of the problem is simplified by introducing the following quantities:

$$
\eta = y\sqrt{\frac{(m+1)U}{2\nu x}}, \quad \psi = f(\eta)\sqrt{\frac{2U\nu x}{m+1}}, \quad \theta(\eta) = \frac{T-T_\infty}{T_w-T_\infty}, \quad \gamma(\eta) = \frac{C-C_\infty}{C_w-C_\infty}, \tag{5.6}
$$

The stream function ψ is defined as $u = \partial\psi/\partial y$ and $v = -\partial\psi/\partial x$, which automatically satisfied the continuity Eq. 5.1. Therefore, upon using these variables, the governing Eqs. 5.2–5.4 can be written as

$$
f''' + ff'' + \frac{2m}{m+1}\left(1-(f')^2\right) = 0, \tag{5.7}
$$

$$
\theta'' + \mathrm{Pr} f\theta' + N_T\left(\theta'\right)^2 + N_{TC}\gamma'' + \frac{2m}{m+1}\mathrm{Pr}\xi^2\delta\theta = 0, \tag{5.8}
$$

$$
\gamma'' + \mathrm{PrLe} f\gamma' + N_{CT}\ \mathrm{Le}\theta'' + \frac{2m}{m+1}\mathrm{PrLe}\xi^2 K^*\gamma = 0, \tag{5.9}
$$

with the corresponding boundary conditions

$$
\begin{aligned}
f = \frac{2}{m+1}F_w, \quad f' = 0, \quad \theta = 1, \quad \gamma = 1, \quad \text{at} \quad \eta = 0, \\
f' \to 1, \quad \theta \to 0, \quad \gamma \to 0, \quad \text{as} \quad \eta \to \infty,
\end{aligned} \tag{5.10}
$$

where prime denotes the partial differentiation with respect to η. Here, $N_T = \tau D_T(T_w - T_\infty)/\alpha T_\infty$ is the thermophoresis parameter, $N_{TC} = D_{TC}(C_w - C_\infty)/\alpha(T_w - T_\infty)$ is the Dufour-type parameter, $N_{CT} = D_{CT}(T_w - T_\infty)/\alpha(C_w - C_\infty)$ is the Soret-type parameter, $\mathrm{Pr} = \nu/\alpha$ is the Prandtl number, $\mathrm{Le} = \alpha/D_S$ is the Lewis number, $\delta = Q/ab^2$ is the heat generation/absorption parameter, $K^* = K_0/ab^2$ is the chemical reaction parameter, $F_w = -v_0\mathrm{Re}_x^{1/2}/U$ is the suction parameter and $\mathrm{Re}_x = Ux/\nu$ is the Reynolds number.

The expression of local skin-friction coefficient, local Nusselt number and local Sherwood number are given by

$$C_{fx} = \frac{\tau_w}{\rho_f U^2}, \quad Nu_x = \frac{xq_w}{k(T_w - T_\infty)}, \quad Sh_x = \frac{xq_m}{D_B(C_w - C_\infty)}, \tag{5.11}$$

where $\tau_w = \mu \left(\frac{\partial u}{\partial y}\right)_{y=0}$, $q_w = -k \left(\frac{\partial T}{\partial y}\right)_{y=0}$ and $q_m = -D_B \left(\frac{\partial C}{\partial y}\right)_{y=0}$ are shear stress, heat flux and mass flux, respectively. Using Eq. 5.6, the local skin friction coefficient, local Nusselt number and local Sherwood number in dimensionless scale are

$$C_{fx}\sqrt{\mathrm{Re}_x} = f''(0)\sqrt{\frac{m+1}{2}}, \quad \frac{Nu_x}{\sqrt{\mathrm{Re}_x}} = -\theta'(0)\sqrt{\frac{m+1}{2}}, \quad \frac{Sh_x}{\sqrt{\mathrm{Re}_x}} = -\gamma'(0)\sqrt{\frac{m+1}{2}}. \tag{5.12}$$

5.2 Results and Discussion

The impact of all physical parameters on the value of $f''(0)$, $-\theta'(0)$ and $-\gamma'(0)$ is given in Table 5.1. It is observed from Table 5.1 that the value of $f''(0)$ increases on increasing the wedge angle and suction parameters. The velocity gradient near the wedge surface is larger when suction is present and the wedge angle parameter increases. This result is consistent with the physical interpretation of the skin friction, which $f''(0)$ represents the velocity gradient at the wedge surface and is also related to the drag coefficient on the wall. However, the value of $f''(0)$ remains unchanged when the value of N_T, N_{TC}, N_{CT}, δ and K^* are changing because those parameters appear only in the energy and solutal concentration equations. The value of $-\theta'(0)$ shows an increasing pattern when the values of all the parameters are increasing except suction parameter. The value of $-\theta'(0)$ decreases on increasing the suction parameter. Therefore, the thermal boundary layer thickness reduces as the suction parameter increases. It is observed that the value of $-\gamma'(0)$ increases as the value of m increases. The value of $-\gamma'(0)$ decreases when N_T, N_{TC}, N_{CT}, δ, F_w and K^* increase as depicted in Table 5.1.

Fig. 5.1(a) shows the dimensionless velocity, temperature and solutal concentration profiles for different values of wedge angle parameter, m. The fluid velocity increases on increasing the values of wedge angle parameter. The results also show that the velocity profiles became steeper for larger values of wedge angle. In addition, the velocity profiles squeeze closer and closer to the surface of the wall, thus the hydrodynamic boundary layer

Table 5.1: The values of $f''(0)$, $-\theta'(0)$ and $-\gamma'(0)$ for various values of m, F_w, N_T, N_{TC}, N_{CT}, δ and K^* when $m = 0.0909$, $F_w = 0.5$ and Le $= 5$.

<table>
<tr><th>m</th><th>F_w</th><th>N_T</th><th>N_{TC}</th><th>N_{CT}</th><th>δ</th><th>K^*</th><th>$f''(0)$</th><th>$-\theta'(0)$</th><th>$-\gamma(0)$</th></tr>
<tr><td>0.0909</td><td rowspan="4">0.5</td><td rowspan="4">0.1</td><td rowspan="4">0.1</td><td rowspan="4">0.1</td><td rowspan="4">0.2</td><td rowspan="4">0.2</td><td>1.34053</td><td>3.25008</td><td>2.42073</td></tr>
<tr><td>0.2000</td><td>1.39035</td><td>2.94983</td><td>2.34354</td></tr>
<tr><td>0.3333</td><td>1.43445</td><td>2.65698</td><td>2.26229</td></tr>
<tr><td>0.5000</td><td>1.47391</td><td>2.37305</td><td>2.17555</td></tr>
<tr><td rowspan="4">0.5</td><td>0.3</td><td rowspan="4">0.1</td><td rowspan="4">0.1</td><td rowspan="4">0.1</td><td rowspan="4">0.2</td><td rowspan="4">0.2</td><td>1.04808</td><td>1.66310</td><td>2.46897</td></tr>
<tr><td>0.7</td><td>1.64951</td><td>4.80176</td><td>2.50337</td></tr>
<tr><td>0.9</td><td>1.97053</td><td>6.32726</td><td>2.61619</td></tr>
<tr><td>1.2</td><td>2.46814</td><td>8.58918</td><td>2.94566</td></tr>
<tr><td rowspan="3">0.0909</td><td rowspan="3">0.5</td><td>0.3</td><td rowspan="3">0.1</td><td rowspan="3">0.1</td><td rowspan="3">0.2</td><td rowspan="3">0.2</td><td rowspan="3">1.34053</td><td>2.17362</td><td>0.25197</td></tr>
<tr><td>0.5</td><td>1.43882</td><td>0.62505</td></tr>
<tr><td>0.7</td><td>0.93610</td><td>2.22326</td></tr>
<tr><td rowspan="3">0.0909</td><td rowspan="3">0.5</td><td rowspan="3">0.1</td><td>0.1</td><td rowspan="3">0.1</td><td rowspan="3">0.2</td><td rowspan="3">0.2</td><td rowspan="3">1.34053</td><td>3.25008</td><td>2.42073</td></tr>
<tr><td>0.3</td><td>1.44491</td><td>4.81450</td></tr>
<tr><td>0.5</td><td>0.52777</td><td>5.11516</td></tr>
<tr><td rowspan="3">0.0909</td><td rowspan="3">0.5</td><td rowspan="3">0.1</td><td rowspan="3">0.1</td><td>0.3</td><td rowspan="3">0.2</td><td rowspan="3">0.2</td><td rowspan="3">1.34053</td><td>1.37060</td><td>5.14912</td></tr>
<tr><td>0.5</td><td>0.90375</td><td>5.33196</td></tr>
<tr><td>0.7</td><td>0.58135</td><td>5.38980</td></tr>
<tr><td rowspan="6">0.0909</td><td rowspan="6">0.5</td><td rowspan="6">0.1</td><td rowspan="6">0.1</td><td rowspan="6">0.1</td><td>-0.6</td><td rowspan="6">0.2</td><td rowspan="6">1.34053</td><td>4.60890</td><td>1.06391</td></tr>
<tr><td>-0.4</td><td>4.31299</td><td>1.35946</td></tr>
<tr><td>-0.2</td><td>3.99280</td><td>1.67933</td></tr>
<tr><td>0.4</td><td>2.80191</td><td>2.86763</td></tr>
<tr><td>0.8</td><td>1.59676</td><td>4.06722</td></tr>
<tr><td>1.0</td><td>0.64325</td><td>5.01408</td></tr>
<tr><td rowspan="3">0.0909</td><td rowspan="3">0.5</td><td rowspan="3">0.1</td><td rowspan="3">0.1</td><td rowspan="3">0.1</td><td rowspan="3">0.2</td><td>0.5</td><td rowspan="3">1.34053</td><td>3.16473</td><td>3.21696</td></tr>
<tr><td>1.0</td><td>3.06087</td><td>4.28092</td></tr>
<tr><td>1.3</td><td>3.01328</td><td>4.81374</td></tr>
</table>

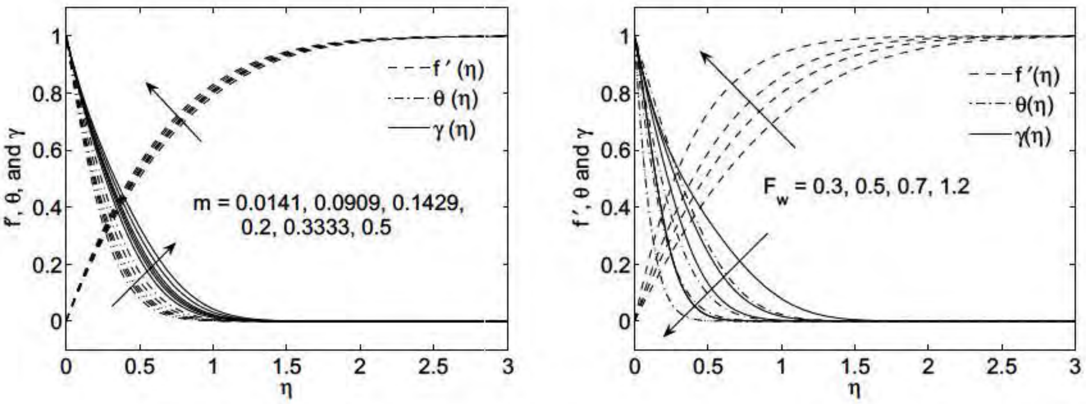

(a) (b)

Figure 5.1: The distributions of f', θ and γ for different values of: (a) m when $F_w = 0.5$; (b) F_w when $m = 0.0909$; with $N_T = N_{TC} = N_{CT} = 0.1$, $\delta = K^* = 0.2$ and $\mathrm{Le} = 5$

becomes thin as m increases. It can be observed from Fig. 5.1(a) that both temperature and solutal concentration profiles increase on increasing wedge angle parameter. Fig. 5.1(b) displays the velocity, temperature and solutal concentration profiles against η for various values of suction parameter, F_w. It can be seen from the Fig. 5.1(b) that the velocity of the fluid increases with an increase of suction velocity. Therefore, the thicknesses of the hydrodynamic and thermal boundary layers are found to decrease with the increase of suction parameter. It is clear that increasing the suction parameter tends to decrease the temperature of the fluid as well as the solutal concentration. The imposition of suction at wedge surface reduces the region of viscous domination close to the wall, which causes decreasing in the fluid's temperature as well as the solutal concentration profiles.

The influences of Dufour, thermophoresis, Soret and chemical reaction parameters on temperature and solutal concentration profiles are depicted in Figs. 5.2((a)−(d)), respectively. The temperature profile shows an increasing pattern when all parameters increase. This means that the N_{TC}, N_T and N_{CT} parameters work to increase the values of temperature in the fluid and then decrease the gradient at the wall. In addition, the thickness of thermal boundary layer increases on increasing the value of N_{TC}, N_T and N_{CT} parameters. The solutal concentration profile shows a decreasing behaviour when the Dufour parameter increases but the opposite results are obtained for thermophoresis and Soret parameters. This fact indicates that the Dufour parameter reduces the nanoparticle diffusion while the thermophoresis and Soret parameters enhance the nanoparticle diffusion.

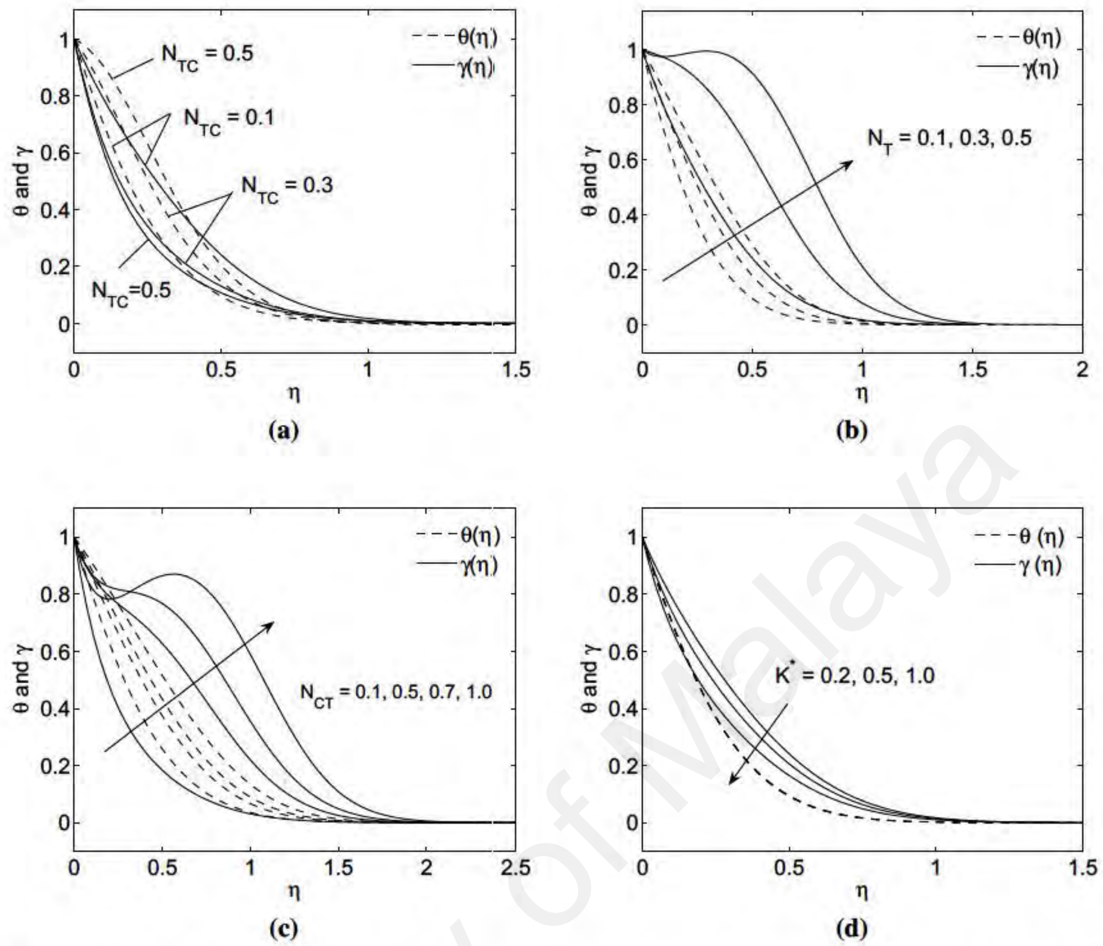

Figure 5.2: The distributions of θ and γ with $m = 0.0909$, $\delta = 0.2$, $F_w = 0.5$ and $\mathrm{Le} = 5$ for different values of: (a) N_{TC} when $K^* = 0.2$, $N_T = N_{CT} = 0.1$; (b) N_T when $K^* = 0.2$, $N_{TC} = N_{CT} = 0.1$; (c) N_{CT} when $K^* = 0.2$, $N_T = N_{TC} = 0.1$; and, (d) K^* when $N_T = N_{TC} = N_{CT} = 0.1$

Fig. 5.2(d) depicts the influence of chemical reaction on the dimensionless temperature and solutal concentration profiles. It is obvious that an increase in the chemical reaction parameter results in the decreasing of solutal concentration profile. The distribution of solutal concentration becomes weak in the presence of chemical reaction. So, the solutal concentration boundary layer becomes thin as the chemical reaction parameter increases. From Fig. 5.2(d), the chemical reaction parameter influences the solutal concentration field, however, it has a minor effect on temperature profile. It is worth mentioning here that, the large values of K^* show small changes on temperature field.

Figs. 5.3(a) and 5.3(b) present the effect of heat generation/absorption for temperature and solutal concentration profiles, respectively. The positive values of δ indicate heat generation (source) and the negative values of δ correspond to heat absorption (sink). It

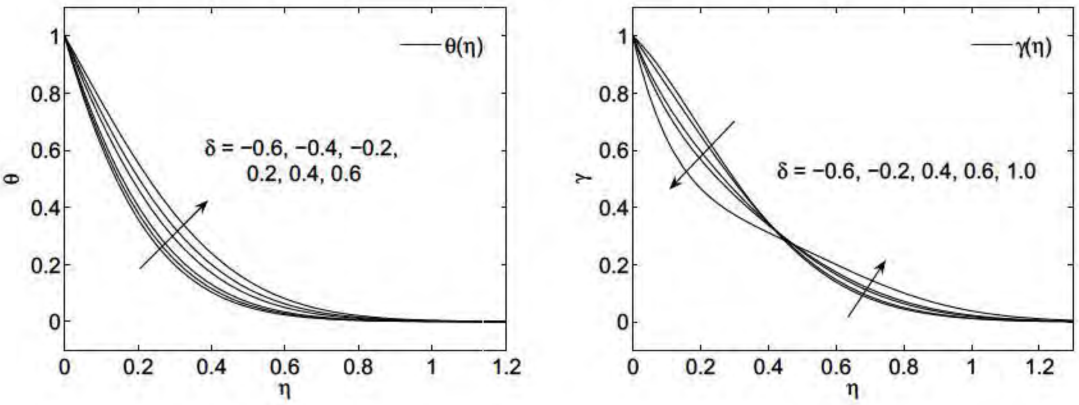

(a) **(b)**

Figure 5.3: Influence of δ on: (a) θ; and (b) γ; when $m = 0.0909$, $N_T = N_{TC} = N_{CT} = 0.1$, $K^* = 0.2$, $F_w = 0.5$ and Le $= 5$

is noted that the temperature of nanofluid increases with the increase of δ. Therefore, the thermal boundary layer thickness becomes high on increasing the heat source/sink parameter. This is due to the fact that heat generation causes the thermal boundary layer becomes thicker and the temperature of the fluid to increases. For the case of heat absorption, the opposite effects are obtained. The solutal concentration profile decreases with an increase of δ when $\eta < 0.5$. However, when η is approximately greater than 0.5 ($\eta > 0.5$), the solutal concentration of the nanoparticles shows an increasing pattern.

CHAPTER 6: DOUBLE DIFFUSIVE CONVECTIVE FLOW OF NANOFLUID OVER A MOVING WEDGE WITH SUCTION, SORET AND DUFOUR EFFECTS

Double diffusive convection occurs when the fluid is subjected by two different density gradients triggered by local variations of temperature and concentration. Diffusion of matter caused by temperature gradient is known as thermophoresis or the Soret effect while diffusion of heat caused by concentration gradient is called the Dufour effect. The aim of the present numerical study is to investigate the Soret and Dufour effects on double diffusive convective boundary layer flow of nanofluid past a moving wedge in the presence of suction.

6.1 Mathematical Formulation

Consider the two-dimensional, steady, incompressible, laminar flow of nanofluid with heat and mass transfer over a moving wedge. The coordinate system is chosen such that x-axis is along the surface of the wedge and y-axis is normal to the surface of the wedge (see Fig. 3.2 for schematic of the physical system). The ambient values attained as y tends to infinity of the temperature T, the solutal concentration C and the nanoparticle volume fraction S are denoted by T_∞, C_∞ and S_∞, respectively. The constant temperature, solutal concentration and nanoparticle volume fraction at the wedge wall are denoted as T_w, C_w and S_w, respectively. The wedge at $y = 0$ is moved in the x-direction with velocity U_w. The nanofluid is a dilute solid-liquid mixture with a uniform volume fraction of nanoparticle dispersed within the base fluid. The base fluid and nanoparticles are in thermally equilibrium. Following Kuznetsov & Nield (2011), the governing equations for total mass, momentum, thermal energy, solute and nanoparticles can be expressed as

$$\frac{\partial u}{\partial x} + \frac{\partial v}{\partial y} = 0, \tag{6.1}$$

$$u\frac{\partial u}{\partial x} + v\frac{\partial u}{\partial y} = \nu\frac{\partial^2 u}{\partial y^2} + U\frac{dU}{dx}, \tag{6.2}$$

$$u\frac{\partial T}{\partial x}+v\frac{\partial T}{\partial y}=\alpha\frac{\partial^2 T}{\partial y^2}+\tau\left[D_B\frac{\partial S}{\partial y}\frac{\partial T}{\partial y}+\left(\frac{D_T}{T_\infty}\right)\left(\frac{\partial T}{\partial y}\right)^2\right]+D_{TC}\frac{\partial^2 C}{\partial y^2}, \tag{6.3}$$

$$u\frac{\partial S}{\partial x}+v\frac{\partial S}{\partial y}=D_B\frac{\partial^2 S}{\partial y^2}+\left(\frac{D_T}{T_\infty}\right)\frac{\partial^2 T}{\partial y^2}, \tag{6.4}$$

$$u\frac{\partial C}{\partial x}+v\frac{\partial C}{\partial y}=D_S\frac{\partial^2 C}{\partial y^2}+D_{CT}\frac{\partial^2 T}{\partial y^2}. \tag{6.5}$$

The boundary conditions are expressed as:

$$\begin{gathered} u=U_w, \quad v=v_0, \quad T=T_w, \quad C=C_w, \quad S=S_w \quad \text{at} \quad y=0, \\ u\to U, \quad T\to T_\infty, \quad C\to C_\infty, \quad S\to S_\infty, \quad \text{as} \quad y\to\infty. \end{gathered} \tag{6.6}$$

The velocity of the moving wedge is denoted by $U_w = b_w x^m$ where b_w is a constant, $U_w > 0$ for a stretching wedge in the same direction as the external flow, $U_w < 0$ for a shrinking wedge in an opposite direction to the outer flow and $U_w = 0$ corresponds to a static wedge.

The mathematical analysis of the problem is simplified by introducing the following quantities:

$$\begin{gathered} \eta=y\sqrt{\frac{(m+1)U}{2\nu x}}, \quad \psi=f(\eta)\sqrt{\frac{2U\nu x}{m+1}}, \quad \theta(\eta)=\frac{T-T_\infty}{T_w-T_\infty}, \\ \gamma(\eta)=\frac{C-C_\infty}{C_w-C_\infty}, \quad \phi(\eta)=\frac{S-S_\infty}{S_w-S_\infty}. \end{gathered} \tag{6.7}$$

The stream function $\psi(x,y)$ is defined by $u=\partial\psi/\partial y$ and $v=-\partial\psi/\partial x$ such that the continuity Eq. 6.1 is automatically satisfies. Therefore using Eq. 6.7, Eqs. 6.2−6.5 can be written as

$$f'''+ff''+\frac{2m}{m+1}\left(1-(f')^2\right)=0, \tag{6.8}$$

$$\theta''+\Pr f\theta'+N_B\phi'\theta'+N_T\left(\theta'\right)^2+N_{TC}\gamma''=0, \tag{6.9}$$

$$\gamma''+\Pr \mathrm{Le} f\gamma'+N_{CT}\,\mathrm{Le}\theta''=0, \tag{6.10}$$

$$\phi''+\Pr \mathrm{Ln} f\phi'+\frac{N_T}{N_B}\theta''=0, \tag{6.11}$$

where primes indicate as the differentiation with respect to η, $\Pr=\nu/\alpha$ is the Prandtl number, $N_B=\tau D_B(S_w-S_\infty)/\alpha$ is the Brownian parameter, $N_T=\tau D_T(T_w-T_\infty)/\alpha T_\infty$

is the thermophoresis parameter, $N_{TC} = D_{TC}(C_w - C_\infty)/\alpha(T_w - T_\infty)$ is the Dufour-type parameter, $N_{CT} = D_{CT}(T_w - T_\infty)/\alpha(C_w - C_\infty)$ is the Soret-type parameter, $\mathrm{Le} = \alpha/D_S$ is the Lewis number and $\mathrm{Ln} = \alpha/D_B$ is the nanofluid Lewis number. The boundary conditions 6.6 become

$$\begin{aligned} &f = \frac{2}{m+1}F_w, \quad f' = \lambda, \quad \theta = 1, \quad \gamma = 1, \quad \phi = 1 \quad \text{at} \quad \eta = 0, \\ &f' \to 1, \quad \theta \to 0, \quad \gamma \to 0, \quad \phi \to 0, \quad \text{as} \quad \eta \to \infty, \end{aligned} \tag{6.12}$$

where $F_w = -v_0 \mathrm{Re}_x^{1/2}/U$ is the suction parameter, $\mathrm{Re}_x = Ux/\nu$ is the Reynolds number and $\lambda = U_w/U$ is the moving wedge parameter.

The local skin friction coefficient C_{fx}, local Nusselt number Nu_x and local Sherwood number Sh_x are of special significance for this type of flow, heat and mass transfer situations. These physical parameters can be defined as

$$C_{fx} = \frac{\tau_w}{\rho_f U^2}, \quad Nu_x = \frac{x q_w}{k(T_w - T_\infty)}, \quad Sh_x = \frac{x q_m}{D_B(C_w - C_\infty)}, \tag{6.13}$$

where $\tau_w = \mu\left(\frac{\partial u}{\partial y}\right)_{y=0}$, $q_w = -k\left(\frac{\partial T}{\partial y}\right)_{y=0}$ and $q_m = -D_B\left(\frac{\partial C}{\partial y}\right)_{y=0}$ are shear stress, heat flux and mass flux, respectively. Using Eq. 6.7, the local skin friction coefficient, local Nusselt number and local Sherwood number can be written, respectively as

$$C_{fx}\sqrt{\mathrm{Re}_x} = f''(0)\sqrt{\frac{m+1}{2}}, \quad \frac{Nu_x}{\sqrt{\mathrm{Re}_x}} = -\theta'(0)\sqrt{\frac{m+1}{2}}, \quad \frac{Sh_x}{\sqrt{\mathrm{Re}_x}} = -\gamma'(0)\sqrt{\frac{m+1}{2}}. \tag{6.14}$$

6.2 Results and Discussion

Computational solutions are performed for the effects of all the thermophysical parameters and are illustrated in Figs. 6.1−6.8 These figures depict the influences of the various controlling parameters on dimensionless velocity, temperature, solutal concentration and nanoparticle volume fraction as well as local skin-friction coefficient, local Nusselt number and local Sherwood number.

Figs. 6.1(a) and 6.1(b) show the influence of wedge angle parameter, m on the dimensionless velocity, temperature, solutal concentration and nanoparticle volume frac-

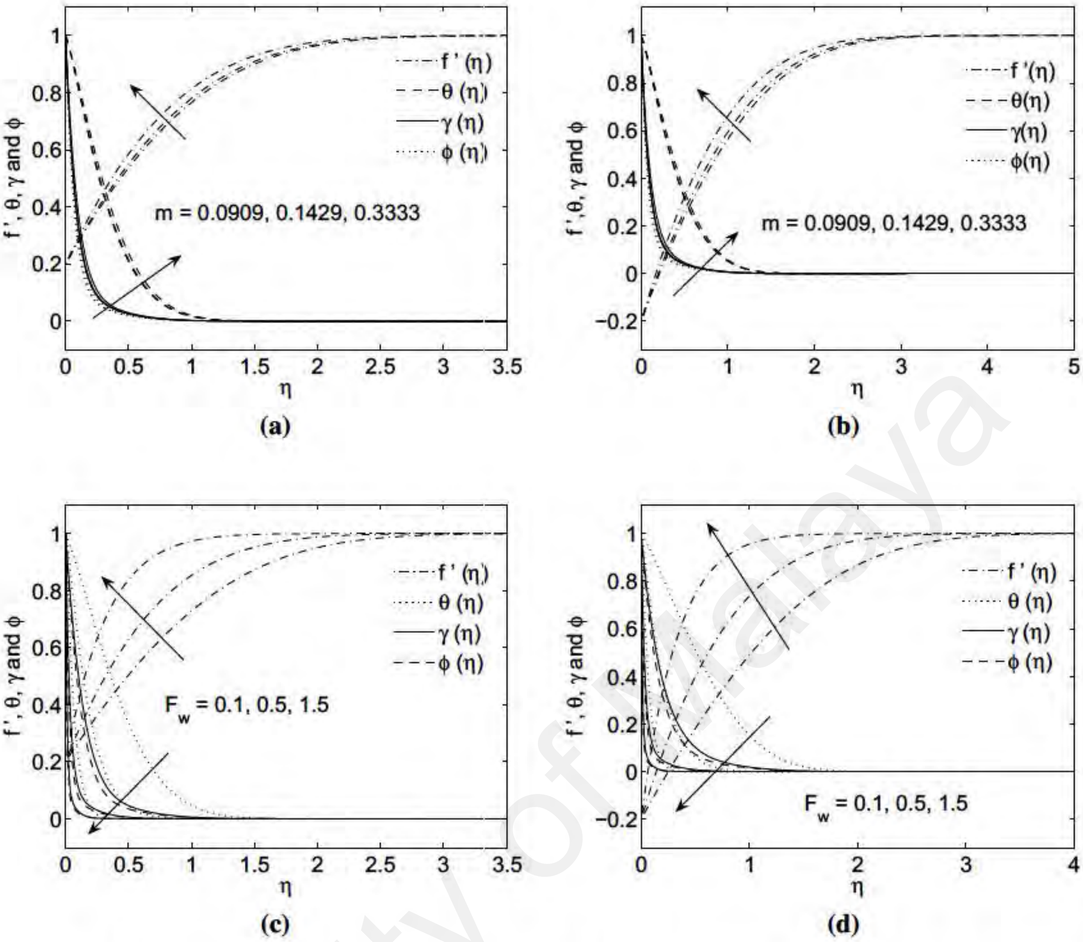

Figure 6.1: The distributions of f', θ, γ and ϕ for different values of: (a) m when $F_w = 0.2$, $\lambda = 0.2$; (b) m when $F_w = 0.2$, $\lambda = -0.2$; (c) F_w when $m = 0.0909$, $\lambda = 0.2$; (d) F_w when $m = 0.0909$, $\lambda = -0.2$; with $N_B = 0.2$, $N_T = N_{CT} = N_{TC} = 0.1$, Le $= 5$ and Ln $= 6$

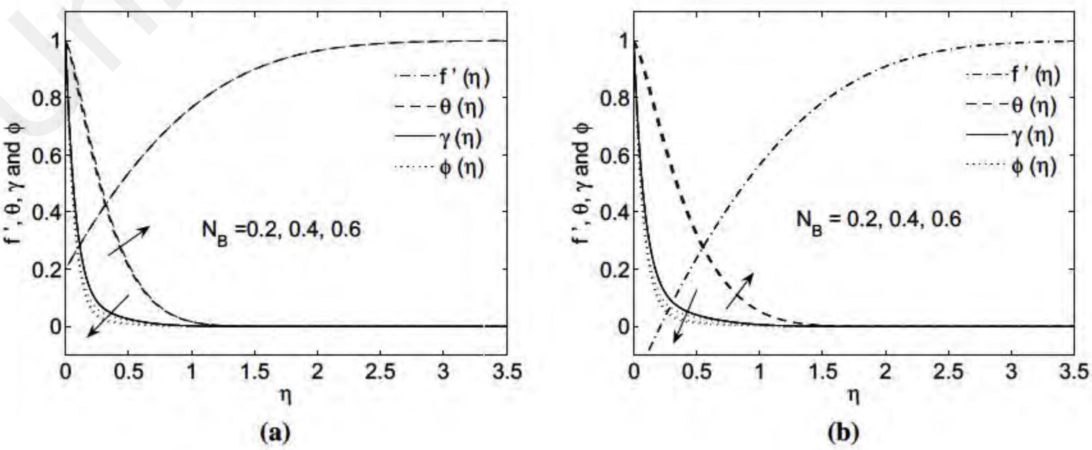

Figure 6.2: Influence of N_B on f', θ, γ and ϕ when: (a) $\lambda = 0.2$; (b) $\lambda = -0.2$; with $m = 0.0909$, $F_w = 0.2$, $N_T = N_{CT} = N_{TC} = 0.1$, Le $= 5$ and Ln $= 6$

tion profiles for the case of $\lambda = 0.2$ and $\lambda = -0.2$, respectively. Figs. 6.1(c) and 6.1(d) illustrate the influence of suction parameter F_w on all dimensionless fields when $\lambda = 0.2$ and $\lambda = -0.2$, respectively. All four figures show that the velocity profile increases as m and F_w increase for both values of $\lambda = 0.2$ and $\lambda = -0.2$. This means that the velocity profile move closer to the surface of the wedge and the hydrodynamic boundary layer decreases for larger values of m and F_w. The increases of wedge angle parameter, m causes an increase in temperature, solutal concentration and nanoparticle volume fraction profiles as depicted in Figs. 6.1(a) and 6.1(b). Furthermore, it can be seen from Figs. 6.1(c) and 6.1(d) that the imposition of suction (F_w) at the wedge surface reduces the region of viscous domination close to the wall, which causes decreasing in the fluid's temperature, solutal concentration and nanoparticle volume fraction distributions. Also, we observed that increasing of suction parameter results in the increasing of the shear stress on the wedge surface and causes the decrease in the thermal, solutal concentration and nanoparticle volume fraction boundary layer thickness.

The effect of Brownian motion parameter on various dimensionless profiles is shown in Figs. 6.2(a) and 6.2(b), respectively for both $\lambda = 0.2$ and $\lambda = -0.2$. Brownian motion is the random motion of nanoparticles within the base fluid and results from continuous collisions between the nanoparticles and the molecules of the base fluid. It is examined that the nanofluid velocity remains unchanged with increasing of N_B. The temperature profile is continued to increase by increasing the Brownian motion parameter for both values of λ. Meanwhile, the solutal concentration and nanoparticle volume fraction profiles decrease as N_B increases. These situations indicate that the Brownian motion parameter works to increase the thermal boundary layer thickness and decrease both the solutal concentration and nanoparticle volume fraction boundary layer thickness.

The dimensionless temperature, solutal concentration and nanoparticle volume fraction as a function of η for $\lambda = 0.2$ and $\lambda = -0.2$ are depicted in Figs. 6.3(a) and 6.3(b), respectively for various values of thermophoresis parameter, N_T. In present study, thermophoresis is assumed as the migration of nanoparticle in water due to nanoscopic temperature gradient. It is observed that an increase in N_T leads to enhance the temperature $\theta(\eta)$, solutal concentration $\gamma(\eta)$ and nanoparticle volume fraction $\phi(\eta)$ profiles within

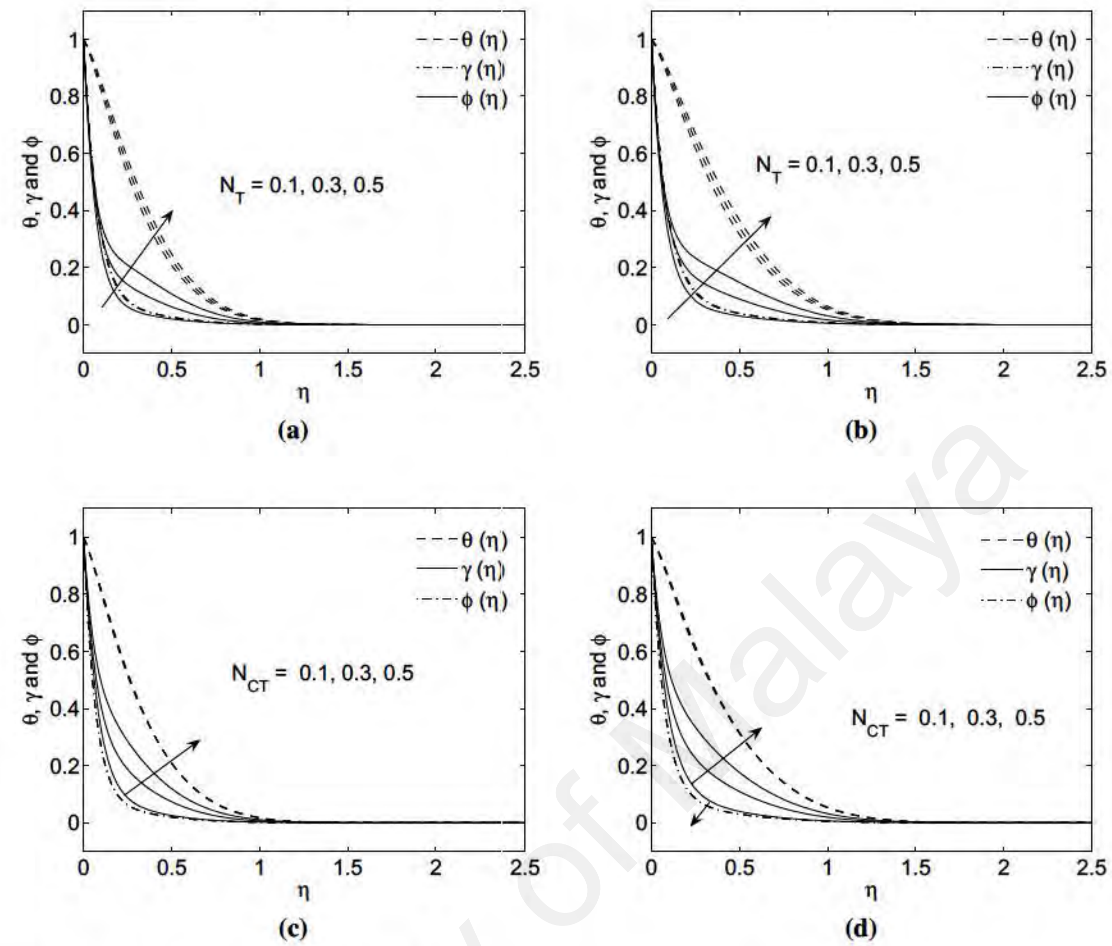

Figure 6.3: The distributions of θ, γ and ϕ for different values of: (a) N_T when $N_{CT} = 0.1$, $\lambda = 0.2$; (b) N_T when $N_{CT} = 0.1$, $\lambda = -0.2$; (c) N_{CT} when $N_T = 0.1$, $\lambda = 0.2$; (d) N_{CT} when $N_T = 0.1$, $\lambda = -0.2$; with $m = 0.0909$, $F_w = N_B = 0.2$, $N_{TC} = 0.1$, Le $= 5$ and Ln $= 6$

the boundary layer region. These situations indicate that the thermal, solutal concentration and volume fraction boundary layers thickness increase when increasing the value of N_T from 0.1 to 0.5. The ratio of the thermal diffusion coefficient and the normal diffusion coefficient is known as the Soret coefficient. The effect of Soret-type parameter, N_{CT} is illustrated in Figs. 6.3(c) and 6.3(d) for $\lambda = 0.2$ and $\lambda = -0.2$, respectively. For both values of $\lambda = 0.2$ and $\lambda = -0.2$, the distribution of nanofluid temperature and solutal concentration become strong as N_{CT} increases. In addition, the nanoparticle volume fraction boundary layer thickness is much thinner compared to thermal and solutal concentration boundary layer thickness.

Dufour effect is the inverse phenomenon to the Soret effect. It is the formation of a temperature gradient as the result of the mixing of different molecular species. Results

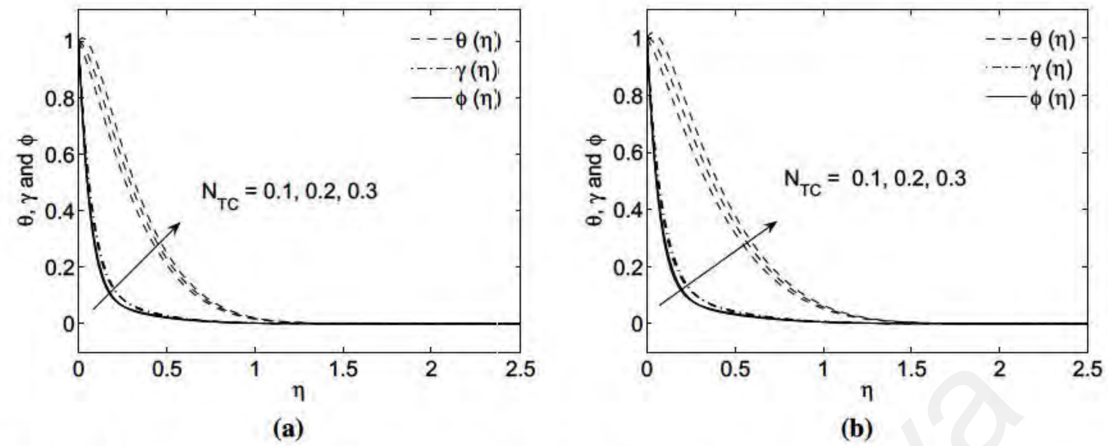

Figure 6.4: Influence of N_{TC} on θ, γ and ϕ when: (a) $\lambda = 0.2$; (b) $\lambda = -0.2$; with $m = 0.0909$, $F_w = N_B = 0.2$, $N_T = N_{CT} = 0.1$, Le $= 5$ and Ln $= 6$

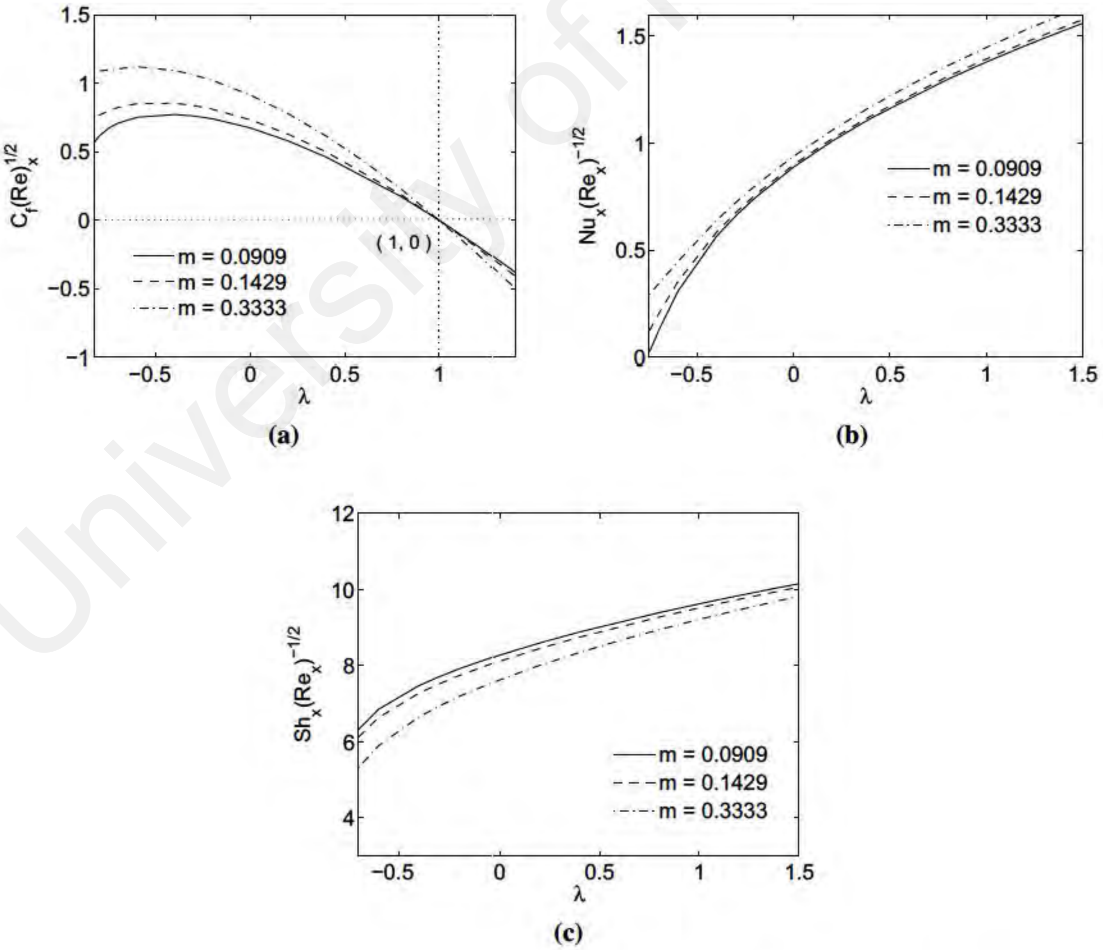

Figure 6.5: Variations of: (a) $C_{fx}(\mathrm{Re})_x^{1/2}$; (b) $Nu_x(\mathrm{Re})_x^{-1/2}$; (c) $Sh_x(\mathrm{Re})_x^{-1/2}$; for different values of m when $F_w = N_B = 0.2$, $N_T = N_{CT} = N_{TC} = 0.1$, Le $= 5$ and Ln $= 6$

for the effect of Dufour-type parameter, N_{TC} on dimensionless temperature, solutal concentration and nanoparticle volume fraction profiles are given in Fig. 6.4(a) for $\lambda = 0.2$. It can be seen that all three dimensionless quantities experience an increase when N_{TC} increases from 0.1 to 0.3. Fig. 6.4(b) shows the similarity solutions of $\theta(\eta)$, $\gamma(\eta)$ and $\phi(\eta)$ for $\lambda = -0.2$ with various values of N_{TC}. The graph follows the same pattern as in Fig. 6.4(a). As one would expect, the thickness of boundary layer for the nanoparticle volume fraction is smaller than the thermal and solutal concentration boundary layer thickness for both cases $\lambda = 0.2$ and $\lambda = -0.2$.

The variations of the local skin friction coefficient for various values of m with fixed values of other parameters is plotted in Fig. 6.5(a). It is observed that an increase in wedge angle parameter, m resulted in an increase in the local skin friction coefficient for $\lambda < 1$, while the reverse behaviour is noticed for $\lambda > 1$. In addition, the positive value of $C_{fx}(\mathrm{Re})_x^{1/2}$ is obtained when $\lambda < 1$ and when $\lambda > 1$, the opposite sign is yielded. This is agreed with the physical interpretation that there is a force that opposes the motion when the wedge moves through the nanofluid. The negative value of skin friction coefficient indicates that the drag force on the fluid is exerted by the moving wedge and the positive value implies the opposite. The variations of local Nusselt number and local Sherwood number for some values of m are depicted in Fig. 6.5(b) and 6.5(c), respectively. As the parameter m increases, the local Nusselt number increases. The reverse trend is seen in Fig. 6.5(c), that is, the local Sherwood number decreases on increasing the wedge angle parameter.

Fig. 6.6(a) presents the variation of local skin friction coefficient against the moving wedge parameter λ for different values of suction parameter, F_w. The skin friction coefficient increases with the increase of F_w for $\lambda < 1$ and it decreases for $\lambda > 1$. All values of $C_{fx}(\mathrm{Re})_x^{1/2}$ are negative as $\lambda > 1$ and decrease to more negativity with larger values of F_w. This negative tendency of skin friction coefficient indicates that the elastic effect will reduce the drag on the wedge wall. A similar trend is observed when the curves from Fig. 6.5(a) and Fig. 6.6(a) are compared. By comparing the curves for both Figs. 6.5(a) and 6.6(a), we noted that all curves are intersect at the point $(1,0)$, where the wedge moving parameter $\lambda = 1$, and the skin friction coefficient is equal to zero. Physically, the zero

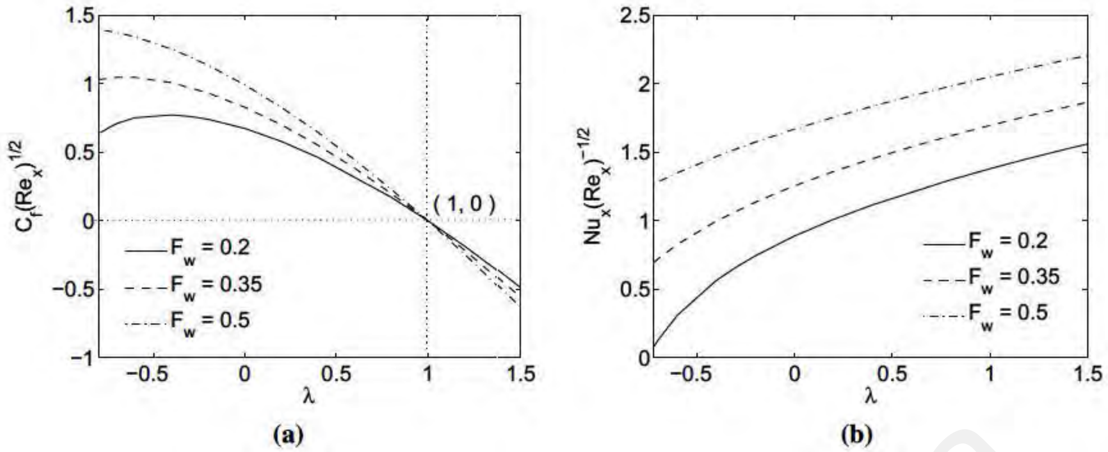

Figure 6.6: Variations of: (a) $C_{fx}(\mathrm{Re})_x^{1/2}$; (b) $Nu_x(\mathrm{Re})_x^{-1/2}$; for different values of F_w when $m = 0.0909$, $N_B = 0.2$, $N_T = N_{CT} = N_{TC} = 0.1$, $\mathrm{Le} = 5$ and $\mathrm{Ln} = 6$

value of skin friction coefficient means that in the absence of shear stress, the wedge and the fluid move with the same velocity. Therefore, the stress on any surface, anywhere in the fluid, can be expressed in terms of a single scalar field. Fig. 6.6(b) exhibits the variation of local Nusselt number for different values of suction parameter. From this figure, it is observed that the local Nusselt number increases with the increase in suction parameter, F_w and moving wedge parameter, λ.

The effect of Brownian motion parameter N_B on the local Nusselt number and Sherwood number is presented in Figs. 6.7(a) and 6.7(b), respectively with fixed values of other parameters. As stated by Buongiorno (2006), the Brownian motion is an important mechanism for nano size particles in nanofluid. The Brownian motion is assumed to enhance the heat transfer properties and promote heat conduction. The energy exchange rates increase due to the random movement (Brownian motion) of the nanoparticles. However, Brownian motion reduces the diffusion of nanoparticle. Therefore, it can be seen in Figs. 6.7(a) and 6.7(b) that with the increase in the values of N_B, a reduction in the local Nusselt number is noted whereas an increase in the local Sherwood number is noticed. Figs. 6.7(c) and 6.7(d) display the variations of the local Nusselt number and Sherwood number, respectively for different values of thermophoresis parameter, N_T. Thermophoresis parameter is also a vital mechanism of nanofluid in determining the heat diffusion and nanoparticle volume fraction in the boundary layer. Therefore this yields strong reduction in the local Nusselt number and an increase in local Sherwood number on increasing the

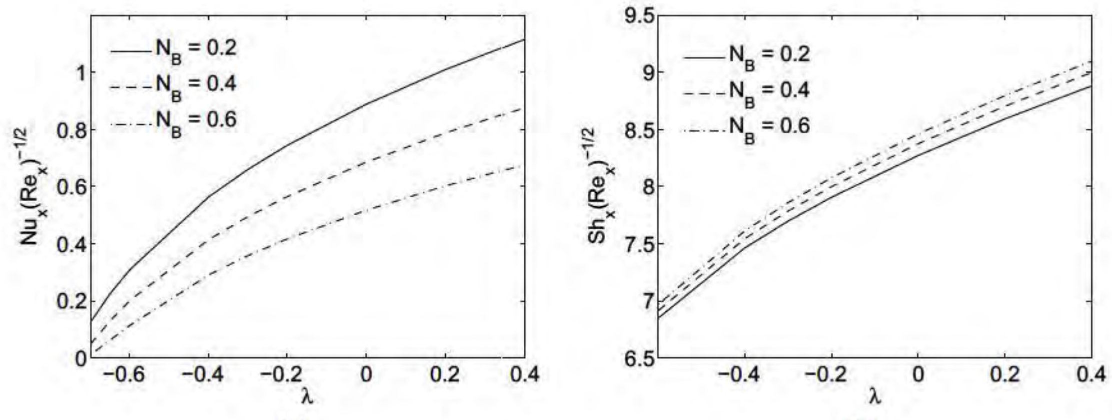

(a) **(b)**

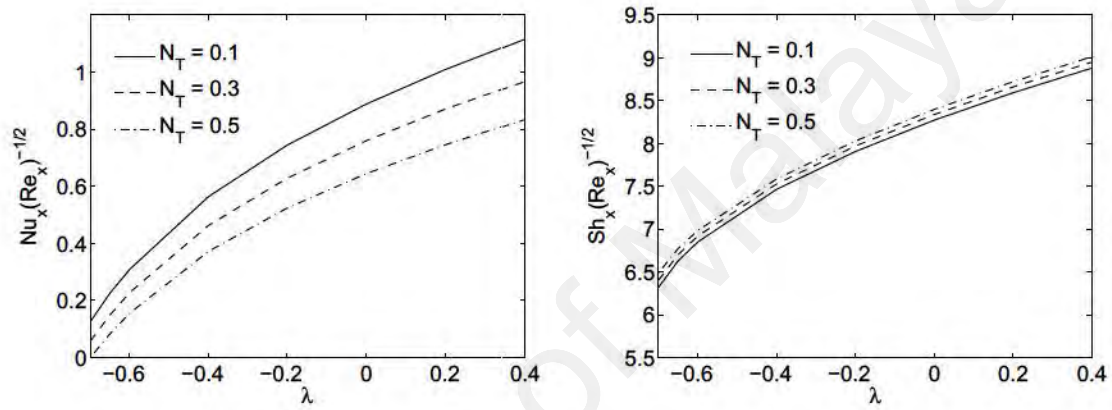

(c) **(d)**

Figure 6.7: Variations of: (a) $Nu_x(\text{Re})_x^{-1/2}$ for different values of N_B when $N_T = 0.1$; (b) $Sh_x(\text{Re})_x^{-1/2}$ for different values of N_B when $N_T = 0.1$; (c) $Nu_x(\text{Re})_x^{-1/2}$ for different values of N_T when $N_B = 0.2$; (d) $Sh_x(\text{Re})_x^{-1/2}$ for different values of N_T when $N_B = 0.2$; with $m = 0.0909$, $N_{CT} = N_{TC} = 0.1$, $F_w = 0.2$, Le $= 5$ and Ln $= 6$

value of N_T. Figs. 6.7((a)$-$(d)) show that the local Nusselt number and local Sherwood number increase as the wedge moving parameter λ increases.

The variations of the local Nusselt number and local Sherwood number are depicted in Figs. 6.8(a) and 6.8(b), respectively for different values of Soret-type parameter, N_{CT}. The Soret-type parameter appears in the solutal concentration equation, therefore it accounts for additional mass diffusion. Thus, this results in strong reduction of the local Sherwood number as the value of N_{CT} increases. The present analysis shows that the local Sherwood number is appreciably influenced by the Soret-type parameter. It is observed from Fig. 6.8(a) that the effects of moving wedge and Soret-type parameters enhance the local Nusselt number. The effect of Dufour-type parameter N_{TC} on both the local Nusselt number and local Sherwood number is plotted in Figs. 6.8(c) and 6.8(d), respectively against

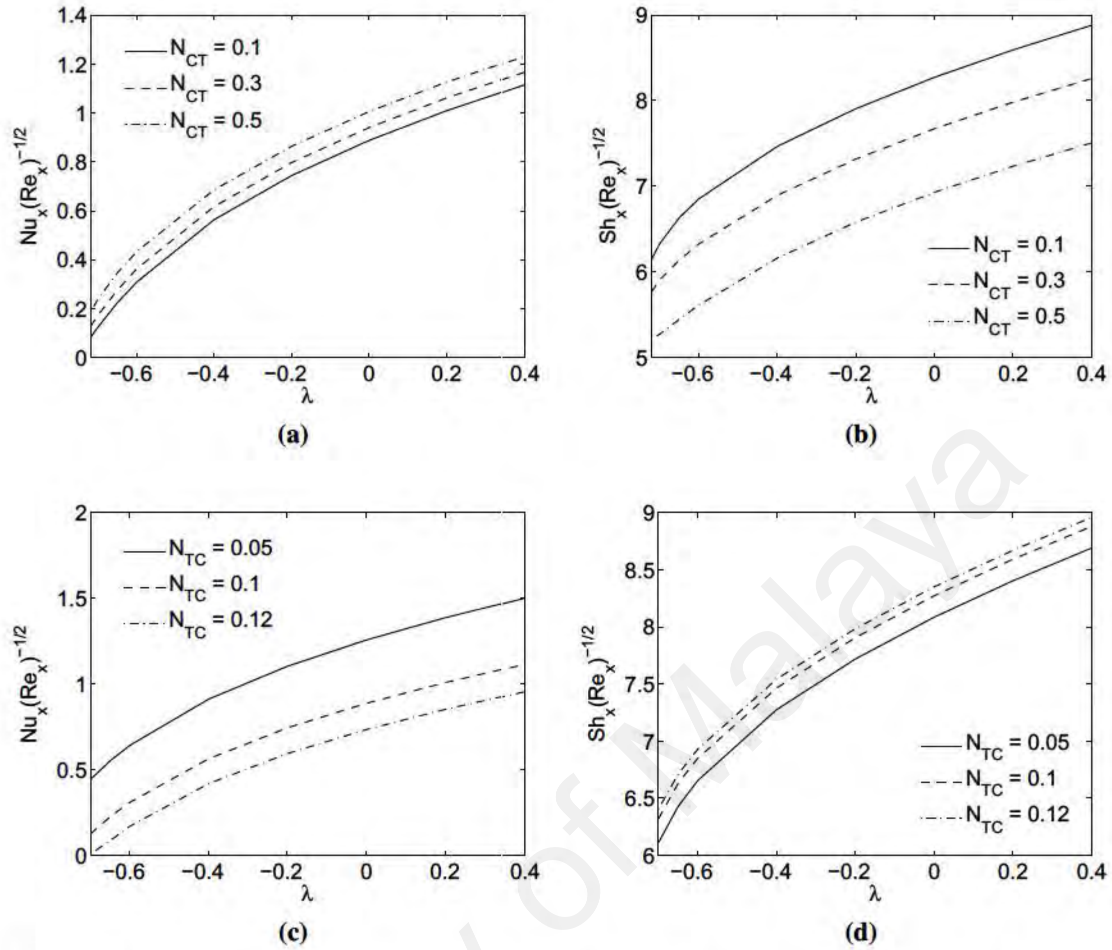

Figure 6.8: Variations of: (a) $Nu_x(\mathrm{Re})_x^{-1/2}$ for different values of N_{CT} when $N_{TC} = 0.1$; (b) $Sh_x(\mathrm{Re})_x^{-1/2}$ for different values of N_{CT} when $N_{TC} = 0.1$; (c) $Nu_x(\mathrm{Re})_x^{-1/2}$ for different values of N_{TC} when $N_{CT} = 0.1$; (d) $Sh_x(\mathrm{Re})_x^{-1/2}$ for different values of N_{TC} when $N_{CT} = 0.1$; with $m = 0.0909$, $F_w = N_B = 0.2$, $N_T = 0.1$, $\mathrm{Le} = 5$ and $\mathrm{Ln} = 6$

the wedge moving parameter, λ. The graphs reveal that the local Nusselt number decreases as the value of the Dufour-type parameter, N_{TC} increases, while a reverse trend is observed for the local Sherwood number. Fig. 6.8(d) shows that the Dufour-type parameter is less pronounced on the local Sherwood number than on the local Nusselt number. Comparing these figures (6.8(a)–6.8(d)), we observed that both Soret-type and Dufour-type parameters provide opposing trends on local Nusselt number and local Sherwood number.

CHAPTER 7: DOUBLE DIFFUSIVE CONVECTIVE FLOW OF NANOFLUID OVER A WEDGE WITH SUCTION, THERMAL RADIATION, SORET AND DUFOUR EFFECTS

This chapter discussed the combined effects of Soret and Dufour on doubly diffusive convective boundary layer flow of nanofluid over a wedge in the presence of thermal radiation and suction. In addition, the pertinent parameters of wedge angle, Brownian motion and thermophoresis are also considered in this study.

7.1 Mathematical Formulation

We consider the steady, two-dimensional flow of an incompressible, laminar heat and mass transfer of nanofluid over a wedge with thermal radiation, suction, Soret and Dufour effects. The nanofluid is a dilute solid-liquid mixture with uniform volume fraction of nanoparticle dispersed within the base liquid. The base liquid and nanoparticles are in thermally equilibrium. The effects of Brownian motion and thermophoresis are included for the nanofluid. Fig. 3.2 shows the flow model and physical configuration. We adopt Cartesian coordinate system in such a way that x- and y-axes are taken along the wedge surface and normal to the wedge surface, respectively. The flow is assumed to be in the x-direction. The wedge surface is assumed to be permeable so as to allow for possible wall suction. T_w, C_w and S_w are constant temperature, solutal concentration and nanoparticle volume fraction at the wall, respectively. T_∞, C_∞, and S_∞ are the free stream temperature, solutal concentration and nanoparticle volume fraction, respectively. The thermal-diffusion (Soret) and diffusion-thermo (Dufour) effects are considered in this study. Thus, in accordance with these assumptions and employing the usual boundary layer approximations, along with Boussinesq's approximation, the governing equations describing the conservation of mass, momentum, thermal energy, solute concentration and nanoparticles volume fraction are given as follows (Buongiorno (2006) and Kuznetsov & Nield (2011)):

$$\frac{\partial u}{\partial x}+\frac{\partial v}{\partial y}=0, \tag{7.1}$$

$$u\frac{\partial u}{\partial x}+v\frac{\partial u}{\partial y}=\nu\frac{\partial^2 u}{\partial y^2}+U\frac{dU}{dx}, \tag{7.2}$$

$$u\frac{\partial T}{\partial x}+v\frac{\partial T}{\partial y}=\alpha\frac{\partial^2 T}{\partial y^2}+\tau\left[D_B\frac{\partial S}{\partial y}\frac{\partial T}{\partial y}+\left(\frac{D_T}{T_\infty}\right)\left(\frac{\partial T}{\partial y}\right)^2\right]+D_{TC}\frac{\partial^2 C}{\partial y^2}-\frac{1}{(\rho c)_f}\frac{\partial q_r}{\partial y}, \tag{7.3}$$

$$u\frac{\partial S}{\partial x}+v\frac{\partial S}{\partial y}=D_B\frac{\partial^2 S}{\partial y^2}+\left(\frac{D_T}{T_\infty}\right)\frac{\partial^2 T}{\partial y^2}, \tag{7.4}$$

$$u\frac{\partial C}{\partial x}+v\frac{\partial C}{\partial y}=D_S\frac{\partial^2 C}{\partial y^2}+D_{CT}\frac{\partial^2 T}{\partial y^2}, \tag{7.5}$$

subject to the following boundary conditions

$$\begin{gathered} u=0, \quad v=v_0, \quad T=T_w, \quad C=C_w, \quad S=S_w \quad \text{at} \quad y=0, \\ u\to U, \quad T\to T_\infty, \quad C\to C_\infty, \quad S\to S_\infty, \quad \text{as} \quad y\to\infty, \end{gathered} \tag{7.6}$$

where the radiative heat flux, $q_r=-(4\sigma/3k_1)(\partial T^4/\partial y)$ is employed by utilizing the Rosseland approximation where σ is the Stefan-Boltzmann constant and k_1 is the mean absorption coefficient. The fluid-phase temperature differences within the flow are assumed to be sufficiently small, so that, T^4 may be expressed as a linear function of temperature by using Taylor's series about the free stream temperature, T_∞ and neglecting the higher-order terms to yield, $T^4 \cong 4T_\infty^3 T-3T_\infty^4$. Applying this approximation, the radiative heat flux in Eq. 7.3 becomes, $q_r=-(16\sigma T_\infty^3/3k_1)(\partial T/\partial y)$.

Defining the stream function ψ such that $u=\dfrac{\partial\psi}{\partial y}$ and $v=-\dfrac{\partial\psi}{\partial x}$, which identically satisfies the Eq. 7.1. Substituting Eq. 6.7 into Eqs. 7.2–7.5 yields the following equations:

$$f'''+ff''+\frac{2m}{m+1}\left(1-(f')^2\right)=0, \tag{7.7}$$

$$\left(1+\frac{4}{3R}\right)\theta''+\Pr f\theta'+N_B\phi'\theta'+N_T\left(\theta'\right)^2+N_{TC}\gamma''=0, \tag{7.8}$$

$$\gamma''+\Pr \mathrm{Le} f\gamma'+N_{CT}\,\mathrm{Le}\theta''=0, \tag{7.9}$$

$$\phi''+\Pr \mathrm{Ln} f\phi'+\frac{N_T}{N_B}\theta''=0, \tag{7.10}$$

with the corresponding boundary condition

$$f = \frac{2}{m+1}F_w, \quad f' = 0, \quad \theta = 1, \quad \gamma = 1, \quad \phi = 1 \quad \text{at} \quad \eta = 0,$$
$$f' \to 1, \quad \theta \to 0, \quad \gamma \to 0, \quad \phi \to 0, \quad \text{as} \quad \eta \to \infty. \tag{7.11}$$

The primes denote the derivatives with respect to η, $\Pr = \nu/\alpha$ is the Prandtl number, $\mathrm{Le} = \alpha/D_S$ is the Lewis number, $\mathrm{Ln} = \alpha/D_B$ is the nanofluid Lewis number, $R = k_1 k/4\sigma T_\infty^3$ is the radiation parameter, $N_B = \tau D_B(S_w - S_\infty)/\alpha$ is the Brownian parameter, $N_T = \tau D_T(T_w - T_\infty)/\alpha T_\infty$ is the thermophoresis parameter, $N_{TC} = D_{TC}(C_w - C_\infty)/\alpha(T_w - T_\infty)$ is the Dufour-type parameter, $N_{CT} = D_{CT}(T_w - T_\infty)/\alpha(C_w - C_\infty)$ is the Soret-type parameter, $F_w = -v_0 \mathrm{Re}_x^{1/2}/U$ is the suction parameter and $\mathrm{Re}_x = Ux/\nu$ is the Reynolds number.

The quantities of interest to be monitored in this study are skin friction coefficient C_{fx}, the local Nusselt Number Nu_x and local Sherwood number Sh_x which are defined by

$$C_{fx} = \frac{\tau_w}{\rho_f U^2}, \quad Nu_x = \frac{x q_w}{k(T_w - T_\infty)}, \quad Sh_x = \frac{x q_m}{D_B(C_w - C_\infty)}, \tag{7.12}$$

where

$$\tau_w = \mu\left(\frac{\partial u}{\partial y}\right)_{y=0}, \quad q_w = -k\left(\frac{\partial T}{\partial y}\right)_{y=0} - \frac{4\sigma}{3k_1}\left(\frac{\partial T^4}{\partial y}\right)_{y=0}, \quad q_m = -D_B\left(\frac{\partial C}{\partial y}\right)_{y=0}, \tag{7.13}$$

are shear stress, heat flux and mass flux, respectively. Using Eq. 6.7, the local skin friction coefficient, local Nusselt number and local Sherwood number can be expressed, respectively, as

$$C_{fx}(\mathrm{Re}_x)^{1/2} = f''(0)\sqrt{\frac{m+1}{2}}, \tag{7.14}$$

$$Nu_x(\mathrm{Re}_x)^{-1/2} = -\theta'(0)\left(1 + \frac{4}{3R}\right)\sqrt{\frac{m+1}{2}}, \tag{7.15}$$

$$Sh_x(\mathrm{Re}_x)^{-1/2} = -\gamma'(0)\sqrt{\frac{m+1}{2}}. \tag{7.16}$$

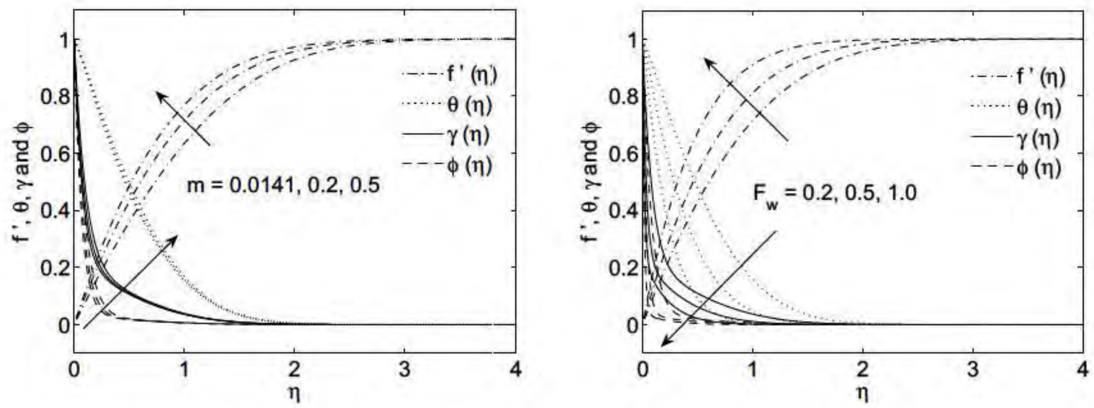

(a) (b)

Figure 7.1: The distributions of f', θ, γ and ϕ with $R = 1$, $N_B = 0.2$, $N_T = 0.1$, $N_{CT} = 0.5$, $N_{TC} = 0.1$, Le $= 5$ and Ln $= 6$ for different values of: (a) m when $F_w = 0.2$; (b) F_w when $m = 0.2$

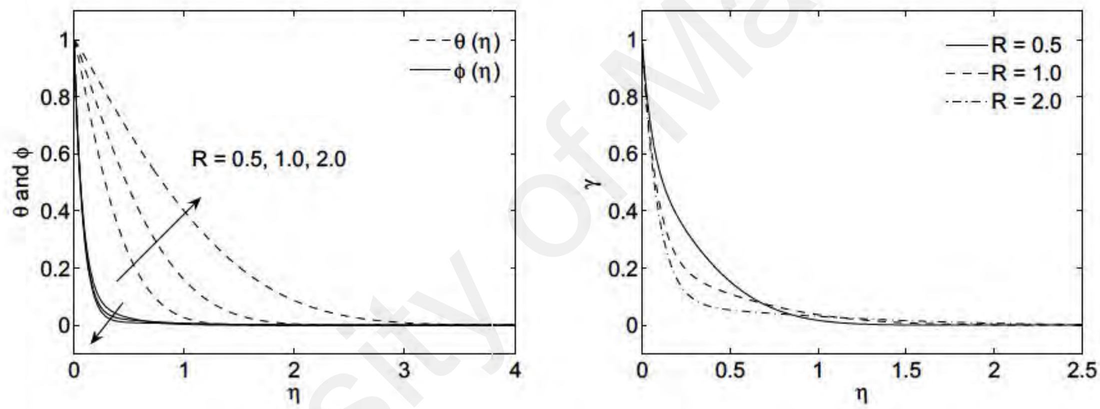

(a) (b)

Figure 7.2: The influence of R on: (a) temperature and nanoparticle volume fraction profiles; (b) solutal concentration profile; when $m = 0.2$, $F_w = 0.2$, $N_B = 0.2$, $N_T = 0.1$, $N_{CT} = 0.5$, $N_{TC} = 0.1$, Le $= 5$ and Ln $= 6$

7.2 Results and Discussion

In this section, the numerical solutions are plotted for values of different parameters. Figs. 7.1−7.7 display the effects of all thermo-physical parameters on dimensionless velocity, temperature, solutal concentration and nanoparticle volume fraction as well as local skin-friction coefficient, local Nusselt number and local Sherwood number.

Figs. 7.1(a) and 7.1(b) display the velocity, temperature, solutal concentration and nanoparticle volume fraction profiles for various values of wedge angle parameter, m and suction parameter, F_w, respectively. Both figures show that the velocity of the fluid

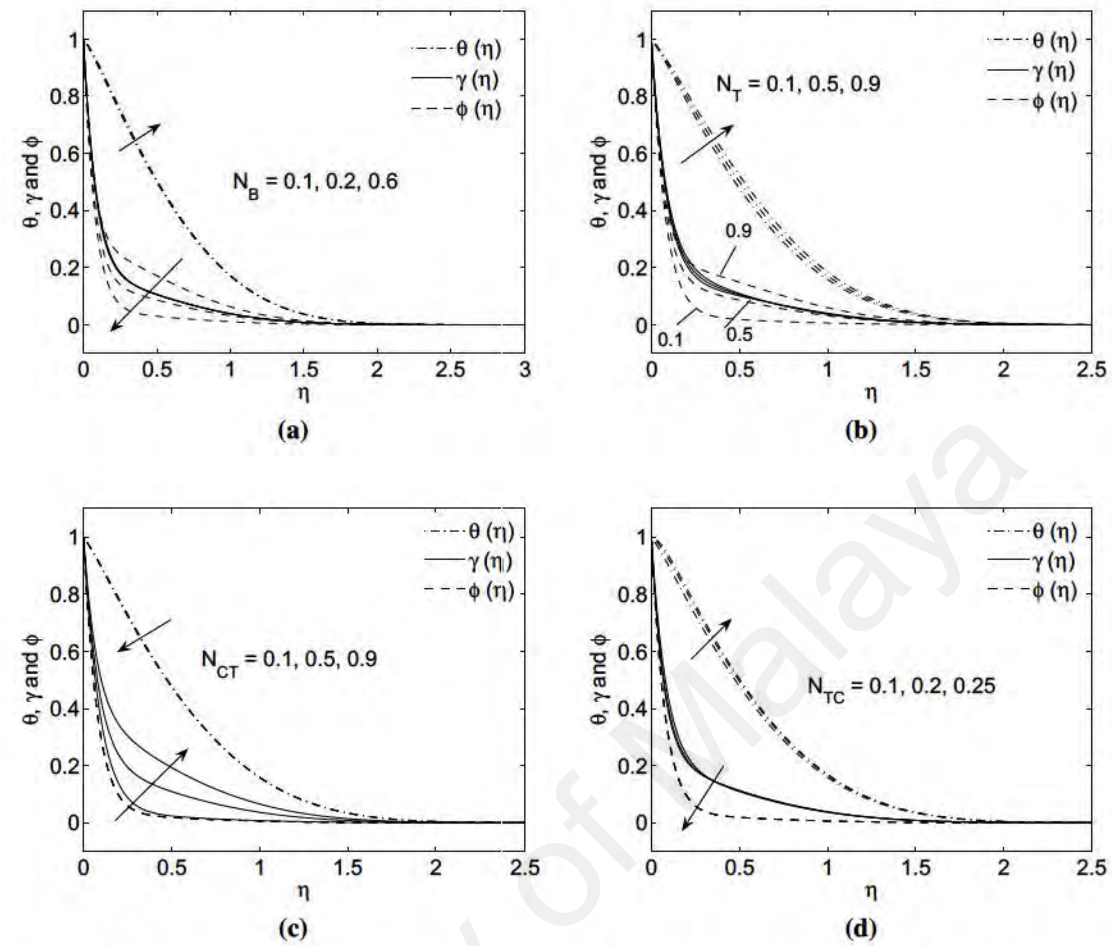

Figure 7.3: The distributions of θ, γ and ϕ with $m = 0.2$, $F_w = 0.2$, $R = 1$, $\mathrm{Le} = 5$ and $\mathrm{Ln} = 6$ for different values of: (a) N_B when $N_T = 0.5$, $N_{CT} = 0.5$, $N_{TC} = 0.1$; (b) N_T when $N_B = 0.2$, $N_{CT} = 0.5$, $N_{TC} = 0.1$; (c) N_{CT} when $N_B = 0.2$, $N_T = 0.1$, $N_{TC} = 0.1$; and (d) N_{TC} when $N_B = 0.2$, $N_T = 0.1$, $N_{CT} = 0.5$;

increases with an increase in m and F_w. This means that the velocity profile move closer to the surface of the wedge and the hydrodynamic boundary layer decreases for larger values of m and F_w. It can be seen from the Fig. 7.1(a) that the increase of wedge angle parameter causes an increase in temperature, solutal concentration and nanoparticle volume fraction profiles. Furthermore, Fig. 7.1(b) shows that the temperature, solutal concentration and nanoparticle volume fraction profiles decrease when increasing the suction parameter. This situation results in the increasing of the shear stress on the wedge surface. Also, we observed that the imposition of suction at the wedge surface reduces the region of viscous domination close to the wall, which causes decreasing in the fluid's temperature, solutal concentration and nanoparticle volume fraction distributions.

The effect of thermal radiation R on temperature and volume fraction profiles is de-

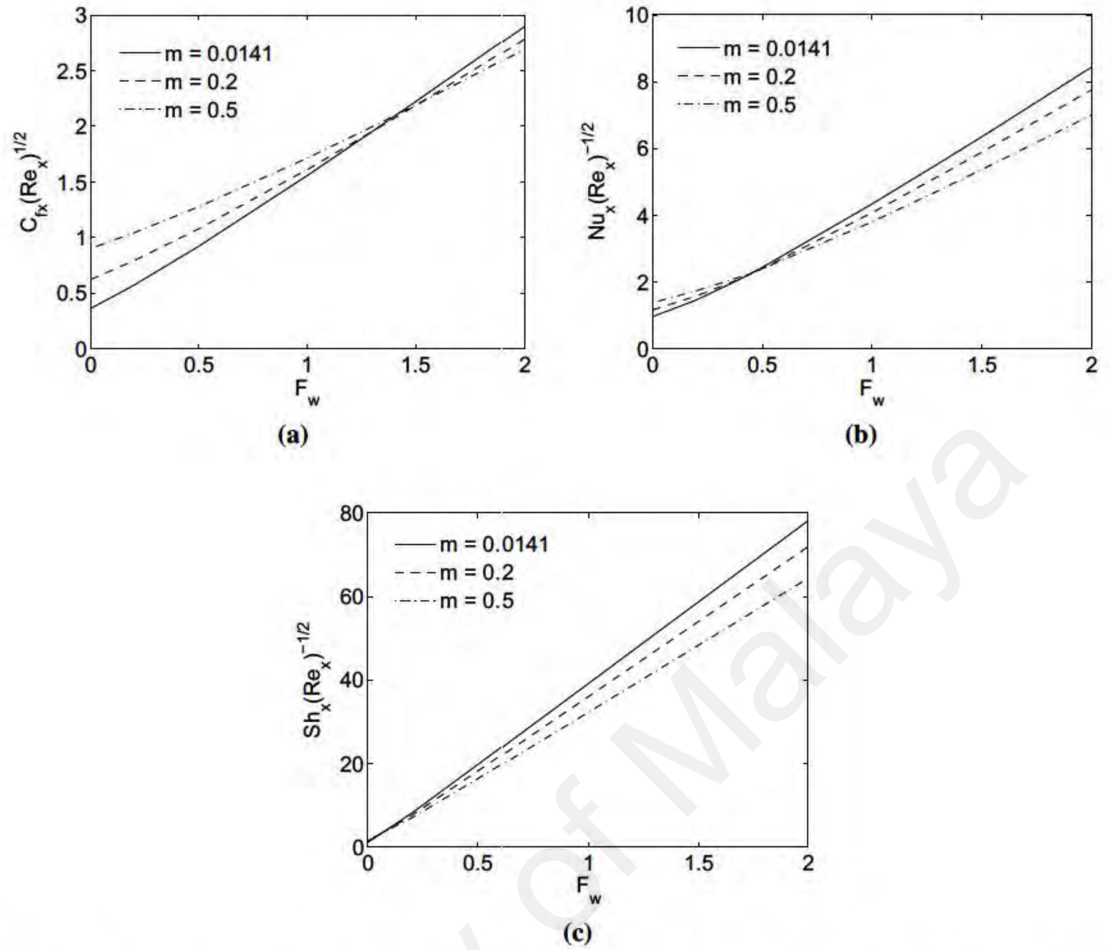

Figure 7.4: Variations of: (a) $C_{fx}(\mathrm{Re})_x^{1/2}$; (b) $Nu_x(\mathrm{Re})_x^{-1/2}$; (c) $Sh_x(\mathrm{Re})_x^{-1/2}$; against F_w for different values of m when $R = 1$, $N_B = 0.2$, $N_T = 0.1$, $N_{CT} = 0.5$, $N_{TC} = 0.1$, $\mathrm{Le} = 5$ and $\mathrm{Ln} = 6$

picted in the Fig. 7.2(a). An increase in the thermal radiation leads to the increase of fluid temperature, θ. Hence this will enhance the temperature at each point away from the wedge surface. The higher value of radiation parameter implies the higher surface heat flux. This situation also accompanied by an increase in thermal boundary layer and the convection effect. In addition, Fig. 7.2(a) shows that the nanoparticle volume fraction decreases on increasing R. The effect of ϕ with R is insignificant compare to θ on R. Even though, the parameter R is not involved in the nanoparticle volume fraction equation, there is a small change in the ϕ profile. Fig. 7.2(b) displays the solutal concentration profile for various values of thermal radiation. It is observed that the solutal concentration distribution decreases on increasing the radiation parameter.

The random motion of nanoparticles within the base fluid is called the Brownian motion. The influence of Brownian motion parameter, N_B for the distribution of temperature,

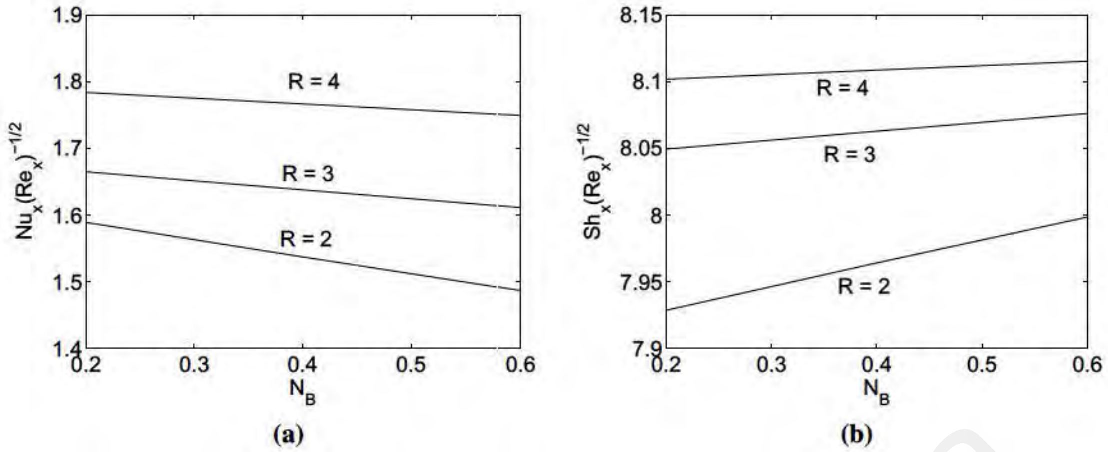

Figure 7.5: Variations of: (a) $Nu_x(\mathrm{Re})_x^{-1/2}$; (b) $Sh_x(\mathrm{Re})_x^{-1/2}$; against N_B for different values of R when $m = 0.2$, $F_w = 0.2$, $N_T = 0.1$, $N_{CT} = 0.5$, $N_{TC} = 0.1$, $\mathrm{Le} = 5$ and $\mathrm{Ln} = 6$

solutal concentration and nanoparticle volume fraction is shown in the Fig. 7.3(a). It can be seen that the fluid temperature is found to increase with an increase in the Brownian motion parameter. This means that the thickness of thermal boundary layer increases as N_B increases, which eventually enhances the temperature. Since the Brownian motion parameter is appeared in thermal energy equation, it gives the enhancement on temperature distribution. The increasing in the temperature distribution is also due to the continuous collisions between the nanoparticles and the molecules of the base fluid (water). In Fig. 7.3(a), we observed that, the solutal concentration and nanoparticle volume fraction decrease with an increase in Brownian motion parameter. An increase in N_B refers to an increase in the intermolecular space of nanoparticles. Thus, this situation results in lowering the nanoparticle volume fraction distribution as well as the solutal concentration.

Fig. 7.3(b) presents the distribution of dimensionless temperature, solutal concentration and nanoparticle volume fraction against η for various values of thermophoresis parameter, N_T. Thermophoresis is referred as the transport of the nanoparticles in base fluid due to the temperature gradient under the influence of the thermophoretic force. It is observed that an increase in N_T leads to the increase in both fluid temperature and nanoparticle volume fraction. This phenomenon shows that the nanoparticles' molecules carry high kinetic energy and resulting in a net force on the particles. These enhancements are due to the nanoparticles of high thermal conductivity being driven away from

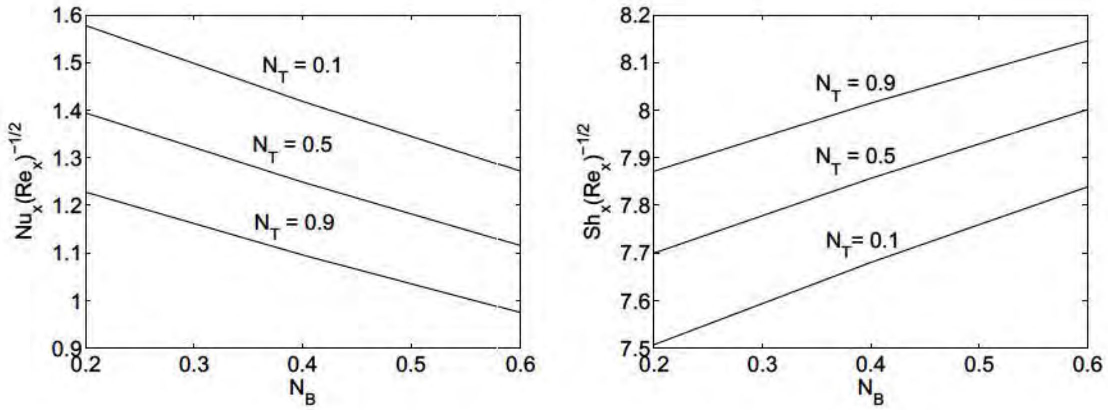

(a) **(b)**

Figure 7.6: Variations of: (a) $Nu_x(\mathrm{Re})_x^{-1/2}$; (b) $Sh_x(\mathrm{Re})_x^{-1/2}$; against N_B for different value of N_T when $m = 0.2$, $F_w = 0.2$, $R = 1$, $N_{CT} = 0.5$, $N_{TC} = 0.1$, Le $= 5$ and Ln $= 6$

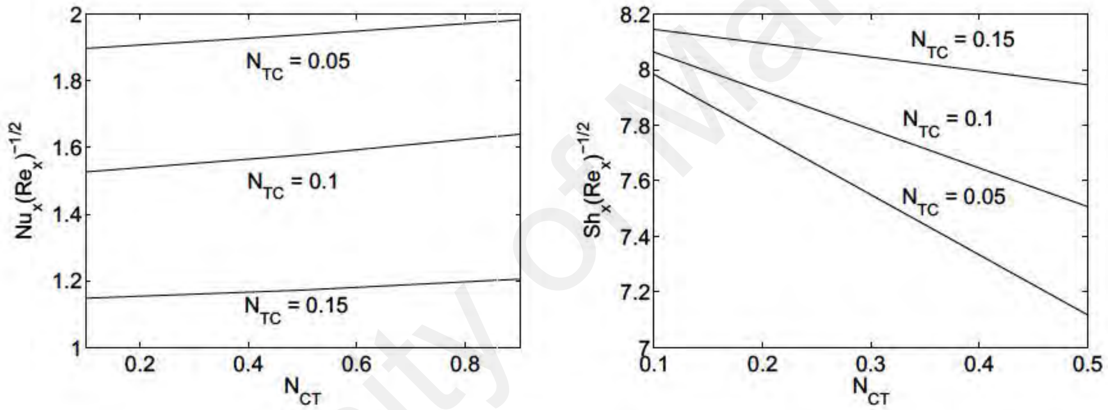

(a) **(b)**

Figure 7.7: Variations of: (a) $Nu_x(\mathrm{Re})_x^{-1/2}$; (b) $Sh_x(\mathrm{Re})_x^{-1/2}$; against N_{CT} for different values of N_{TC} when $m = 0.2$, $F_w = 0.2$, $R = 1$, $N_B = 0.2$, $N_T = 0.1$, Le $= 5$ and Ln $= 6$

the hot surface to the quiescent nanofluid. This net force is called thermophoretic. Also, it can be seen from the Fig. 7.3(b) that the solutal concentration decreases on increasing the value of N_T. These situations indicate that the thermophoresis parameter works to increase the volume fraction and thermal boundary layer thickness and decrease the solutal concentration boundary layer thickness.

Fig. 7.3(c) depicts the temperature, solutal concentration and nanoparticle volume fraction profiles for different values of Soret-type parameter, N_{CT}. It is observed that an increase in the Soret-type parameter leads to a decrease in the temperature distribution. The solutal concentration and nanoparticle volume fraction increase on increasing the value of N_{CT}. Fig. 7.3(d) shows the influence of Dufour effect, N_{TC} on the temperature, solutal concentration and nanoparticle volume fraction profiles. The temperature distribution of the fluid increases when the value of N_{TC} increases, which in turn leads to a decrease in nanoparticle volume fraction and lowering the concentration of species.

The variations of local skin friction coefficient against suction parameter, F_w for various values of wedge angle parameter, m is shown in the Fig. 7.4(a). It is observed that an increase in wedge angle parameter leads to an increase in the local skin friction coefficient for approximately when $F_w < 1.4$. The opposite behaviour is noticed for $F_w > 1.4$. Fig. 7.4(b) exhibits the variation of local Nusselt number for different values of m. It can be seen that the value of local Nusselt number shows different behaviour before and after certain points of F_w as the wedge angle parameter increases, particularly $F_w = 0.45$. Before $F_w \approx 0.5$, the local Nusselt number increases and after this point, it decreases. The variation of local Sherwood number for various values of m is displayed in Fig. 7.4(c). The local Sherwood number decreases as the wedge angle parameter increases and it increases with an increase in suction parameter. The local mass transfer rate vanishes when the suction parameter approaching zero (i.e,$F_w \to 0$).

The variations of local Nusselt number and local Sherwood number are plotted against N_B in the Figs. 7.5(a) and 7.5(b), respectively for various values of thermal radiation, R. It is observed that, an increase in Brownian motion parameter obviously decreases the local Nusselt number, whereas the reverse effect is seen in the local Sherwood number. It can be seen from the Figs. 7.5(a) and 7.5(b) that, both the local Nusselt and Sherwood number increase on increasing the value of thermal radiation.

The effects of Brownian motion and thermophoresis parameters on local Nusselt number and Sherwood number are presented in the Figs. 7.6(a) and 7.6(b), respectively. The local Nusselt number decreases as both the Brownian motion and thermophoresis parameters increase. Meanwhile, the local Sherwood number increases as N_B and N_T increase. This is due to the fact that an increase in energy exchange rate causes an enhancement in the random movement of nanoparticles and promote heat conduction.

The variations of local Nusselt number and local Sherwood number are plotted in Figs. 7.7(a) and 7.7(b), respectively, against N_{CT} for various values of Dufour-type parameter, N_{TC}. The graphs reveal that the local Nusselt number decreases as the value of the Dufour-type parameter increases, while a reverse trend is observed for the local Sherwood number. Fig. 7.7(b) shows that the local Sherwood number increases as the Dufour-type and suction parameters increase. It is observed from Fig. 7.7(a) that, the local Nusselt number increases on increasing the Soret-type parameter. The Soret-type parameter appears in the solutal concentration equation, therefore it accounts for additional mass diffusion. Thus, the local Sherwood number reduces as the value of N_{CT} increases. Comparing these Figs. 7.7(a) and 7.7(b), we observed that both Soret-type parameter and Dufour-type parameter provide opposing trends on local Nusselt number and local Sherwood number.

CHAPTER 8: DOUBLE DIFFUSIVE MIXED CONVECTIVE FLOW OF NANOFLUID OVER A WEDGE WITH POWER LAW VARIATION IN THE PRESENCE OF SUCTION AND THERMAL RADIATION, SORET AND DUFOUR EFFECTS

Mixed (or combined) convection flow occurs when natural and forced convections mechanism are determined simultaneously. The flow is pronounced in situations where both pressure forces and buoyant forces interact. This chapter discussed the effects of thermal radiation, Soret and Dufour on double diffusive mixed convection of nanofluid flow past a wedge in the presence of suction with power-law variation of the wall temperature and concentration.

8.1 Mathematical Formulation

We consider heat and mass transfer analysis in steady, two-dimensional, incompressible flow of nanofluid over a wedge. Fig. 3.2 shows that the x-axis is extending along the wedge surface, while the y-axis is normal to the surface. The flow is assumed to be in the x direction. The nanofluid is a dilute solid-liquid mixture with a uniform volume fraction of nanoparticle dispersed within the base liquid. It is assumed that the nanoparticles and base liquid are in thermal equilibrium. The effects of Brownian motion and thermophoresis are included for the nanofluid. The Boussinesq approximation is valid. The thermal radiation, Soret and Dufour effects are considered. Following the nanofluid model proposed by Buongiorno (2006) and Kuznetsov & Nield (2011), the governing equations describing the conservation of mass, momentum, thermal energy, solute concentration and nanoparticles volume fraction are

$$\frac{\partial u}{\partial x}+\frac{\partial v}{\partial y}=0, \tag{8.1}$$

$$u\frac{\partial u}{\partial x}+v\frac{\partial u}{\partial y}=\nu\frac{\partial^2 u}{\partial y^2}+U\frac{dU}{dx}+\left[g\beta_T\left(T-T_\infty\right)+g\beta_C\left(C-C_\infty\right)\right]\sin\frac{\Omega}{2}, \tag{8.2}$$

$$u\frac{\partial T}{\partial x}+v\frac{\partial T}{\partial y}=\alpha\frac{\partial^2 T}{\partial y^2}+\tau\left[D_B\frac{\partial S}{\partial y}\frac{\partial T}{\partial y}+\left(\frac{D_T}{T_\infty}\right)\left(\frac{\partial T}{\partial y}\right)^2\right]+D_{TC}\frac{\partial^2 C}{\partial y^2}-\frac{1}{(\rho c)_f}\frac{\partial q_r}{\partial y}, \tag{8.3}$$

$$u\frac{\partial S}{\partial x}+v\frac{\partial S}{\partial y}=D_B\frac{\partial^2 S}{\partial y^2}+\left(\frac{D_T}{T_\infty}\right)\frac{\partial^2 T}{\partial y^2}, \tag{8.4}$$

$$u\frac{\partial C}{\partial x}+v\frac{\partial C}{\partial y}=D_S\frac{\partial^2 C}{\partial y^2}+D_{CT}\frac{\partial^2 T}{\partial y^2}, \tag{8.5}$$

where g is the gravity, β_T is the volumetric thermal expansion coefficient and β_C is the volumetric concentration expansion coefficient. It is important to note that β_T is positive in most fluids at normal pressures. However, β_C can be positive or negative depending on the contribution of the diffusing species to the density of the ambient medium.

The initial and boundary conditions are given as follows:

$$\begin{aligned} &u=0, \quad v=v_0, \quad T=T_w=T_\infty+b_1x^{n_1}, \quad C=C_w=C_\infty+b_2x^{n_2}, \quad S=S_w \quad \text{at} \quad y=0,\\ &u\to U, \quad T\to T_\infty, \quad C\to C_\infty, \quad S\to S_\infty, \quad \text{as} \quad y\to\infty. \end{aligned} \tag{8.6}$$

The wall temperature and concentration are assumed to have power-law variation forms where b_1 and b_2 are constants and n_1 and n_2 are the power-law exponent that signifies the change of amount of temperature and solute along the surface.

The continuity Eq. 8.1 is automatically satisfied by defining the stream function $\psi(x,y)$ such that $u=\partial\psi/\partial y$ and $v=-\partial\psi/\partial x$. Substituting Eq. 6.7 into Eqs. 8.2–8.5, yield the non-dimensional equations as follows:

$$f'''+ff''+\frac{2m}{m+1}\left(1-(f')^2\right)+\frac{2}{m+1}Ri(\theta+N\gamma)\sin\frac{\Omega}{2}=0, \tag{8.7}$$

$$\left(1+\frac{4}{3R}\right)\theta''+\Pr f\theta'-\frac{2n_1}{m+1}\Pr\theta+N_B\phi'\theta'+N_T\left(\theta'\right)^2+N_{TC}\gamma''=0, \tag{8.8}$$

$$\gamma''+\Pr\,\mathrm{Le}f\gamma'-\frac{2n_2}{m+1}\Pr\mathrm{Le}\gamma+N_{CT}\,\mathrm{Le}\theta''=0, \tag{8.9}$$

$$\phi''+\Pr\,\mathrm{Ln}f\phi'+\frac{N_T}{N_B}\theta''=0, \tag{8.10}$$

with the corresponding boundary conditions

$$\begin{aligned} &f=\frac{2}{m+1}F_w, \quad f'=0, \quad \theta=1, \quad \gamma=1, \quad \phi=1 \quad \text{at} \quad \eta=0,\\ &f'\to 1, \quad \theta\to 0, \quad \gamma\to 0, \quad \phi\to 0, \quad \text{as} \quad \eta\to\infty, \end{aligned} \tag{8.11}$$

where prime denotes the partial differentiation with respect to η, $\mathrm{Re}_x = Ux/\nu$ is the Reynold number, $N = Ri^*/Ri$ is the ratio of buoyancy parameter, $Ri = Gr_x/\mathrm{Re}_x^2$ is thermal Richardson number, $Ri^* = Gr_x^*/\mathrm{Re}_x^2$ is solutal Richardson number, $Gr_x = g\beta_T(T_w - T\infty)x^3/\nu^2$ is thermal Grashof number, $Gr_x^* = g\beta_C(C_w - C\infty)x^3/\nu^2$ is solutal Grashof number, $R = k_1 k/4\sigma T_\infty^3$ is the thermal radiation parameter, $\mathrm{Pr} = \nu/\alpha$ is the Prandtl number, $\mathrm{Le} = \alpha/D_S$ is the Lewis number, $N_B = \tau D_B(S_w - S_\infty)/\alpha$ is the Brownian motion parameter, $N_T = \tau D_T(T_w - T_\infty)/\alpha T_\infty$ is the thermophoresis parameter, $N_{CT} = D_{CT}(T_w - T_\infty)/\alpha(C_w - C_\infty)$ is the Soret-type parameter, $N_{TC} = D_{TC}(C_w - C_\infty)/\alpha(T_w - T_\infty)$ is the Dufour-type parameter, $\mathrm{Ln} = \alpha/D_B$ is the nanofluid Lewis number and $F_w = -v_0\mathrm{Re}_x^{1/2}/U$ is the suction parameter.

The local skin friction, local Nusselt number and local Sherwood number are defined as follows.

$$C_{fx} = \frac{\tau_w}{\rho_f U^2}, \quad Nu_x = \frac{xq_w}{k(T_w - T_\infty)}, \quad Sh_x = \frac{xq_m}{D_B(C_w - C_\infty)}, \tag{8.12}$$

where

$$\tau_w = \mu\left(\frac{\partial u}{\partial y}\right)_{y=0}, \quad q_w = -k\left(\frac{\partial T}{\partial y}\right)_{y=0} - \frac{4\sigma}{3k_1}\left(\frac{\partial T^4}{\partial y}\right)_{y=0}, \quad q_m = -D_B\left(\frac{\partial C}{\partial y}\right)_{y=0}, \tag{8.13}$$

are shear stress, heat flux and mass flux, respectively. Using Eq. 6.7, the local skin friction coefficient, local Nusselt number and local Sherwood number can be written, respectively as

$$C_{fx}(\mathrm{Re}_x)^{1/2} = f''(0)\sqrt{\frac{m+1}{2}}, \tag{8.14}$$

$$Nu_x(\mathrm{Re}_x)^{-1/2} = -\theta'(0)\left(1 + \frac{4}{3R}\right)\sqrt{\frac{m+1}{2}}, \tag{8.15}$$

$$Sh_x(\mathrm{Re}_x)^{-1/2} = -\gamma'(0)\sqrt{\frac{m+1}{2}}. \tag{8.16}$$

8.2 Results and Discussion

Table 8.1 shows the values of $f''(0)$, $-\theta(0)$, $-\gamma(0)$ and $-\phi(0)$ for different values of Richardson number, Ri and the buoyancy ratio parameter, N. The buoyancy ratio parameter represents the ratio between concentration and thermal buoyancy forces. When $N = 0$, there is no mass transfer and the buoyancy force is due to the thermal diffusion only. When $N > 0$, the buoyancy forces are cooperating and act in the same direction (assisting flow). When $N < 0$ means that concentration and thermal buoyancy forces act in the opposite direction (opposing flow). It is observed that, the value of $f''(0)$ increases on increasing the parameter N for the case of assisting flow $(N > 0)$ when $n_1 = 0.3$ and $n_2 = 0.1$. Meanwhile, for the case of opposing flow $(N < 0)$, the value of $f''(0)$ decreases on increasing the values of N. It is important to note that Richardson number, Ri plays the role of a buoyancy or a mixed convection parameter. $Ri > 0$ and $Ri < 0$ are for the situation when the bouyancy forces assist the main flow and when they oppose the main flow, respectively. The case $Ri \gg 1.0$ corresponds to free convection, $Ri = 1.0$ corresponds to mixed convection and $Ri \ll 1.0$ corresponds to pure forced convection. The results presented in Table 8.1 also indicated that when $n_1 = 0$ and $n_2 = 0$, the value of $f''(0)$ increases on increasing the Richardson number for the case of assisting flow $(Ri > 0)$. Further, the value of $f''(0)$ decreases on increasing Ri for the case of opposing flow $(Ri < 0)$. Both $(Ri > 0)$ and $(N > 0)$ parameters act as a favorable pressure gradient which accelerated the fluid flow and this situation leads to enhance the value of $f''(0)$. For the opposing flow, an adverse pressure gradient occurs which decelerates the velocity of the fluid. The effects of N and Ri on the values of $-\theta(0)$, $-\gamma(0)$ and $-\phi(0)$ are very small because of the physical parameters N and Ri appear only in the momentum equation. Thus, the buoyancy ratio parameter and Richardson number are strongly affect the value of $f''(0)$, whereas the effect of these parameters on $-\theta(0)$, $-\gamma(0)$ and $-\phi(0)$ are not much significant.

Figs. 8.1((a)$-$(c)) depict the velocity, temperature, solutal concentration and volume fraction profiles against η for various values of wedge angle, suction and thermal radiation parameters, respectively. The velocity increases on increasing the values of m, F_w and R. The effect of increasing m is to show that the fluid velocity became faster and thereby the velocity profiles squeeze faster and move nearer to the surface of the wedge wall. In addition, the hydrodynamic boundary layer decreases for larger values of m. Furthermore, the fluid particles intensify the velocity on increasing the suction and ther-

Table 8.1: The values of $f''(0)$, $-\theta(0)$, $-\gamma(0)$ and $-\phi(0)$ for various values of N, Ri, n_1 and n_2 when $m = 0.0435$, $F_w = N_B = 0.2$, $N_T = N_{TC} = 0.1$, $N_{CT} = 0.5$, Le $= 5$ and Ln $= 6$

N	Ri	n_1	n_2	$f''(0)$	$-\theta(0)$	$-\gamma(0)$	$-\phi(0)$
-5	1	0.3	0.1	0.74106	1.42398	10.53373	13.89749
-3				0.82465	1.42849	10.55119	13.91043
-1				0.90796	1.43298	10.56837	13.92318
0				0.94920	1.43518	10.57673	13.92941
0.2				0.95742	1.43561	10.57839	13.93064
1				0.99019	1.43735	10.58496	13.93555
2				1.03092	1.43949	10.59304	13.94160
3				1.07488	1.44203	10.60236	13.94840
0.2	-5	0	0	0.08287	0.75221	10.85139	14.07351
	-3			0.42134	0.81416	10.92261	14.12697
	-1			0.71207	0.85889	10.97739	14.16989
	-0.5			0.78018	0.86854	10.98957	14.17961
	0			0.84686	0.87773	11.00128	14.18903
	0.01			0.84818	0.87791	11.00151	14.18921
	0.1			0.86004	0.87951	11.00357	14.19088
	1			0.97644	0.89490	11.02349	14.20703
	5			1.45692	0.95223	11.10049	14.27087

mal radiation parameters. It can be seen from the Fig. 8.1(a) that the increase of wedge angle parameter causes an increase in temperature, solutal concentration and nanoparticle volume fraction profiles. It is clear from Fig. 8.1(b) that the effect of increasing F_w is to decrease the temperature of the fluid. The imposition of suction at wedge surface reduces the region of viscous domination close to the wall, which causes decreasing in the fluid's temperature. However, an increase in the thermal radiation leads to enhance the fluid temperature. Hence this will boost the temperature at each point away from the wedge surface. The higher value of radiation parameter implies the higher surface heat flux. This situation also accompanied by an increase in thermal boundary layer thickness and the convection effect. It can be seen from the Figs. 8.1(b) and 8.1(c) that the solutal concentration and nanoparticle volume fraction profiles decrease on increasing the suction and thermal radiation parameters. The effects of θ, γ and ϕ on m are insignificant

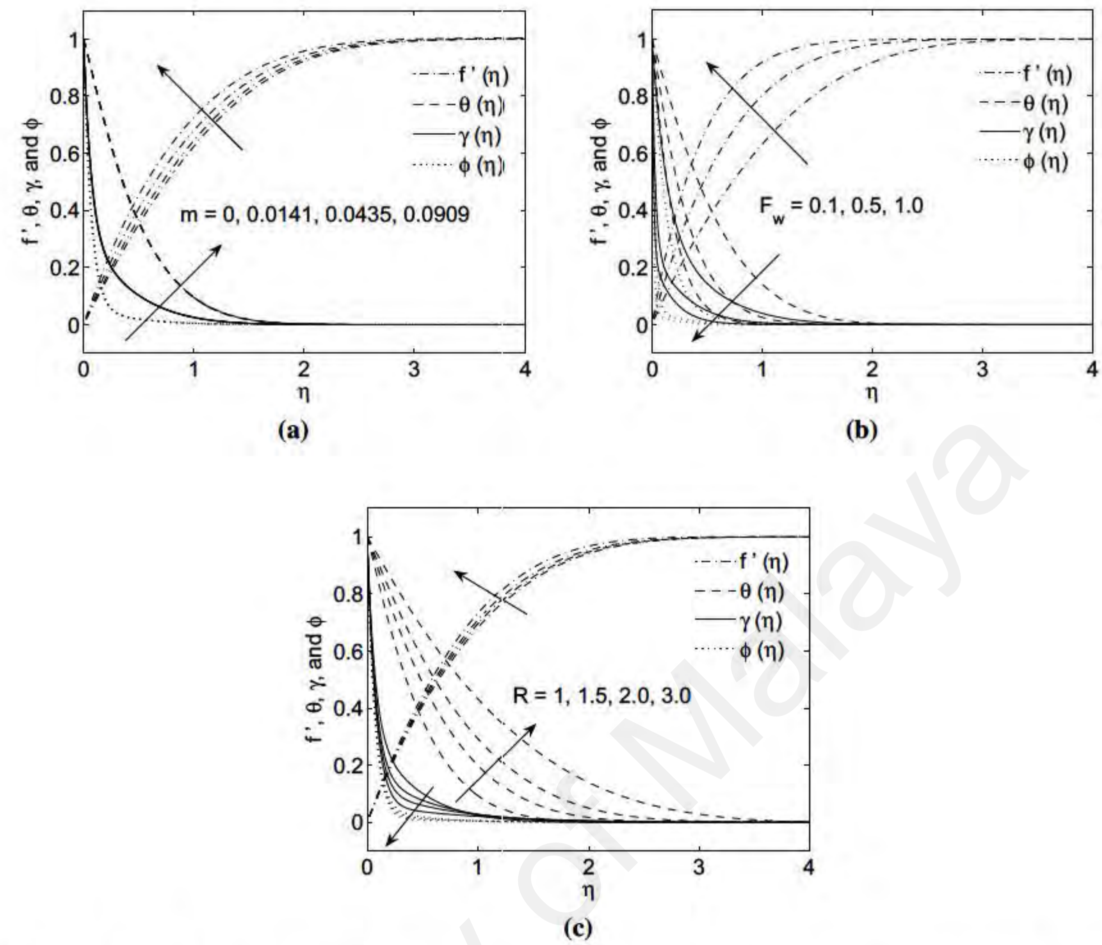

Figure 8.1: The velocity, temperature, solutal concentration and nanoparticle volume fraction profiles with $Ri = 1$, $N_B = 0.2$, $N_T = 0.1$, $N_{CT} = 0.5$, $N_{TC} = 0.1$, $n_1 = 0.3$, $n_2 = 0.1$, $N = 1$, Le $= 5$ and Ln $= 6$ for different values of: (a) m when $F_w = 0.2$ and $R = 1$; (b) F_w when $m = 0.0435$ and $R = 1$; (c) R when $m = 0.0435$ and $F_w = 0.2$

compared to f' on m. This is because the wedge angle plays a dominant role on velocity of the flow than other properties of the fluid such as temperature, solutal concentration and nanoparticle volume fraction.

Fig. 8.2(a) presents the temperature, solutal concentration and volume fraction profiles for various values of Brownian motion parameter, N_B. Brownian motion is one of the key physical forces in nanofluid. This motion caused by the particles suspended in liquid seem to constantly move at random as they are pushed to and fro by collisions with the atoms that comprise the liquid. As a result of this random movement, all particles are distributed throughout the fluid. Thus, it is observed from Fig. 8.2(a) that the temperature rises as the Brownian motion parameter increases. The solutal concentration decreases on increasing N_B due to the rapid movement of the fluid molecules and nanoscopic particles.

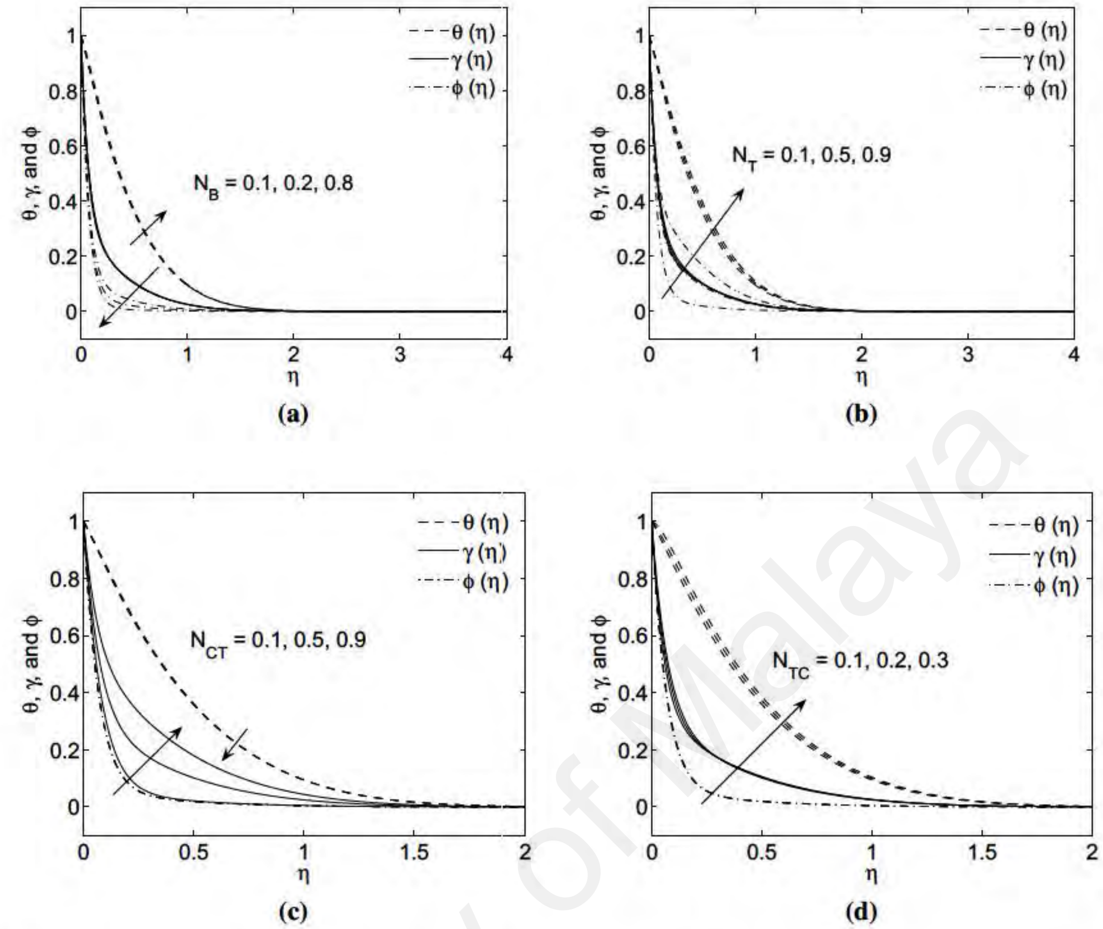

Figure 8.2: The temperature, solutal concentration and volume fraction profiles with $m = 0.0435$, $Ri = 1$, $F_w = 0.2$, $R = 1$, $n_1 = 0.3$, $n_2 = 0.1$, $N = 1$, $\mathrm{Le} = 5$ and $\mathrm{Ln} = 6$ for different values of: (a) N_B when $N_T = 0.1$, $N_{CT} = 0.5$, $N_{TC} = 0.1$; (b) N_T when $N_B = 0.2$, $N_{CT} = 0.5$, $N_{TC} = 0.1$; (c) N_{CT} when $N_B = 0.2$, $N_T = 0.1$, $N_{TC} = 0.1$; and (d) N_{TC} when $N_B = 0.2$, $N_T = 0.1$, $N_{CT} = 0.5$

An increase in N_B refers to an increase in the intermolecular space of nanoparticles. Thus, this situation results in lowering the nanoparticle volume fraction distribution, ϕ.

Thermophoresis is referred as the transport of the nanoparticles in base fluid due to the temperature gradient under the influence of thermophoretic force. Fig. 8.2(b) depicts the influence of thermophoresis, N_T on temperature, solutal concentration and volume fraction profiles. It is noticed that an increase in thermophoresis parameter leads to the increase in fluid temperature, solutal concentration and nanoparticle volume fraction distributions. This situation indicates that N_T works to increase the volume fraction, thermal boundary layer thickness and solutal concentration boundary layer thickness. In addition, this phenomenon shows that the nanoparticles' molecules contain high kinetic energy and resulting in a net force on the particles. This net force is called thermophoretic. More-

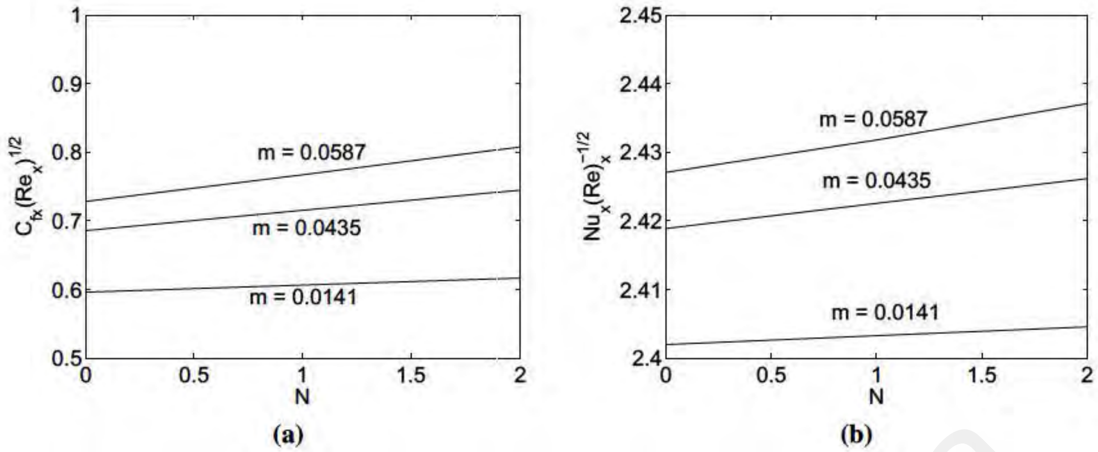

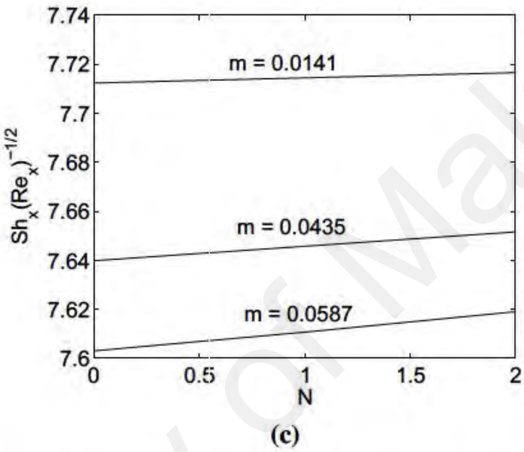

Figure 8.3: Variations of: (a) $C_{fx}(\mathrm{Re})_x^{1/2}$; (b) $Nu_x(\mathrm{Re})_x^{-1/2}$; (c) $Sh_x(\mathrm{Re})_x^{-1/2}$; against N for different values of m when $Ri = 1$, $F_w = 0.2$, $N_B = 0.2$, $N_T = 0.1$, $N_{CT} = 0.5$, $N_{TC} = 0.1$, $n_1 = 0.3$, $n_2 = 0.1$, $R = 1$, $\mathrm{Le} = 5$ and $\mathrm{Ln} = 6$

over, these enhancements are due to the nanoparticles of high thermal conductivity being driven away from the hot surface to the quiescent nanofluid.

The effects of Soret-type parameter, N_{CT} and Dufour-type parameter, N_{TC} on temperature, solutal concentration and volume fraction distributions are shown in Figs. 8.2(c) and 8.2(d), respectively. It is observed that the temperature decreases on increasing N_{CT} and it increases on increasing N_{TC}. Figs. 8.2(c) and 8.2(d) also show that the solutal concentration and nanoparticle volume fraction profiles increase on increasing the Soret-type parameter and Dufour-type parameter. The influence of N_{CT} on γ is more significant compared to N_{CT} on ϕ.

The variations of local skin friction coefficient, local Nusselt number and local Sherwood number against the buoyancy ratio, N for various values of the wedge angle parameter, m are presented in Figs. 8.3((a)–(c)), respectively. It is observed that an increase

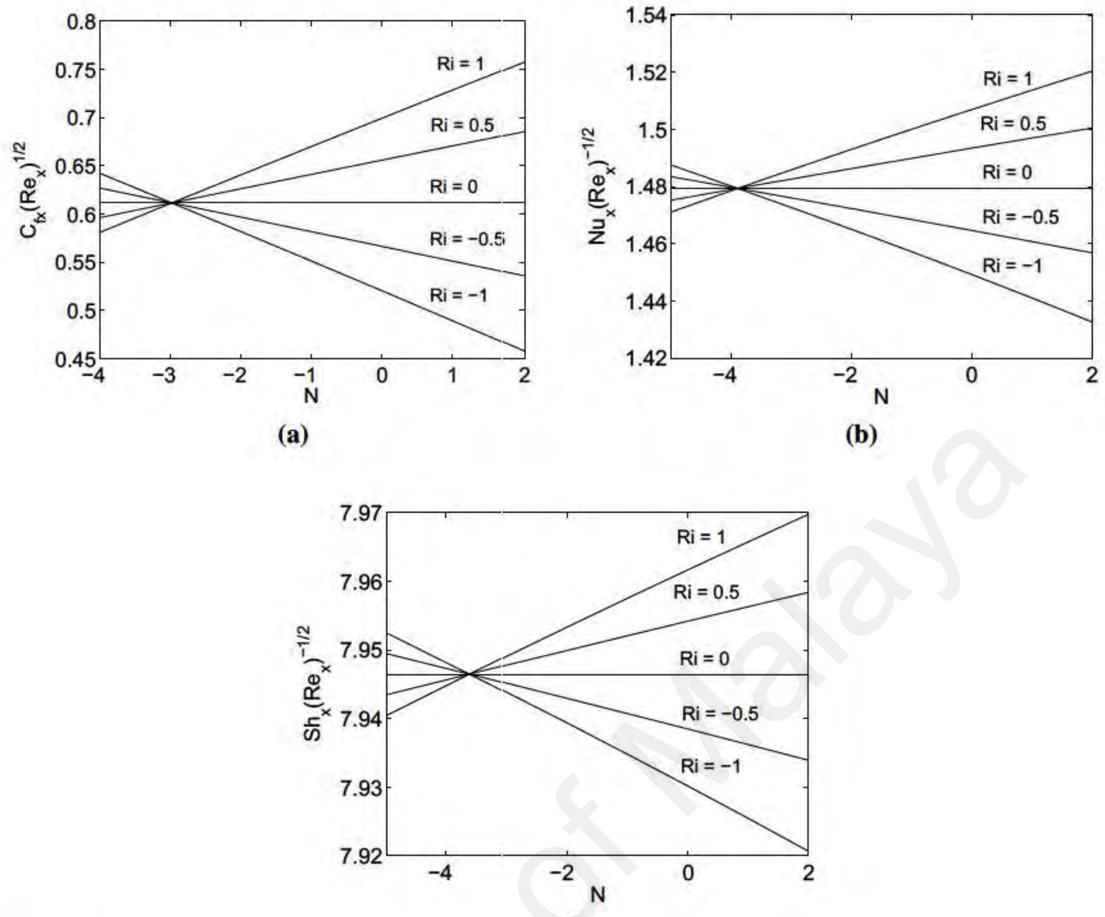

Figure 8.4: Variations of: (a) $C_{fx}(\text{Re})_x^{1/2}$; (b) $Nu_x(\text{Re})_x^{-1/2}$; (c) $Sh_x(\text{Re})_x^{-1/2}$; against N for different values of Ri when $m = 0.0435$, $F_w = 0.2$, $N_B = 0.2$, $N_T = 0.1$, $N_{CT} = 0.5$, $N_{TC} = 0.1$, $n_1 = 0$, $n_2 = 0$, $R = 1$, Le $= 5$ and Ln $= 6$

in wedge angle and buoyancy ratio parameter leads to an increase in local skin friction coefficient and local Nusselt number. Meanwhile, the local Sherwood number decreases on increasing m but opposite behaviour is observed on increasing N. This is due to the fact that the ratio of buoyancy acts like a favorable pressure gradient which accelerated the nanofluid.

The influences of Richardson number, Ri and the buoyancy ratio parameter, N on the local skin friction coefficient, local Nusselt number and local Sherwood number are shown in Figs. 8.4((a)−(c)). Both assisting ($Ri > 0$) and opposing ($Ri < 0$) flow cases are considered. It can be seen that, there is a single intersection point of all the curves plotted in Figs. 8.4((a)−(c)) when N changes within the range $-5 \leq N \leq 2$ for various values of Ri and 1. Based on our computations, we obtained $C_{fx}(\text{Re})_x^{1/2} = 0.61171$ when $N_c = -2.98$, $Nu_x(\text{Re})_x^{-1/2} = 0.63400$ when $N_c = -3.89$ and $Sh_x(\text{Re})_x^{-1/2} = 7.94647$ when $N_c = -3.62$.

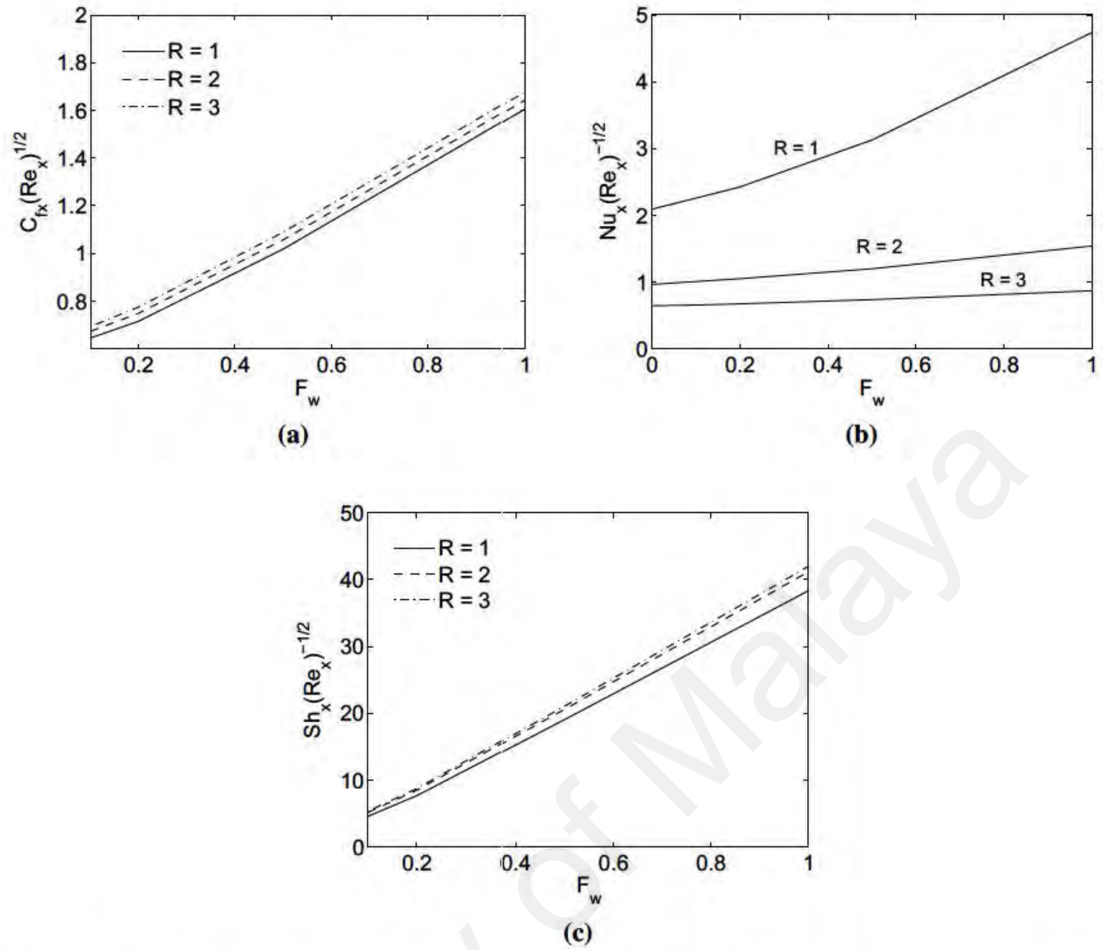

Figure 8.5: Variations of: (a) $C_{fx}(\mathrm{Re})_x^{1/2}$; (b) $Nu_x(\mathrm{Re})_x^{-1/2}$; (c) $Sh_x(\mathrm{Re})_x^{-1/2}$; against F_w for different values of R when $m = 0.0435$, $N = 1$, $N_B = 0.2$, $N_T = 0.1$, $N_{CT} = 0.5$, $N_{TC} = 0.1$, $n_1 = 0.3$, $n_2 = 0.1$, $Ri = 1$, $\mathrm{Le} = 5$ and $\mathrm{Ln} = 6$

Here, N_c is the value of buoyancy ratio parameter for which the intersections exist. It is worth mentioning that the curves of local skin friction coefficient, local Nusselt number and local Sherwood number are parallel to x-axis when $Ri = 0$. This is not surprising since there is no buoyancy effect at the surface of the wedge. As it can be noticed in Figs. 8.4((a)−(c)), the local skin friction coefficient, local Nusselt number and local Sherwood number increase for the case of assisting flow ($Ri > 0$). The variation of local skin friction coefficient, local Nusselt number and local Sherwood number showed a decrease pattern for the case of opposing flow ($Ri < 0$). However, the opposite behaviour is observed when $N < N_c$.

Fig. 8.5(a) displays the variations of local skin friction coefficient against suction parameter, F_w for different values of R. It is observed that the local skin friction coefficient shows an increasing pattern when both parameters, F_w and R increase. The same be-

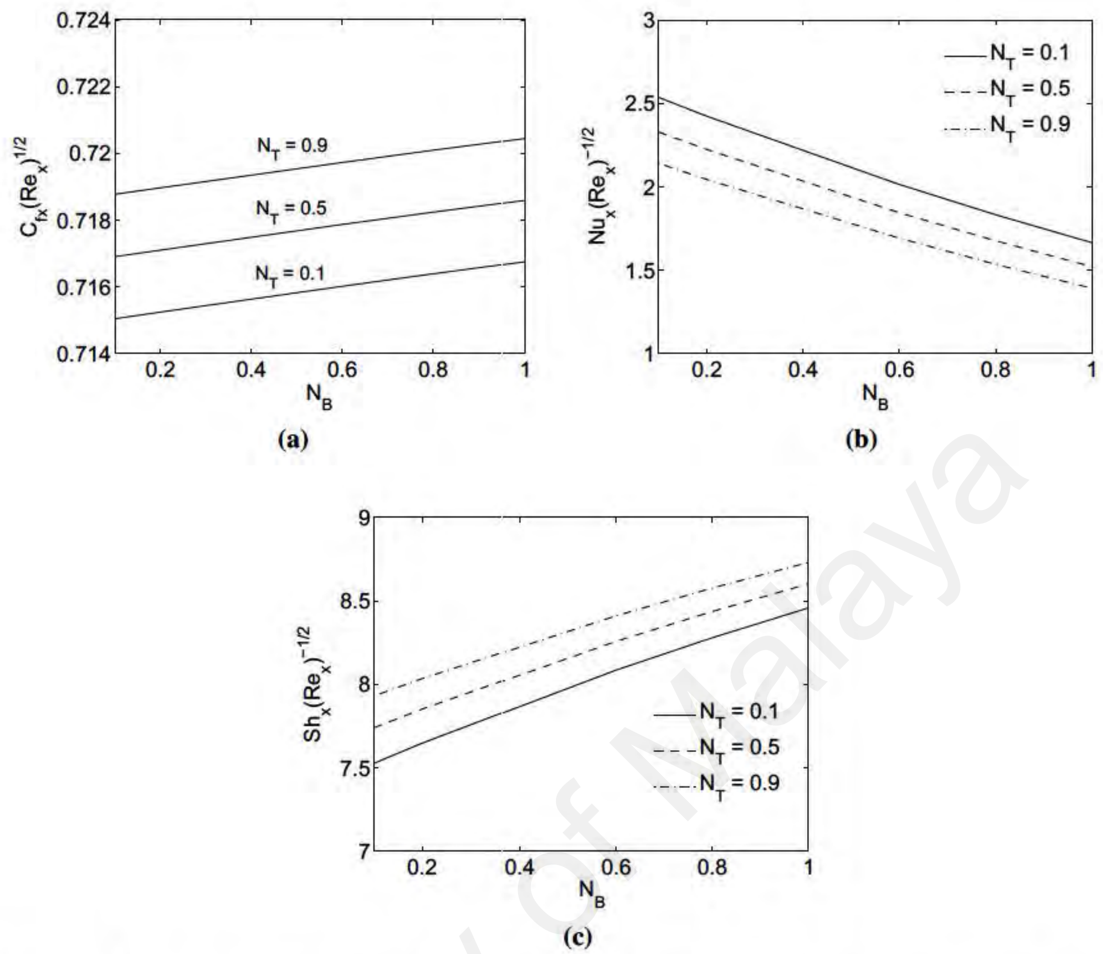

Figure 8.6: Variations of: (a) $C_{fx}(\mathrm{Re})_x^{1/2}$; (b) $Nu_x(\mathrm{Re})_x^{-1/2}$; (c) $Sh_x(\mathrm{Re})_x^{-1/2}$; against N_B for different values of N_T when $m = 0.0435$, $N = 1$, $F_w = 0.2$, $R = 1$, $N_{CT} = 0.5$, $N_{TC} = 0.1$, $n_1 = 0.3$, $n_2 = 0.1$, $Ri = 1$, Le $= 5$ and Ln $= 6$

haviour can be observed in Fig. 8.5(c), that is the local Sherwood number increases on increasing F_w and R. Fig. 8.5(b) shows that, the local Nusselt number decreases on increasing the radiation parameter and it increases on increasing the values of suction. The value of local Nusselt number is higher for the case of $R = 1$, comparing with $R = 2$ and $R = 3$. This is due to the fact that once the fluid is drawn across the suction wall, both the hydrodynamic and thermal boundary layer lead to increase the temperature gradients on the wedge and rises the heat transfer rate.

The simultaneous effects of thermophoresis and Brownian motion parameters on local skin friction coefficient, local Nusselt number and local Sherwood number are presented in Figs. 8.6((a)−(c)), respectively. Thermophoresis involves nanoparticle migration due to the imposed temperature gradient across the fluid. Meanwhile, Brownian motion experiences the random drifting of suspended nanoparticles. Therefore, the numerical results

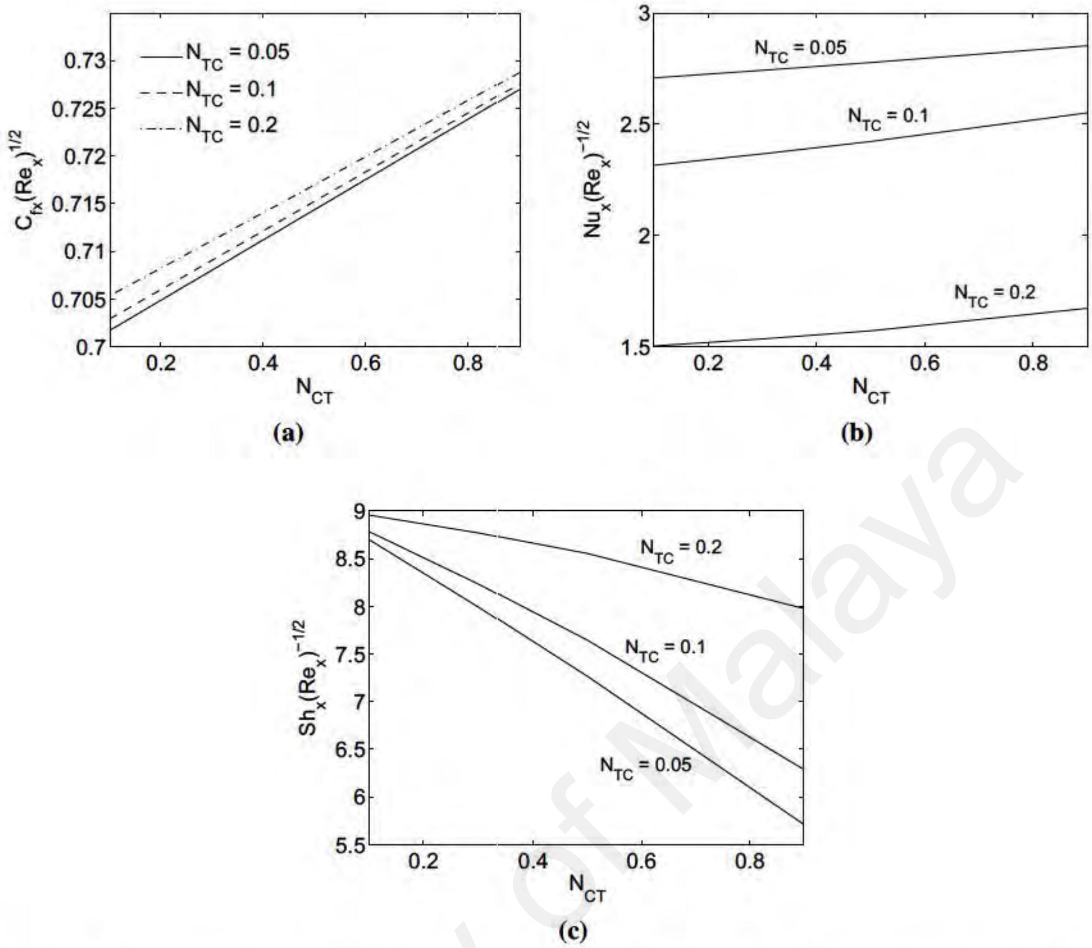

Figure 8.7: Variations of: (a) $C_{fx}(\mathrm{Re})_x^{1/2}$; (b) $Nu_x(\mathrm{Re})_x^{-1/2}$; (c) $Sh_x(\mathrm{Re})_x^{-1/2}$; against N_{CT} for different values of N_{TC} when $m = 0.0435$, $N = 1$, $F_w = 0.2$, $R = 1$, $N_B = 0.2$, $N_T = 0.1$, $n_1 = 0.3$, $n_2 = 0.1$, $Ri = 1$, $\mathrm{Le} = 5$ and $\mathrm{Ln} = 6$

should be carried out for a wide range of Brownian motion and thermophoretic parameters to reveal their effects. Figs. 8.6(a) and 8.6(c) show that the local skin friction coefficient and local Sherwood number increase on increasing N_T and N_B parameters. It is observed that, the local Nusselt number decreases as N_T and N_B increase. This reduction occurs due to the fact that an increase in energy exchange rate causes an enhancement in the random movement of nanoparticles and promote heat conduction.

The influences of N_{CT} and N_{TC} on local skin friction coefficient, local Nusselt number and local Sherwood number are displayed in Figs. 8.7((a)–(c)). It is observed from Fig. 8.7(a) that the local skin friction coefficient increases on increasing both N_{CT} and N_{TC} parameters. The local Nusselt number increases on increasing the Soret-type parameter while a reverse trend is observed for local Sherwood number. This is due to the fact that, the Soret-type parameter produces a mass flux from lower to higher solute concen-

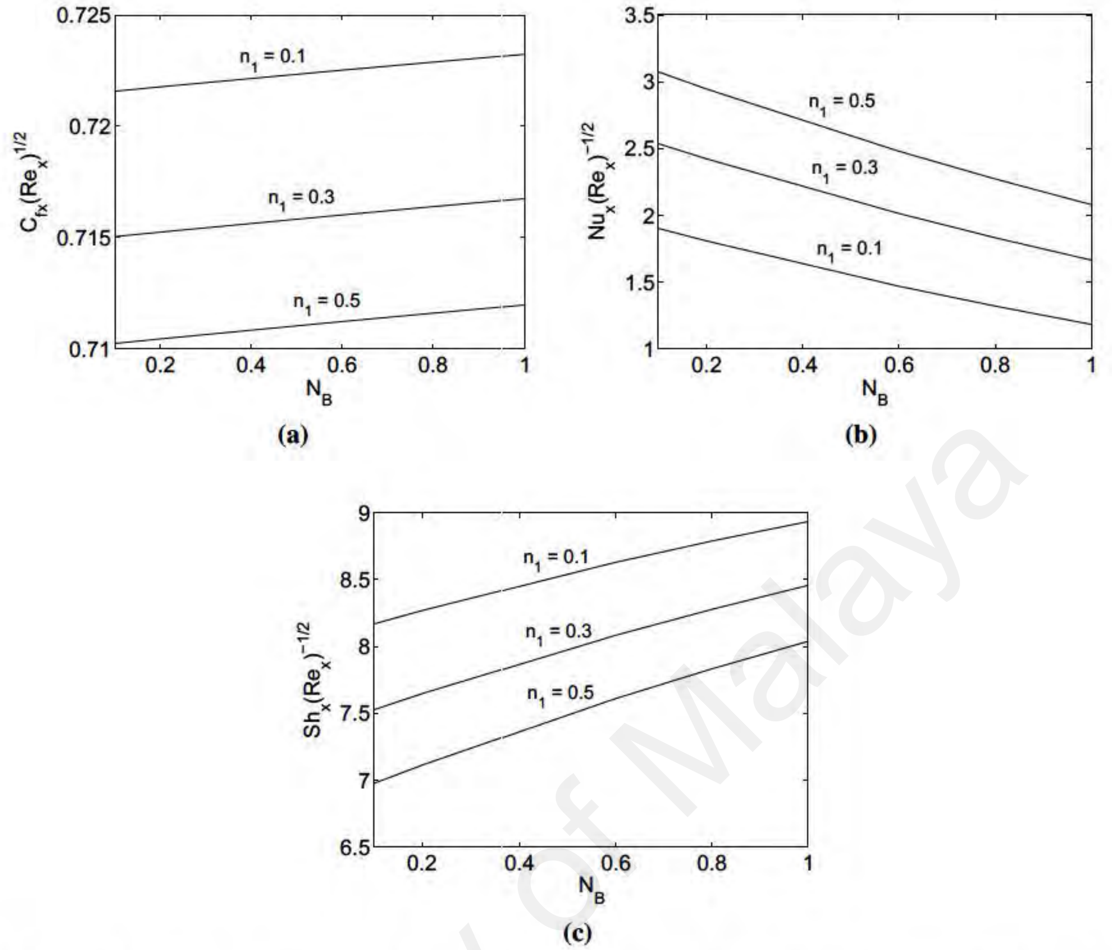

Figure 8.8: Variations of: (a) $C_{fx}(\mathrm{Re})_x^{1/2}$; (b) $Nu_x(\mathrm{Re})_x^{-1/2}$; (c) $Sh_x(\mathrm{Re})_x^{-1/2}$; against N_B for different values of n_1 when $m = 0.0435$, $N = 1$, $F_w = 0.2$, $R = 1$, $N_T = 0.1$, $N_{CT} = 0.5$, $N_{TC} = 0.1$, $n_2 = 0.1$, $Ri = 1$, $\mathrm{Le} = 5$ and $\mathrm{Ln} = 6$

tration driven by the temperature gradient. It can be seen from Fig. 8.7((c)) that the local Sherwood number increases on increasing the Dufour-type parameter and it decreases as the Soret-type parameter increases.

The variations of $C_{fx}(\mathrm{Re})_x^{1/2}$, $Nu_x(\mathrm{Re})_x^{-1/2}$ and $Sh_x(\mathrm{Re})_x^{-1/2}$ against the Brownian motion parameter, N_B for various values of temperature power-law exponent, n_1 are presented in Figs. 8.8((a)−(c)), respectively. It is observed that an increase in n_1 leads to a decrease in local skin friction coefficient as well as local Sherwood number. However, a reverse behaviour is observed for the variation of local Nusselt number. The local Nusselt number increases on increasing the values of surface temperature exponent. In other words, increasing the temperature power-law exponent tends to increase the buoyancy force, accelerating the flow and thus increasing the heat transfer rate.

Figs. 8.9((a)−(c)) show the variations of local skin friction coefficient, local Nusselt

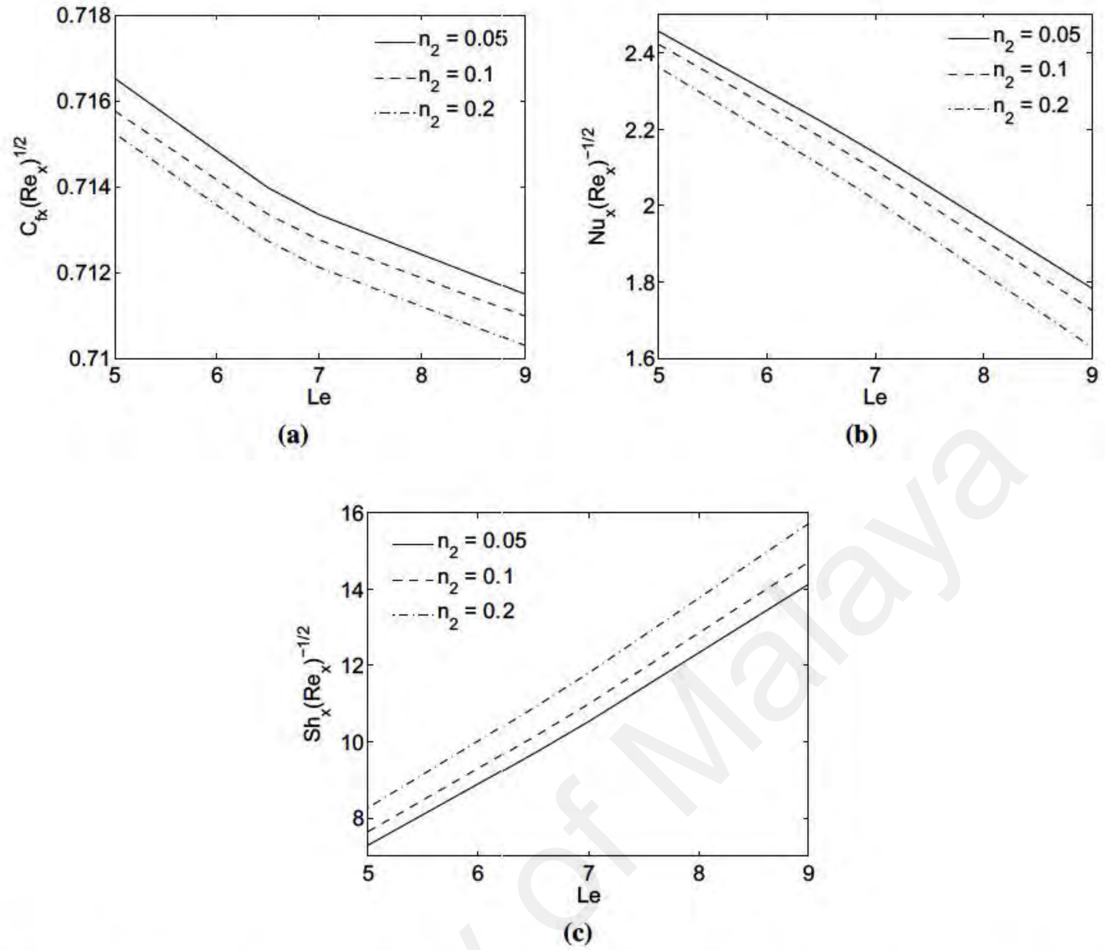

Figure 8.9: Variations of: (a) $C_{fx}(\mathrm{Re})_x^{1/2}$; (b) $Nu_x(\mathrm{Re})_x^{-1/2}$; (c) $Sh_x(\mathrm{Re})_x^{-1/2}$; against Le for different values of n_2 when $m = 0.0435$, $N = 1$, $F_w = 0.2$, $R = 1$, $N_B = 0.2$, $N_T = 0.1$, $N_{CT} = 0.5$, $N_{TC} = 0.1$, $n_1 = 0.3$, $Ri = 1$ and $\mathrm{Ln} = 6$

number and local Sherwood number against Lewis number, Le for various values of concentration power-law exponent, n_2. Lewis number is defined as the ratio of thermal diffusivity to mass diffusivity. It is an effective parameter which is used to characterize the fluid flow where simultaneous heat and mass transfer occur because of convection. Obviously, an increase in the values of Le leads to decrease the local skin friction coefficient and local Nusselt number. It is observed from Figs. 8.9((a)−(b)) that both local skin friction coefficient and local Nusselt number exert the decreasing behavior when the value of n_2 increases. Comparing the curves in Fig. 8.9(c), it can be seen that the local Sherwood number increases as the Lewis number and n_2 increase. This is due to the fact that a larger Lewis number has relatively lower molecular diffusivity.

CHAPTER 9: CONCLUSIONS AND RECOMMENDATIONS

This Doctoral thesis addresses the numerical study on convective boundary layer flow and heat transfer of nanofluid over a wedge. Starting with a brief introduction to fluid dynamics and boundary layer, Chapter 1 evolves through the mode of heat transfer and the classification of convection. This chapter also underlined the general introduction to nanofuid and listed its advantages as compared to conventional fluid. Chapter 2 focuses on a comprehensive literature review on the boundary layer flow over a wedge. The thorough discussion in the review led to one significant outcome which is the boundary layer flow of nanofluid along a wedge. Besides that, the seven specification effects such as the moving wedge, suction, chemical reaction, heat generation or absorption, thermal radiation, Soret and Dufour are emphasized. Chapter 3 gives the details of the derivation of the governing equations which satisfied the flow field along the wedge. The solution of the governing equations is achieved with the aid of similarity and local similarity concepts. The reduced boundary layer equations, complete with transformed boundary conditions are solved by using the fourth-order Runge-Kutta-Gill method along with the shooting technique and Newton Raphson method. On the basis of the present numerical investigations on boundary layer flow of nanofluid along a wedge, the following conclusions can be drawn:

The velocity profile increases on increasing the value of wedge angle and suction parameters. The velocity profile also increases for both cases of stretching and shrinking wedge. This means that the fluid velocity became faster and thereby the velocity profiles squeeze faster and move closer to the surface of the wedge wall. In addition, the hydrodynamic boundary layer becomes thin for larger values of the wedge angle and suction parameters. The velocity profile seems insignificant on increasing the values of Brownian motion, thermophoresis, Soret and Dufour because these parameters are not appeared in momentum equation.

The temperature profile increases on increasing the wedge angle, thermal radiation, heat generation/absorption, Brownian motion, thermophoresis and Dufour-type parameters. An increase in the thermal radiation leads to enhance the temperature at each point away from the wedge surface. However, the temperature of the fluid decreases on increasing the suction parameter. The imposition of suction at the wedge surface reduces the region of viscous domination close to the wall, which causes decreasing in the temperature profile. Besides that, the sheer stress enhances when increasing the suction parameter and causes the decrease in thermal boundary layer thickness. It is noted that the dimensionless temperature profile decreases on increasing the value of Soret-type parameter. However, the temperature rises as the Soret-type parameter increases in the presence of chemical reaction or stretching or shrinking wedge.

The nanoparticle volume fraction profile decreases on increasing the value of suction, thermal radiation and Brownian motion parameters. An increase in Brownian motion parameter refers to an increase in the intermolecular space of nanoparticles. Thus, this situation results in lowering the nanoparticle volume fraction distribution.

The solutal concentration profile increases on increasing wedge angle and Soret-type parameters. The increasing value of thermophoresis parameter also enhances the solutal concentration profile in the presence of chemical reaction and moving wedge. Thermophoresis is associated with the migration of nanoparticle in water due to nanoscopic temperature gradient. Thus, this yields strong increment in solutal concentration profile. The solutal concentration profile decreases on increasing suction, thermal radiation and Brownian motion parameters. The higher value of suction parameter implies the increasing of the sheer stress on the wedge surface. Adding to that, an increase in thermal radiation parameter leads to enhance the surface heat flux. Both situations indicate to the decrease in solutal concentration profile.

The local skin friction coefficient increases on increasing the value of wedge angle and suction parameters when the moving wedge parameter is less than 1 ($\lambda < 1$) and it decreases for $\lambda > 1$. The results also showed that the positive value of local skin friction coefficient is obtained for $\lambda < 1$ and for the case of $\lambda > 1$, the opposite sign is obtained. All values of skin friction coefficient are negative as $\lambda > 1$ and decrease to more negativity on increasing the value of wedge angle and suction parameters. As mentioned in Chapter 6, this situation happened when there is a force that opposes the motion when the wedge moves through the nanofluid. The negative value of skin friction coefficient indicates that the drag force on the fluid is exerted by the moving wedge and the positive value implies the opposite. In the presence of thermal radiation, the local skin friction coefficient increases on increasing the value of wedge angle parameter when the suction value is less than 1.4 ($F_w < 1.4$), while the reverse behaviour is noticed for $F_w > 1.4$. An increase in buoyancy ratio parameter leads to an increase in the local skin friction coefficient. The local skin friction coefficient also increases for the case of assisting flow ($Ri > 0$), while it decreases for the case of opposing flow ($Ri < 0$).

The local Nusselt number increases on increasing the value of wedge angle, suction, moving wedge, Soret-type and buoyancy ratio parameters. The local Nusselt number reduces as the value of Lewis number, Brownian motion, thermophoresis and Dufour-type parameters increase. An increase in thermal radiation parameter leads to increase the local Nusselt number. However for the case of mixed convection, a strong reduction in local Nusselt number is obtained as the value of thermal radiation increases. The local Nusselt number increases on increasing the temperature power-law exponent and it decreases as the concentration power-law exponent increases. The local Nusselt number showed an increasing pattern for the case of assisting flow ($Ri > 0$). The opposite result is obtained for the case of opposing flow ($Ri < 0$).

The local Sherwood number decreases on increasing the value of wedge angle and Soret-type parameters as well as temperature power-law exponent. The Soret-type parameter appears in the solutal concentration equation, therefore it accounts for additional mass diffusion. Thus, this results in strong reduction of the local Sherwood number as the value of Soret-type parameter increases. Meanwhile, the local Sherwood number increases on increasing the value of suction, thermal radiation, buoyancy ratio, Brownian motion, thermophoresis and Dufour-type parameters. In addition, the local Sherwood number increases as the Lewis number and concentration power-law exponent increase. This is due to the fact that a larger Lewis number has relatively lower molecular diffusivity.

9.1 Recommendations for Future Work

As a result of the work done for this thesis, the following have emerged as work for the future.

9.1.1 Flow Regimes

The boundary layer nanofluid model can be extended for various flow regimes such as turbulance flow, flow through porous media and MHD flow.

9.1.2 Experimental

An experimental investigation could be set up in order to simulate the boundary layer flow of nanofluid along a wedge. The experimental results can be used to validate the present numerical results and extended to the use of practical applications.

REFERENCES

Ahmad, R., & Khan, W. A. (2013). Effect of viscous dissipation and internal heat generation/absorption on heat transfer flow over a moving wedge with convective boundary condition. *Heat Transfer–Asian Research*, *42*(7), 589–602.

Ahmad, R., & Khan, W. A. (2014). Numerical study of heat and mass transfer MHD viscous flow over a moving wedge in the presence of viscous dissipation and heat source/sink with convective boundary condition. *Heat Transfer–Asian Research*, *43*(1), 17–38.

Ahmed, S. E., Hussein, A. K., Mohammed, H. A., Adegun, I. K., Zhang, X., Kolsi, L., & Sivasankaran, S. (2014). Viscous dissipation and radiation effects on MHD natural convection in a square enclosure filled with a porous medium. *Nuclear Engineering and Design*, *266*, 34–42.

Akçay, M., & Yükselen, M. A. (2011). Flow of power-law fluids over a moving wedge surface with wall mass injection. *Archive of Applied Mechanics*, *81*, 65–76.

Ashwini, G., & Eswara, A. T. (2012). MHD Falkner-Skan boundary layer flow with internal heat generation or absorption. *World Academy of Science, Engineering and Technology*, *65*, 662–665.

Bazaraa, M. S., Sherali, H. D., & Shetty, C. M. (2006). *Nonlinear programming: Theory and algorithms* (3rd ed.). John Wiley & Sons, Incorporated.

Bhuvaneswari, M., Sivasankaran, S., & Kim, Y. J. (2012). Lie group analysis of radiation natural convection flow over an inclined surface in a porous medium with internal heat generation. *Journal of Porous Media*, *12*, 1155–1164.

Brown, S. N., & Stewartson, K. (1966). On the reversed flow solutions of the Falkner-Skan equation. *Mathematika*, *13*(1), 1–6.

Buongiorno, J. (2006). Convective transport in nanofluids. *ASME Journal of Heat Transfer*, *128*, 240–250.

Butt, A. S., & Ali, A. (2013). Thermodynamical analysis of the flow and heat transfer over a static and a moving wedge. *ISRN Thermodynamics*, *2013*, 264095.

Cebeci, T., & Keller, H. B. (1971). Shooting and parallel shooting methods for solving the Falkner-Skan boundary-layer equation. *Journal Of Computational Physics*, *7*, 289–300.

Chamkha, A. J., Abbasbandy, S., Rashad, A., & Vajravelu, K. (2012). Radiation effects on mixed convection over a wedge embedded in a porous medium filled with a nanofluid. *Transport in Porous Media*, *91*(1), 261–279.

Chamkha, A. J., Khaled, A. R. A., & Al-Hawaj, O. (2000). Simultaneous heat and mass transfer by natural convection from a cone and a wedge in porous media. *Journal of Porous Media*, *3*(2), 155–164.

Chamkha, A. J., Mujtaba, M., Quadri, A., & Issa, C. (2003). Thermal radiation effects on

MHD forced convection flow adjacent to a non-isothermal wedge in the presence of a heat source or sink. *Heat and Mass Transfer*, *39*, 305–312.

Chamkha, A. J., & Rashad, A. M. (2014). MHD forced convection flow of a nanofluid adjacent to a non-isothermal wedge. *Computational Thermal Sciences*, *6*(1), 27–39.

Chamkha, A. J., Rashad, A. M., & Gorla, R. S. R. (2014). Non-similar solutions for mixed convection along a wedge embedded in a porous medium saturated by a non-Newtonian nanofluid. *International Journal of Numerical Methods for Heat and Fluid Flow*, *24*(7), 1471–1486.

Chandrasekar, M. (2003). Analytical study of heat transfer and boundary layer flow with suction and injection. *Heat and Mass Transfer*, *40*, 157–165.

Chandrasekar, M., & Baskaran, S. (2008). Analytic study of magnetohydrodynamic flow and boundary layer control over a wedge. *Acta Mathematicae Applicatae Sinica, English Series*, *24*(4), 541–552.

Chandrasekar, M., & Shanmugapriya, M. (2008). Analytic solution of a free and forced convection with suction and injection over a non-isothermal wedge. *Bulletin of the Malaysian Mathematical Sciences Society*, *31*(1), 11–24.

Chao, B. T., & Cheema, L. S. (1971). Forced convection in wedge flow with non-isothermal surfaces. *International Journal of Heat and Mass Transfer*, *14*(9), 1363–1375.

Chen, L. S., & Chao, B. T. (1970). Thermal response behavior of laminar boundary layers in wedge flow. *International Journal of Heat and Mass Transfer*, *13*(7), 1101–1114.

Chen, L. S., & Radulovic, P. T. (1973). Heat transfer in non-Newtonian flow past a wedge with nonisothermal surfaces. *Journal of Heat Transfer*, *95*(4), 498–504.

Chen, Y. M. (1985). Heat transfer of a laminar flow passing a wedge at small Prandtl number: A new approach. *International Journal of Heat and Mass Transfer*, *28*(8), 1517–1523.

Chen, Y. M. (1986). A higher order asymtotic solution for heat transfer of a laminar flow passing a wedge at small Prandtl number. *International Journal of Heat and Mass Transfer*, *29*(3), 490–492.

Cheng, C. Y. (2012). Soret and Dufour effects on mixed convection heat and mass transfer from a vertical wedge in a porous medium with constant wall temperature and concentration. *Transport in Porous Media*, *94*(1), 123–132.

Choi, S. U. S. (1995). Enhancing thermal conductivity of fluids with nanoparticles. In *Developments and Applications of Non-Newtonian Flows: International Mechanical Engineering Congress & Exposition.*

Curle, N. (1962). *The laminar boundary layer equations* (First ed.). Great Britain: Oxford University Press.

Das, S. K., Choi, S. U. S., Yu, W., & Pradeep, T. (2007). *Nanofluids: Science and* *technology*. John Wiley and Sons, Inc.

Deka, R. K., & Sharma, S. (2013). Magnetohydrodynamic mixed convection flow past a wedge under variable temperature and chemical reaction. *American Journal of Computational and Applied Mathematics*, *3*(2), 74–80.

Drake, D. G., & Riley, D. S. (1975). On the heat transfer from a wedge with non-isothermal surfaces. *Journal of Applied Mathematics and Physics*, *26*, 199–202.

Elbashbeshy, E. M. A., & Dimian, M. F. (2002). Effect of radiation on the flow and heat transfer over a wedge with variable viscosity. *Applied Mathematics and Computation*, *132*, 445–454.

Evans, H. L. (1968). *Laminar boundary layer theory*. Addison-Wesley Publishing Company.

Falkner, V. M., & Skan, S. W. (1931). Some approximate solutions of the boundary layer equations. *Philosophical Magazine*, *12*(80), 865–896.

Ganapathirao, M., Ravindran, R., & Momoniat, E. (2015). Effects of chemical reaction, heat and mass transfer on an unsteady mixed convection boundary layer flow over a wedge with heat generation/absorption in the presence of suction or injection. *Heat and Mass Transfer*, *51*(2), 289–300.

Ganapathirao, M., Ravindran, R., & Pop, I. (2013). Non-uniform slot suction (injection) on an unsteady mixed convection flow over a wedge with chemical reaction and heat generation or absorption. *International Journal of Heat and Mass Transfer*, *67*, 1054–1061.

Gill, S. (1951). A process for the step-by-step integration of differential equations in an automatic digital computing machine. *Mathematical Proceedings of the Cambridge Philosophical Society*, *47*(1), 96–108.

Gorla, R. S. R., Chamkha, A. J., & Rashad, A. M. (2011). Mixed convective boundary layer flow over a vertical wedge embedded in a porous medium saturated with a nanofluid: Natural convection dominated regime. *Nanoscale Research Letters*, *6*, 207.

Griffiths, D. F., & Higham, D. J. (2010). *Numerical methods for ordinary differential equations*. Springer-Verlag London.

Gunness, R. C., & Gebhart, B. (1965). Combined forced and natural convection flow for the wedge geometry. *International Journal of Heat and Mass Transfer*, *8*(1), 43–53.

Hartree, D. R. (1937). On an equation occuring in Falkner and Skan's approximate treatment of the equations of the boundary layer. *Proceedings of the Cambridge Philosophical Society*, *33*, 223--239.

Herwig, H. (1987). An asymptotic approach to compressible boundary layer flow. *International Journal of Heat and Mass Transfer*, *30*(1), 59–68.

Hossain, M. A., Munir, M. S., & Rees, D. A. S. (2000). Flow of viscous incompressible fluid with temperature dependent viscosity and thermal conductivity past a permeable wedge with uniform surface heat flux. *International Journal of Thermal Sciences*, *39*(6), 635–644.

Hsiao, K. L. (2011). MHD mixed convection for viscoelastic fluid past a porous wedge. *International Journal of Non-Linear Mechanics*, *46*, 1-8.

Hsu, C. H., Chen, C. S., & Teng, J. T. (1997). Temperature and flow fields for the flow of a second grade fluid past a wedge. *International Journal of Non-Linear Mechanics*, *32*(5), 933–946.

Ishak, A., Nazar, R., & Pop, I. (2006). Moving wedge and flat plate in a micropolar fluid. *International Journal of Engineering Science*, *44*, 1225–1236.

Ishak, A., Nazar, R., & Pop, I. (2007). Falkner-Skan equation for flow past a moving wedge with suction or injection. *Journal of Applied Mathematics and Computing*, *25*(1), 67–83.

Ishak, A., Nazar, R., & Pop, I. (2011). Moving wedge and flat plate in a power-law fluid. *International Journal of Non-Linear Mechanics*, *46*, 1017–1021.

Jafar, K., Nazar, R., Ishak, A., & Pop, I. (2013). MHD boundary layer flow due to a moving wedge in a parallel stream with the induced magnetic field. *Boundary Value Problems*, *20*, 1–14.

Jaluria, Y. (1980). *Natural convection heat and mass transfer*. United Kingdom: Pergamon Press.

James, M., Mureithi, E. W., & Kuznetsov, D. (2015). Effects of variable viscosity of nanofluid flow over a permeable wedge embedded in saturated porous medium with chemical reaction and thermal radiation. *International Journal of Advances in Applied Mathematics and Mechanics*, *2*(3), 101–118.

Jeng, D. R., Lee, M. H., & DeWitt, K. J. (1978). Convective heat transfer through boundary layers with arbitrary pressure gradient and non-isothermal surfaces. *International Journal of Heat and Mass Transfer*, *21*(4), 499–509.

Kafoussias, N. G., & Nanousis, N. D. (1997). Magnetohydrodynamic laminar boundary-layer flow over a wedge with suction or injection. *Canadian Journal of Physics*, *75*(10), 733–745.

Kameswaran, P. K., Narayana, M., Shaw, S., & Sibanda, P. (2014). Heat and mass transfer from an isothermal wedge in nanofluids with Soret effect. *The European Physical Journal Plus*, *129*(7), 154.

Kandasamy, R., Muhaimin, I., Hashim, I., & Ruhaila, M. K. (2008). Thermophoresis and chemical reaction effects on non-Darcy mixed convective heat and mass transfer past a porous wedge with variable viscosity in the presence of suction or injection. *Nuclear Engineering and Design*, *238*, 2699–2705.

Kandasamy, R., Muhaimin, I., Khamis, A. B., & Roslan, R. (2013). Unsteady Hiemenz flow of Cu-nanofluid over a porous wedge in the presence of thermal stratification due to solar energy radiation: Lie group transformation. *International Journal of Thermal Sciences*, *65*, 196–205.

Kandasamy, R., Muhaimin, I., Ram, N. S., & Prabhu, K. K. S. (2012). Thermal stratification effects on Hiemenz flow of nanofluid over a porous wedge sheet in the presence of suction/injection due to solar energy: Lie group transformation. *Transport in Porous Media*, *94*, 399–416.

Kandasamy, R., Muhaimin, I., & Rosmila, A. K. (2014). The performance evaluation of unsteady MHD non-Darcy nanofluid flow over a porous wedge due to renewable (solar) energy. *Renewable Energy*, *64*, 1–9.

Kandasamy, R., & Palanimani, P. G. (2007). Effects of chemical reactions, heat and mass transfer on nonlinear magnetohydrodynamic boundary layer flow over a wedge with a porous medium in the presence of Ohmic heating and viscous dissipation. *Journal of Porous Media*, *10*(6), 489–501.

Kandasamy, R., Periasamy, K., & Prabhu, K. K. S. (2005). Effects of chemical reaction, heat and mass transfer along a wedge with heat source and concentration in the presence of suction or injection. *International Journal of Heat and Mass Transfer*, *48*, 1388–1394.

Kays, W. M., & Crawford, M. E. (1980). *Convective heat and mass transfer* (Second ed.). USA: McGraw-Hill.

Khan, M. S., Karim, I., Islam, M. S., & Wahiduzzaman, M. (2014). MHD boundary layer radiative, heat generating and chemical reacting flow past a wedge moving in a nanofluid. *Nano Convergence*, *1*, 20.

Khan, W. A., & Pop, I. (2013). Boundary layer flow past a wedge moving in a nanofluid. *Mathematical Problems in Engineering*, *2013*, ID637285.

Khan, Z., Khan, W., & Pop, I. (2013). Triple diffusive free convection along a horizontal plate in porous media saturated by a nanofluid with convective boundary condition. *International Journal of Heat and Mass Transfer*, *66*, 603–612.

King, W. S., & Varwig, R. L. (1971). The hypersonic boundary layer on a wedge with uniform mass addition and viscous interaction. *International Journal of Heat and Mass Transfer*, *14*(1), 41–48.

Kumari, M. (1998). MHD flow over a wedge with large blowing rates. *International Journal of Engineering Science*, *36*(3), 299–314.

Kumari, M., Takhar, H. S., & Nath, G. (2001). Mixed convection flow over a vertical wedge embedded in highly porous medium. *Heat and Mass Transfer*, *37*, 139–146.

Kuznetsov, A. V., & Nield, D. A. (2011). Double-diffusive natural convective boundary-layer flow of a nanofluid past a vertical plate. *International Journal of Thermal Sciences*, *50*, 712–717.

Levy, S. (1952). Heat transfer to constant-property laminar boundary-layer flows with power-function free stream velocity and wall temperature variations. *Journal of the Aeronautical Sciences*, *19*(5), 341–348.

Libby, P. A., & Li, T. M. (1967). Further solutions of the Falkner-Skan equation. *AIAA Journal*, *5*(5), 1040–1042.

Lin, H. T., & Lin, L. K. (1987). Similarity solutions for laminar forced convection heat transfer from wedges to fluids of any Prandtl number. *International Journal of Heat and Mass Transfer*, *30*(6), 1111–1118.

Loganathan, P., Puvi-Arasu, P., & Kandasamy, R. (2010). Local non-similarity solution to impact of chemical reaction on MHD mixed convection heat and mass transfer flow over porous wedge in the presence of suction/injection. *Applied Mathematics and Mechanics (English Edition)*, *31*(12), 1517–1526.

Massoudi, M., & Ramezan, M. (1989). Effect of injection or suction on the Falkner-Skan flows of second grade fluids. *International Journal of Non-Linear Mechanics*, *24*(3), 221–227.

Midya, C. (2012). Exact solutions of chemically reactive solute distribution in MHD boundary layer flow over a shrinking surface. *Chinese Physics Letters*, *29*, 014701.

Mohamad, R., Kandasamy, R., & Muhaimin, I. (2013). Enhance of heat transfer on unsteady Hiemenz flow of nanofluid over a porous wedge with heat source/sink due to solar energy radiation with variable stream condition. *Heat and Mass Transfer*, *49*(9), 1261–1269.

Muhaimin, I., Kandasamy, R., & Hashim, I. (2009). Thermophoresis and chemical reaction effects on non-Darcy MHD mixed convective heat and mass transfer past a porous wedge in the presence of variable stream condition. *Chemical Engineering Research And Design*, *87*, 1527–1535.

Mukhopadhyay, S. (2009). Effects of radiation and variable fluid viscosity on flow and heat transfer along a symmetric wedge. *Journal of Applied Fluid Mechanics*, *12*(2), 29–34.

Nanbu, K. (1971). Unsteady Falkner-Skan flow. *Zeitschrift für Angewandte Mathematik und Physik*, *22*(6), 1167–1172.

Nanousis, N. D. (1999). Theoretical magnetohydrodynamic analysis of mixed convection boundary-layer flow over a wedge with uniform suction or injection. *Acta Mechanica*, *138*(21–30).

Olsson, U. (1973). Laminar flow heat transfer from wedge-shaped bodies with limited heat conductivity. *International Journal of Heat and Mass Transfer*, *16*(2), 329–336.

Pal, D., & Mondal, H. (2009). Influence of temperature-dependent viscosity and thermal radiation on MHD forced convection over a non-isothermal wedge. *Applied Mathematics and Computation*, *212*(1), 194–208.

Pal, D., & Mondal, H. (2013). Influence of thermophoresis and Soret-Dufour on magnetohydrodynamic heat and mass transfer over a non-isothermal wedge with thermal radiation and Ohmic dissipation. *Journal of Magnetism and Magnetic Materials*, *331*, 250–255.

Postelnicu, A., & Pop, I. (2011). Falkner-Skan boundary layer flow of a power-law fluid past a stretching wedge. *Applied Mathematics and Computation*, *217*, 4359–4368.

Prasad, K. V., Datti, P. S., & Vajravelu, K. (2013). MHD mixed convection flow over a permeable non-isothermal wedge. *Journal of King Saud University–Science*, *25*, 313–324.

Prober, R., & Stewart, W. E. (1963). Transport phenomena in wedge flows: Perturbation solutions for small mass transfer rates. *International Journal of Heat and Mass Transfer*, *6*(3), 221–229.

Rahman, M. M., & Al-Hadhrami, A. M. K. (2013). Nonlinear slip flow with variable transport properties over a wedge with convective surface. In *Chaos and Complex Systems: Proceedings of the 4th International Interdisciplinary Chaos Symposium.*

Rahman, M. M., Al-Lawatia, M. A., Eltayeb, I. A., & Al-Salti, N. (2012). Hydromagnetic slip flow of water based nanofluids past a wedge with convective surface in the presence of heat generation or absorption. *International Journal of Thermal Sciences*, *57*, 172–182.

Raman, N. S., Prabhu, K. K. S., & Kandasamy, R. (2014). Heat transfer effects on Hiemenz flow of nanofluid over a porous wedge sheet in the presence of suction/injection due to solar energy: Lie group transformation. *Journal of Engineering Thermophysics*, *23*(1), 66–78.

Rashad, A. M., & Bakier, A. Y. (2009). MHD effects on non-Darcy forced convection boundary layer flow past a permeable wedge in a porous medium with uniform heat flux. *Nonlinear Analysis: Modelling and Control*, *14*(2), 249–261.

Rashidi, M. M., Ali, M., Freidoonimehr, N., Rostami, B., & Hossain, M. A. (2014). Mixed convective heat transfer for MHD viscoelastic fluid flow over a porous wedge with thermal radiation. *Advances in Mechanical Engineering*, *2014*, 10.

Riley, N., & Wiedman, P. D. (1989). Multiple solutions of the Falkner-Skan equation for flow past a stretching boundary. *SIAM Journal of Applied Mathematics*, *49*(5), 1350-1358.

Saaty, T. L., & Bram, J. (1964). *Nonlinear mathematics*. McGraw-Hill, New York.

Salem, A. M. (2010). Temperature-dependent viscosity effects on non-Darcy hydrodynamic free convection heat transfer from a vertical wedge in porous media. *Chinese Physics Letters*, *27*(6), 064401.

Salem, A. M., Ismail, G., & Fathy, R. (2014). Hydromagnetic flow of a Cu-water nanofluid past a moving wedge with viscous dissipation. *Chinese Physics B*, *23*(4), 044402.

Schlichting, H., & Gersten, K. (2000). *Boundary layer theory* (Eight ed.). German: Springer.

Schuh, H. (1947). Laminar heat transfer in boundary layers at high velocities. *Reports and Transaction, 180*.

Singh, P. J., Roy, S., & Ravindran, R. (2009). Unsteady mixed convection flow over a vertical wedge. *International Journal of Heat and Mass Transfer*, *52*, 415–421.

Smith, S. H. (1967). The impulsive motion of a wedge in a viscous fluid. *Zeitschrift für Angewandte Mathematik und Physik*, *18*(4), 508–522.

Stewart, W. E., & Prober, R. (1962). Heat transfer and diffusion in wedge flows with rapid mass transfer. *International Journal of Heat and Mass Transfer*, *5*(12), 1149–1152.

Stewartson, K. (1954). Further solutions of the Falkner-Skan equation. *Mathematical Proceedings of the Cambridge Philosophical Society*, *50*(3), 454–465.

Su, X., & Zheng, L. (2013). Hall effect on MHD flow and heat transfer of nanofluids over a stretching wedge in the presence of velocity slip and Joule heating. *Central European Journal of Physics*, *11*(12), 1694–1703.

Su, X., Zheng, L., Zhang, X., & Zhang, J. (2012). MHD mixed convective heat transfer over a permeable stretching wedge with thermal radiation and Ohmic heating. *Chemical Engineering Science*, *78*, 1–8.

Thamelis, N. J. (1995). *Transport and chemical rate phenomena*. Taylor and Francis Group.

Tiwari, R. K., & Das, M. K. (2007). Heat transfer augmentation in a two-sided lid-driven differentially heated square cavity utilizing nanofluids. *International Journal of Heat and Mass Transfer*, *50*, 2002–2018.

Unsworth, K., & Chiam, T. C. (1980). A numerical solution for the heat transfer from a wedge with non-isothermal surfaces. *Journal of Applied Mathematics and Physics*, *31*, 4941–8501.

Watanabe, T. (1990). Thermal boundary layers over a wedge with uniform suction or injection in forced flow. *Acta Mechanica*, *83*, 119–126.

Watanabe, T., Funazaki, K., & Taniguchi, H. (1994). Theoretical analysis on mixed convection boundary layer flow over a wedge with uniform suction or injection. *Acta Mechanica*, *105*, 133–141.

Watkins, C. B. (1976). Unsteady heat transfer in impulsive Falkner-Skan flows. *International Journal of Heat and Mass Transfer*, *19*(4), 395–403.

Yacob, N. A., Ishak, A., Nazar, R., & Pop, I. (2011a). Falkner-Skan problem for a static and moving wedge with prescribed surface heat flux in a nanofluid. *International Communications in Heat and Mass Transfer*, *38*, 149–153.

Yacob, N. A., Ishak, A., & Pop, I. (2011b). Falkner-Skan problem for a static or moving wedge in nanofluids. *International Journal of Thermal Sciences*, *50*, 133–139.

Yao, B. (2009). Approximate analytical solution to the Falkner-Skan wedge flow with the permeable wall of uniform suction. *Communications in Nonlinear Science and Numerical Simulation*, *14*(8), 3320–3326.

Yih, K. A. (1998). Uniform suction/blowing effect on about a wedge: Uniform heat flux. *Acta Mechanica*, *128*, 173–181.

Yih, K. A. (2001). Radiation effect on mixed convection over an isothermal wedge in porous media: The entire regime. *Heat Transfer Engineering*, *22*(3), 26–32.

LIST OF PUBLICATIONS

The journal articles and manuscripts constituting the thesis are:

Published

- Kasmani, R. M., Sivasankaran, S., Bhuvaneswari, M. & Siri, Z. (2016). Effect of chemical reaction on convective heat transfer of boundary layer flow in nanofluid over a wedge with heat generation/absorption and suction. *Journal of Applied Fluid Mechanics*, *9*(1), 379−388.
- Kasmani, R. M., Sivasankaran, S., Bhuvaneswari, M. & Siri, Z. (2015). Effect of thermal radiation and suction on convective heat transfer of nanofluid along a wedge in the presence of heat generation/absorption. *AIP Conference Proceedings*, *1682*, 020008.
- Kasmani, R. M., Sivasankaran, S. & Siri, Z. (2014). Convective heat transfer of nanofluid past a wedge in the presence of heat generation/absorption with suction/injection. *AIP Conference Proceedings*, *1605*, 506−511.

Submitted

- Kasmani, R. M., Sivasankaran, S. & Siri, Z. (2015). Thermal radiation, Soret and Dufour effects on mixed convection of nanofluid over a wedge with power-law variation in surface temperature and species concentration. Submitted to Neural Computing and Applications.
- Kasmani, R. M., Sivasankaran, S. & Siri, Z. (2016). Soret and Dufour effects on double-diffusive convection of nanofluid past a moving wedge with suction. Submitted to International Journal of Numerical Method for Heat and Fluid Flow.
- Kasmani, R. M., Sivasankaran, S. & Siri, Z. (2016). Soret and Dufour effects on doubly diffusive convection of nanofluid over a wedge in the presence of thermal radiation and suction. Submitted to Scientia Iranica.